NASA Technical Memorandum 101550

ACOUSTIC TEST OF A MODEL ROTOR AND TAIL ROTOR: RESULTS FOR THE ISOLATED ROTORS AND COMBINED CONFIGURATION

R. M. MARTIN
C. L. BURLEY
J. W. ELLIOTT

FEBRUARY 1989

National Aeronautics and Space Administration

Langley Research Center
Hampton, Virginia 23665-5225

Introduction

One of the earliest flight investigations of main rotor/tail rotor interaction noise (ref. 1-3) was directed at understanding and reducing what was called the "burble" noise observed during forward flight and approach of the Lynx Helicopter. Narrowband analysis of this subjectively annoying noise source showed that it consisted of acoustic energy in the 1-2 kHz spectral range, of discrete frequencies ("interaction harmonics") at $mf_{BPF-M}+nf_{BPF-T}$ (where f_{BPF} is the blade passage frequency of each rotor). Similar spectra exhibiting "interaction harmonics" were reported in reference 4. It was concluded that the "burble" was a result of the interaction of the main rotor tip vortices with the tail rotor. A theoretical study (ref. 3) indicated that this noise source could be reduced by reversing the tail rotor rotation direction from top blade moving forward to bottom blade moving forward. A flight test was subsequently undertaken (ref. 1), and indicated that although the peak level during flyover was the same for each rotation direction, lower far-field approach levels and reduced "burble" noise levels were observed for the reversed direction tail rotor.

Leverton proposed (ref. 3) that there are two types of main rotor/tail rotor interaction noise, "burble" noise and "overhead interaction" noise. The first, "burble noise," was reported to have high acoustic levels at the the "interaction" harmonics, to have strong forward radiation, to be due to the main rotor tip vortices interacting with the tail rotor, and to be dependent on the direction of tail rotor rotation. The second, "overhead interaction noise," was said to affect only the main rotor harmonic levels, to propagate mainly downwards, to be due to the passage of main rotor vortices through the center of the tail rotor disc, and to be related only to tail rotor tip speed. As a result of this study, it was recommended that a reversed direction tail rotor rotation would reduce the interaction noise.

During the same time frame, a small scale acoustic wind tunnel program was conducted (refs. 5-7) using a two-bladed rotor. The test program investigated the parametric effects of both the pusher and tractor tail rotors on main rotor/tail rotor interaction noise. The general results showed that the major acoustic parameters are the direction of tail rotor rotation and the tail rotor tip speed (a confirmation of the conclusions of references 1-3). Interestingly, this test found that the reversed tail rotor rotation created higher acoustic levels. This work also found that changes in acoustic levels from both pusher and tractor tail rotors were more attributable to tail rotor installation effects than main rotor/tail rotor interaction effects.

Schlinker and Amiet (ref. 8) published the results of a rotor-vortex interaction experiment with particular application to the intersection of a wing tip vortex with a tail rotor. This study indicated that the BVI noise has a linear dependence on blade number and vortex strength, a low sensitivity to blade pitch changes and a high dependence on local Mach number.

Analytic work done by George and Chou (refs. 9-10) has tried to assess the relative importance of various components of tail rotor noise. Reference 9 addresses the contributions of broadband and harmonic noise sources of an isolated tail rotor, and the interactions of a tail rotor with the main rotor wake, fuselage wake and the exhaust. This work concluded that the main rotor wake created the strongest tail rotor noise sources. The interaction

noise was generally higher than the isolated tail rotor noise. Reference 10 continued this work to consider (1) the main rotor tip-vortex/tail rotor interaction noise, (2) the fuselage mean wake/tail rotor interaction and (3) turbulent vortex shedding from tail rotor blades. This work concluded that the noise due to tail rotor blade/main rotor tip vortex interaction is as important as tail rotor high speed impulsive noise. Broadband noise (due to blunt trailing edge turbulent vortex shedding) was also shown to be a very important tail rotor noise source.

Due to the recognized importance of tail rotor noise to rotorcraft system noise, and due to the paucity of experimental data on the main rotor/tail rotor interaction problem, a joint experimental program was undertaken by the NASA Langley Research Center, the U. S. Army Aerostructures Directorate, and Sikorsky Aircraft. The program was conducted in three seperate experiments. The first of these considered the isolated main rotor, and was conducted in 1983 in the Langley 14 by 22 Foot Subsonic Tunnel with two one-sixth scale rotor systems and several interchangeable blade tips (refs. 11-14). The primary objectives of this first phase were (1) to characterize the impulsive noise due to main rotor blade-vortex interaction (BVI) created by various tip geometries as a function of rotor operating parameters, (2) to make comparisons with other scale acoustic data, and (3) to acquire an acoustic data base for use in the development and validation of a main rotor BVI noise prediction method.

The second phase of the program was conducted in 1984 by Sikorsky at the United Technologies Research Center (UTRC) anechoic wind tunnel with two one-sixth scale tail rotor models and various pylon-stabilator configurations (ref. 15). This program investigated the installation effects of pylon-stabilator geometry and cant angle on both a pusher and tractor tail rotor. The advancing blade tip Mach number was found to be the primary parameter (as found in ref. 8), with thrust coefficient and advance ratio having a secondary effect on tail rotor noise. Installation effects on noise were found to be more important for the pusher mode than the tractor mode.

The third phase was conducted in 1985 in the Langley 14 by 22 Foot Subsonic Tunnel. The results of the first and second phases were used to choose the main and tail rotors for the third phase. The phase three experiment included three operating configurations : (1) an isolated main rotor, (2) an isolated tail rotor, and (3) the combined main/tail rotor configuration. The main rotor chosen was the design which exhibited the lowest BVI noise during the first experimental phase. The tail rotor chosen was the design which exhibited the least installation effects from the second experimental phase. This final experiment was aimed at studying main rotor wake effects on the tail rotor acoustic signal. The test was designed to place the tail rotor in and out of the main rotor wake while maintaining the same main and tail rotor flight conditions.

This paper presents the acoustic results from the third phase. General trends of directivity and spectral characteristics of the isolated main rotor, the isolated tail rotor and the combined rotor configuration are presented. The acoustic content are discussed in terms of the contributions of the main and tail rotor fundamental frequencies, the first four harmonics of the main and tail rotor, tail rotor broadband noise and tail rotor discrete noise levels. Additional 1/12-th octave band spectra results are also reported in reference 16.

Symbols

a_1	coefficient of first harmonic of longitudinal flapping, deg
b_1	coefficient of first harmonic of lateral flapping, deg
C_T	rotor thrust coefficient
R	rotor radius, (4.7 ft (1.45 m))
r_M	radial distance from center of main rotor tip-path-plane to microphone, $(x_M^2 + y_M^2 + z_M^2)^{1/2}$, m (see figure 7)
r_T	radial distance from center of tail rotor tip-path-plane to microphone, $(x_T^2 + y_T^2 + z_T^2)^{1/2}$, m (see figure 7)
T	tail rotor thrust, lb
V	tunnel free-stream velocity, m/sec (knots)
x	microphone coordinate relative to center of rotor tip-path-plane, positive upstream, m (see figure 7)
y	microphone coordinate relative to center of rotor tip-path-plane, positive to left looking upstream, m (see figure 7)
z	microphone coordinate relative to center of rotor tip-path-plane, positive up, m (see figure 7)
α_s	rotor shaft angle, positive when vehicle nose is up, deg
α_{TPP}	rotor tip-path-plane angle, positive when vehicle nose is up, deg
θ_M	polar angle, angle from main rotor tip-path-plane, deg (see figure 7)
θ_T	polar angle, angle from tail rotor tip-path-plane, deg (see figure 7)
ψ_M	azimuth angle, angle in the plane of main rotor, deg (see figure 7)
ψ_T	azimuth angle, angle in the plane of tail rotor, deg (see figure 7)

Abbreviations

BPF	blade passage frequency, Hz
BVI	blade-vortex interaction
LM1	sound pressure level of first main rotor harmonic, dB
LM4	sound pressure level of first four main rotor harmonics, dB
LT1	sound pressure level of first tail rotor harmonic, dB
LT4	sound pressure level of first four tail rotor harmonics, dB
LTB	sound pressure level of isolated tail rotor broadband noise in 560 to 4600 Hz band, dB
LTD	sound pressure level of isolated tail rotor discrete noise in 560 to 4600 Hz band, dB
OASPL	overall sound pressure level (0 to 12,630 Hz), dB (re 0.0002 dynes per cm^2)

Subscripts

M	isolated main rotor configuration
MT	combined main and tail rotor configuration
T	isolated tail rotor configuration

Description of Experiment

Wind Tunnel Facility

The Langley 14 by 22 Foot Subsonic Tunnel is a closed-circuit atmospheric wind tunnel that can be operated either in the open-jet or closed-jet mode. The open-jet mode is accomplished by removing test section walls, raising a movable ceiling, and introducing a bell-mouth collector. The floor of the test section remains in place so that three sides of the jet are open. The dimensions of the open-jet test section are 4.42 m (14.50 ft) high and 6.63 m (21.75 ft) wide. The ceiling in the open-throat configuration is completely out of the flow, approximately 7.50 m (24.60 ft) above the test chamber floor. Photographs of the rotor model and test rig in the open-jet test chamber are shown in figure 1, and a schematic diagram of the test section is shown in figure 2.

The acoustic characteristics of this facility as originally constructed have been documented in references 17 and 18. Subsequent to these reports, the walls and ceiling of the entire test chamber were covered with permanently installed 12.7 cm (5 in) panels filled with fiberglass material and covered with perforated sheet metal. Because this facility was not originally designed for acoustic testing, acoustic treatment was applied during this test. The test section floor was lined with 12.7 cm (5 in) fiberglass panels covered with perforated sheet metal. The floor areas adjacent to the test section were covered with 15.2 cm (6 in) open-cell polyurethane foam. The raised test section ceiling was covered with the same foam but with a 15.2 cm (6 in) air gap above the foam. The details of the test section acoustic treatment are shown in figure 2.

Model Rotor Test Rig

Sikorsky Aircraft's Basic Model Test Rig number one (BMTR No. 1) was used for the experiment. The fuselage is a 1/5.727 scale representation of a currently operational helicopter. The test rig includes three seperate balances which measure the fuselage loads, tail assembly loads and main rotor loads. All three balance loads are resolved to the center of the main rotor to simplify determination of model trim conditions. A load cell between the transmission and transmission frame monitors main rotor torque. The tail rotor is driven by a 20 horsepower motor mounted on the vertical tail. The model was supported by an aerodynamically faired strut covered with acoustic treatment to dampen acoustic reflections. The BMTR No. 1 has an articulated main rotor head. Main rotor control inputs (collective and cyclic pitch) as well as blade flapping and tail rotor collective pitch were monitored.

Main Rotor and Tail Rotor Model Blades

The main rotor system model was a 1/5.727 scale version of a currently operational main rotor system. The model has a radius of 4.7 ft (1.45 m), and the planform, twist and tip shape are shown in figure 3. The tip, called the large swept tapered tip, employs the Sikorsky SCCA07 airfoil section. Other pertinent data for this model are reported in reference 19. This rotor design was tested during the first phase of the program, and was chosen because it exhibited the lowest BVI noise levels. Performance results for this rotor are reported in reference 11. The nominal tip and rotational speeds were 728 ft/sec (223 m/s) and 1480 rpm.

Two sets of tail rotor blades were employed. The first set was employed for the data acquired with both the main and tail rotors. Due to a tail rotor drive system failure, the first set of tail rotor blades was destroyed, and a second set of tail rotor blades was installed to complete the program. The second set was employed only for the isolated tail rotor data.

Both sets of tail rotor blades were 1/5.727 scale versions of a currently operational tail rotor. The tail rotor model has a radius of 0.97 ft (0.30 m) and the blades have the same planform and twist distribution as the full-scale blades, shown in figure 4. The two tail rotors differ in blade chord length and airfoil section. The blades of the first tail rotor had a chord length of 1.714 in and employed the SC1095RN airfoil section. The blades of the second tail rotor (used only for the isolated tail rotor configuration) had a chord length of 1.697 in and used the SC1095 airfoil section. Details of these airfoil sections are given in reference 16. The nominal tip and rotational speeds were 687 ft/s (209 m/s) and 6800 rpm, respectively.

The tail rotor was installed in a relatively low forward position, whereas the standard position for this tail rotor is a relatively high aft position (ref. 16). In addition, the tail rotor of the full scale is canted 20 degrees, whereas the model tail rotor was not canted during this test.

Test Plan Objectives

The experimental program was aimed at studying the noise created by main rotor wake ingestion by the tail rotor, by moving the tail rotor in and out of the main rotor wake. The main rotor was chosen from the Phase I configurations as the design exhibiting the least BVI noise under most operating conditions (ref. 12). Since main rotor BVI and tail rotor noise occur in roughly the same frequency range, the intent was to minimize the BVI noise so that the tail rotor effects would be more easily measured.

The tractor tail rotor was chosen based on the results from Phase II of the program (ref. 15) as the design exhibiting the least installation related effects. The tractor tail rotor design minimized the noise created by sources other than the effect of the main rotor wake on the tail rotor. The tail rotor location was based on wake predictions which indicated that this location would create the largest variation in main rotor wake/tail rotor wake geometry. Unfortunately, due to physical and practical limitations, the tail rotor was almost always submerged in the main rotor wake (ref. 16). Because of this, an evaluation of the main rotor wake effect on tail rotor noise is difficult to make.

The matrix of test conditions included level flight and descent conditions in the moderate speed range (50 to 80 knots) where acoustic data are best measured in the 14 by 22 Foot Subsonic Tunnel. A tabulation of the test conditions obtained for the main rotor/tail rotor configuration is presented in table 1.

Experimental Procedure

In order to change the tail rotor position in the main rotor wake, while maintaining the same main rotor operating conditions, the following procedure was followed. For a given test condition, the main rotor tip-path-plane angle and thrust coefficient were maintained at a constant value. The main rotor shaft angle relative to the tip-path-plane was changed approximately $\pm 5.^{\circ}$ The main rotor longitudinal flapping was varied

accordingly to maintain the fixed tip-path-plane angle. This change in shaft angle caused the tail rotor to be moved up and down behind the main rotor, changing its intersection location with the main rotor wake. The geometry of this procedure is illustrated in figure 5. The relatively high and low tail rotor positions are designated as "High" and "Low." The designations "High" and "Low" are also noted in table 1.

Data were initially acquired with both main rotor and tail rotor present. The tail rotor thrust was set to counteract the main rotor anti-torque requirements. The same conditions were then repeated for the isolated main rotor and then for the isolated tail rotor, matching the set points of the combined main and tail rotor conditions. As mentioned above, due to mechanical failure, two slightly different sets of tail rotor blades were used for the main rotor/tail rotor data and the isolated tail rotor data.

Rotor Performance Data Acquisition and Corrections

The main rotor and tail rotor performance data were acquired by the tunnel's computerized mean data acquisition system in a similar manner as is described in reference 11. The tip-path-plane angle is obtained from the sum of the measured geometric shaft angle, the longitudinal flapping angle and a correction angle due to the open jet boundary effects (ref. 20).

The correlation of tail rotor performance for the isolated and combined rotor configurations is complicated by the fact that the tail balance measured not only the tail rotor loads but also the loads on the vertical pylon and tail rotor motor fairing. During post-test analyses, it was discovered that the tail pylon generated a significant amount of additional thrust due to the main rotor's wake. Thus, for equivalent total tail side force conditions, the tail rotor thrust is substantially different for the isolated and combined rotor configurations. It was deemed necessary to remove the tail pylon thrust from the total tail thrust, so that test conditions could be compared on the basis of the same tail rotor thrust setting.

A post-test correction procedure was developed to estimate the contributions of the tail rotor and the tail pylon to the total measured tail thrust for the combined rotor test conditions. Reference 16 gives a complete description of the correction employed. The estimated tail rotor thrust levels for the combined rotors are given in table 1 in addition to the measured tail rotor thrust for the isolated tail rotor. In many cases, the two thrust levels are quite different and thus a comparsion of the acoustic levels for both cases is not valid. The conditions where the two thrust levels are within 5 percent are marked with an asterisk, and are considered acceptable for acoustic comparison purposes.

Microphone Locations

The microphone locations are shown in the schematic of figure 6, and the Cartesian coordinates (x, y, z) relative to the rotor hub at zero pitch are given in table 2. A more convenient description of the relative microphone locations is given in terms of the radial distance r from the hub, polar angle θ from the rotor tip-path-plane, and azimuth angle ψ in the tip-path-plane. These coordinates are given both referenced to the main rotor (subscript M) and to the tail rotor (subscript T) as shown in figure 7.

Microphones 1 and 3 were mounted to the model support strut under the fuselage. The geometry between both rotors and these microphones remained constant with fuselage

attitude change. Microphones 2, 4 and 10 were mounted on streamlined stands fixed to the tunnel floor. Microphones 2 and 4 were located to each side of the model, approximately 25° out of the tail rotor plane. Microphone 10 was mounted upstream of the model and nominally in the plane of the main rotor. Microphones 5 through 9 were installed on a wing-like structure as shown in figure 8. This device was mounted on two rods bolted to the tunnel floor and could traverse about 12 ft streamwise from the jet exit nozzle to the vertical model support strut. For most of the data reported herein, this traversing array was fixed in a nominal position of 8.3 ft upstream of the main rotor hub.

Since all the microphones (except numbers 1 and 3) were fixed to the test chamber floor, their relative locations change with changes in main rotor tip-path-plane angle and shaft angle. The changes in location with changes in rotor tip-path-plane angle are presented for the coordinates relative to the main and tail rotors in tables 3 and 4 respectively.

Acoustic Data Acquisition

Ten 1.27 cm diameter (0.50 in) pressure-type condenser microphones fitted with standard "bullet" nosecones were installed in the open-throat test section. The acoustic data were recorded on a 14-channel frequency-modulated magnetic tape recorder. A once-per-revolution impulse signal from both the main rotor and tail rotor and IRIG-A time code were recorded simultaneously with the acoustic signals. The recording method was Wideband I with a tape speed of 76.2 cm/sec (30 in/sec), resulting in a useful frequency response of 20 kHz. Daily calibrations were performed using a standard pistonphone calibrator at a frequency of 250 Hz and level of 124 dB. The analog signals were high-pass filtered at 50 Hz to remove low-frequency wind noise.

Acoustic Data Reduction

The analog acoustic signals were digitized at 25,258 samples per second (1024 samples per main rotor revolutiion) with anti-aliasing filters set at 12.5 kHz. A 2048-point fast Fourier transform algorithm was employed to calculate 50 independent power spectra with a bandwidth of 12.33 Hz. Each of these 50 power spectra were then averaged to obtain an average power spectrum with a maximum frequency of 12.5 kHz and a spectral bandwidth of approximately 12 Hz. Considering each power spectrum as a Chi-squared random variable, the statistical accuracy of the spectral results is ± 0.8 dB for an 80 percent confidence interval.

To help identify general trends in the data, several specific noise metrics were calculated from the averaged narrowband spectra: the overall sound pressure level, OASPL; the main rotor fundamental frequency (about 100 Hz) sound pressure level, LM1; the summed sound pressure level of the first four main rotor harmonics, LM4; the tail rotor fundamental frequency (about 460 Hz) sound pressure level, LT1; and the summed sound pressure level of the first four tail rotor harmonics, LT4. The bandwidth of the fundamental frequency level is 36 Hz, and the bandwidth of the summed first four harmonics is 144 Hz.

In addition, noise metrics to quantify the midfrequency discrete and broadband noise levels were calculated for the isolated tail rotor test conditions. The tail rotor discrete level (LTD) was determined by summing the tail rotor blade-passage harmonics and shaft harmonics between 560 Hz and 4600 Hz (bandwidth of 420 Hz). This frequency range includes the second through the tenth tail rotor harmonic and the fifth through the

sixteenth tail rotor shaft harmonic. Not all shaft harmonics were included because for some test conditions they were much lower than the broadband noise level. The tail rotor broadband level (LTB) was determined by summing the energy between 560 and 4600 Hz (bandwidth of 4040 Hz), excluding the harmonics and shaft harmonics. The harmonics and shaft harmonics were excluded by replacing them with values linearly interpolated from adjacent spectral values.

Acoustic Data Quality

Microphone response correction. The pressure response of each complete microphone system (including the microphone, preamplifier, and adapter) was calibrated using the electrostatic actuator method prior to the experiment. This response was found to be flat to approximately 3 kHz (where the correction is nearly 0 dB) and as much as 2 dB at 10 kHz.

The published free-field correction is flat to approximately 3 kHz (where the correction is approximately 0.5 dB) and becomes as much as 9 dB at 12 kHz. The correction is a function of source angle of incidence to the microphone.

The free-field correction was added to the microphone pressure response to obtain the microphone's free-field response correction. This correction was then subtracted from the measured spectra as a function of frequency and angle of incidence from the source. The angle of incidence was estimated for each microphone location relative to the main rotor hub.

Background noise correction. The background noise data were acquired for all microphone locations with the model installed, both rotor hubs spinning (without rotor blades), and for tunnel speeds of 50 to 80 knots in 5-knot increments. For the fixed microphones (microphones 1 to 4 and 10), the predominant noise is low frequency tunnel background noise, shown in (figure 9(a)) for microphone 10. For the microphones located on the wing the predominant noise is also at low frequencies but an additional tonal noise source appears at higher frequencies as shown in (figure 9(b)) for microphone 7. This source appears between 800 and 1300 Hz at 50 knots and increases in frequency to between 1200 and 2000 Hz at 80 knots. This source is atttributed to Aeolian tones shed from the stiffening cables installed between the vertical wing supports (see figure 8). The background noise above 4500 Hz for all microphones is generally flat and 10 to 30 dB down from the rotor data. Figure 10 shows the signal-to-noise ratio of a typical rotor noise spectrum to the background noise for microphones 4, 7 and 10. The averaged acoustic spectra were corrected by subtracting the background noise on an acoustic power (mean-squared pressure) basis.

Acoustic reflections. To measure reflections at each microphone, small explosive charges were ignited near the main rotor and tail rotor hubs at 0 and 80 knots tunnel speed. The acoustic signals were recorded on tape and analyzed to quantify the amplitude and time delay of the reflections at each location. Due to the close proximity of microphones 1 through 4 to the impulsive noise source, and due to insufficient signal attenuation, the signals measured from these microphones saturated the tape. Conclusions based on absolute amplitudes of the direct and echoed signals from these locations are difficult to make. The acoustic signals from microphones 5 through 10 were properly recorded. An

example of the impulse data measured at zero tunnel speed is shown in figure 11. The direct and echo signals are labelled on this figure. Table 5 contains the estimated echo delay times and relative echo amplitudes for microphones 5 through 10. The relative amplitudes of the reflections are in the range of 0.30 to 0.70, or 3.0 to 10.2 dB down from the direct wave.

A power cepstrum technique has been successfully used in the past (refs. 21-23) to correct the major effects of acoustic reflections from the power spectra. An attempt was made to apply this technique to these data, however, the effort was largely unsuccessful. The power cepstrum technique has been found to be highly data dependent, and is complicated when the source signal is non-compact and of a highly periodic nature, as is rotor noise. These data are further complicated by having two large, periodic noise sources. Thus, corrections have not been made for acoustic reflections.

Discussion of Results

The results will be discussed in the following order: first, the isolated main rotor results; second, the isolated tail rotor results; third, the combined main and tail rotor results.

Isolated Main Rotor Results

Comparisons of acoustic signals for flapping and non-flapping conditions at constant tip-path-plane angle. Although a full scale rotor in flight typically has some component of longitudinal flapping, for wind tunnel tests the model is often flown with zero longitudinal flapping. This is done for two reasons, (1) to simplify the setting and measurement of the tip-path-plane angle α_{TPP}, and (2) to simplify the process of setting the model rotor at a specified test condition. The tip-path-plane angle α_{TPP} is not a measured quantity but is computed as the sum of the shaft angle α_s and the first coefficient of longitudinal flapping a_1 ($\alpha_{TPP} = \alpha_s + a_1$). Thus different combinations of α_s and a_1 may be used to obtain the same α_{TPP}. Researchers have generally assumed that as long as α_{TPP} is constant, different combinations of α_s and a_1 should produce the same performance and acoustic results.

To check this assumption, acoustic data were measured at zero, negative and positive longitudinal flapping angles a_1 for two constant α_{TPP}. Figure 5 shows the relation between the rotor and fuselage for zero, negative and positive longitudinal flapping angles a_1 at a constant α_{TPP}. The spectra taken at the positive and negative longitudinal flapping angles were compared to the spectrum for zero longitudinal flapping. In general, the negative longitudinal flapping data are more tonal in character than those with positive longitudinal flapping angles. Figure 12(a) compares the signal for positive longitudinal flapping with that for negative flapping for $\alpha_{TPP} = -3.^\circ$ The amplitude envelope of the harmonics for the negative flapping data is traced on the curve for the positive flapping. Tones are prevalent in the negative flapping data to about 5000 Hz, whereas the spectra for positive longitudinal flapping typically show tones only up to 4000 Hz. Figure 12(b) shows the same comparison for $\alpha_{TPP} = 2^\circ$ for a different microphone. Again the midfrequency tone levels are increased for the negative flapping data.

Blade vortex interaction noise typically appears as an increase in spectral levels in the midfrequency range, anywhere from 500 Hz to 5000 Hz at model scale. This is similar to

the characteristics seen in the negative longitudinal flapping angle data. It is speculated that the increase in the spectral levels for the negative longitudinal flapping levels is a result of increased blade-vortex interaction. The increased BVI activity may be partly explained by considering the path of the blade tips for a given α_{TPP}. A constant α_{TPP} means that the vertical position of the blades at 0 ° and 180 ° azimuth is the same, but the blade tips at other azimuth locations may be in different vertical positions depending on the flapping. For the test conditions of this experiment, the position of the tip-path-plane deviates at the most $\pm.8$ in for different settings of a_1, b_1 and α_s. If the tip vortex core radius is estimated to be approximately ten percent of the chord, .36 in, a tip-path-plane deviation of .8 inches is very significant, and could possibly make a significant difference in the blade vortex interaction geometry.

In summary, for a given α_{TPP}, negative longitudinal flapping increased the spectral levels of the harmonics between approximately 500 and 6000 Hz. The increase was typically on the order of 5 dB. Thus, for a given α_{TPP} different combinations of α_s and a_1 will produce different acoustic results. The experimentalist should exercise great care in setting rotor conditions, especially when acoustic measurements will be made for matching other scale acoustic data. The position of the blades tips are strongly affected by small changes in flapping and shaft angle settings, and can change the resulting midfrequency harmonic noise.

Overall sound pressure levels $OASPL_M$. The overall sound pressure levels of the isolated main rotor are given in table 6. The results for microphones 1 and 3, located symmetrically under the main rotor advancing and retreating sides show a difference of several decibels. Microphone 1 generally shows higher levels for the positive α_{TPP} cases, while microphone 3 has higher levels for the negative α_{TPP} cases. The highest microphone 3 levels are seen at the highest main rotor thrust coefficient (.0085), indicating that at this location the levels are created by loading noise.

Comparing microphones 2 and 4, located symmetrically downstream of the retreating and advancing sides respectively, the OASPL for microphone 2 is at least equal to but typically 2 to 3 dB higher than microphone 4, with some conditions as much as 6 dB higher.

Inspection of the data for the traversing wing microphones (locations 5 through 9) shows a steady monotonic increase in $OASPL_M$ moving from microphone 5 to microphone 9, typcially an increase of 3 to 5 dB.

The OASPL for microphone 10 range from 107 to 112 dB with no clear trend with operating condition except that it is somewhat higher (1 to 2 dB) for the positive α_s cases (rather than the negative α_s) and for positive α_{TPP} (rather than negative α_{TPP}).

Main rotor fundamental frequency level $LM1_M$. The main rotor fundamental frequency levels for the isolated main rotor cases, $LM1_M$, are given in table 7. The $LM1_M$ is almost always several decibels (3 to 12 dB) higher at microphone 3 than at microphone 1. Comparing microphones 2 and 4, the $LM1_M$ at microphone 2 is usually 2 to 3 dB higher than microphone 4. Since the $OASPL_M$ at microphone 2 is also usually 2 to 3 dB higher, this indicates that the $OASPL_M$ at this location must be driven by the $LM1_M$. These results indicate that the fundamental frequency has stronger levels in the retreating side region (locations 2 and 3) than in the advancing side region (locations 1 and 4).

Microphones 1 through 4 tend to show an increase in $LM1_M$ for decreasing α_s (at a constant α_{TPP}). Microphone 10 shows an opposite trend. For the traversing array microphones, there are no clear trends of the $LM1_M$ with microphone position, although the maximum $LM1_M$ is often aimed at microphones 5, 6 and 7.

Main rotor harmonic level LM4. The summed sound levels of the first four main rotor harmonics are given in table 8. The $LM4_M$ of microphones 2 and 3 again are usually higher than those of microphone 1 and 4, indicating higher levels measured under and downstream of the retreating side than the advancing side.

Spectral characteristics. The occurrence of advancing side blade vortex-interaction noise for descent cases (positive α_{TPP}) can be clearly seen at microphone 1 in the increased harmonic levels between approximately 500 and 2000 Hz. This increase in midfrequency noise is not measured at microphone 3. Two examples of data from both microphones are shown in figures 13(a) and (b) for 50 and 80 knots. For most test conditions, the fundamental frequency for microphone 3 is several decibels higher than for microphone 1, but the second and third harmonics of microphone 3 are several decibels lower than for microphone 1.

The spectra at microphones 2 and 4 are quite similar in general shape. However, microphone 2 exhibits increased midfrequency harmonic content at the same conditions as microphone 1. This indicates that when BVI occurs on the advancing side, it is also occuring on the rotor's retreating side, and that the retreating side content radiates downwind of the retreating side. This is illustrated in figure 14, the same test conditions as figure 13. (A similar result showing impulsive content radiating downstream of the retreating side was also reported in reference 24.)

For microphones 5 through 9, the fundamental frequency upstream of the advancing side (microphone 9) is usually the lowest, with the locations more directly upstream (microphones 5 and 7) having higher levels (figure 15). At these locations, the second harmonic is typically much lower than the fundamental. The third through fifth harmonics are typically as high in level as the fundamental. However, the third through fifth harmonics are typically the highest at microphone 9, with location 7 having the next highest levels, and microphone 5 having the lowest levels. This is probably the cause of the increase in $OASPL_M$ from locations 5 to 9.

At microphone 10, for most test conditions the second harmonic is less than the first and the third harmonics, as was also seen in the data from the microphones on the wing. For positive α_{TPP} the higher harmonic levels (above the 5th) remain at a relatively high constant level out to a frequency of about 2000 Hz (see figure 16(a)). For negative α_{TPP} the higher harmonic levels are much lower (by at least 15 dB) and the peaks are less distinct (see figure 16(b)).

Isolated Tail Rotor Results

Overall sound pressure levels $OASPL_T$. Microphones 1 and 3 were located quite close to the tip-path-plane of the tail rotor ($\theta_T = 10^\circ$ and -13°, $\psi_T \approx 205^\circ$ respectively). The $OASPL_T$ measurements at microphone 1 are consistently higher (up to 8 dB) than those at microphone 3 (table 8). Recall that this is a tractor tail rotor which thrusts in the negative y-direction (towards the main rotor advancing side). While microphone 1

is somewhat closer to being in the tail rotor plane than microphone 3, the higher levels at location 1 suggest that the tail rotor radiation pattern is strongest in the thrusting direction, due to loading noise. An additional possible cause for lower levels at location 3 could be blockage of the acoustic signal by the fuselage.

The levels at microphone 4 are consistently 1 to 2 dB higher than at microphone 2. This again indicates a stronger acoustic radiation in the thrusting direction although blockage by the fuselage is again a possible explanation.

The levels are 2 to 3 dB higher at location 9 than at 5, again increasing towards the thrusting direction. The levels at each microphone also increase steadily with an increase in forward velocity. The levels at microphone 10 range from 100 to 105 dB, with levels increasing with velocity. There is no clear trend of $OASPL_T$ with the low or high tail position.

Tail rotor fundamental frequency level $LT1_T$. The $LT1_T$ values are given in table 9. The levels at microphone 1 are consistently several decibels higher (3 to 7 dB) than those at microphone 3. The level of the tail rotor fundamental is usually a few decibels higher at microphone 4 than at 2. These trends follow those found for the $OASPL_T$, an increase in acoustic level in the thrusting direction.

The traversing array microphones are all located at radial distances approximately 28 ft directly upstream of the tail rotor hub. The location of microphone 7 is nominally in the tail rotor plane. The polar angle θ_T ranges from -11° to 16° for microphones 5 through 9. The highest $LT1_T$ are at microphones 6 and 7, in the tail rotor plane, with a decreasing level at microphone 8 and then an increase at microphone 9, indicating that the measurements are being made further out in the loading noise dipole.

For the majority of cases, the $LT1_T$ levels increase from the low to high tail rotor position.

First four tail rotor harmonic level $LT4_T$. The same general trends as noted for the $LT1_T$ are seen in the $LT4_T$ levels (table 10). The wing microphones also show a high $LT4_T$ at microphones 6 and 7, a decrease at microphone 8 and then an increase at microphone 9, but in some cases there is a steady increase in $LT4_T$ from microphones 5 to 9. This indicates higher harmonic levels measured at increasingly out-of-plane locations.

As for the $LT1_T$, for the majority of cases, the $LT4_T$ levels increase from the low to high tail rotor position.

Spectral characteristics. The rotor harmonics at microphones 1 and 3 are very discrete up to about the fifth harmonic, where they begin to broaden out into humps. For most cases microphone 1 shows distinct peaks on the left or increasing side of the tone humps, as shown in Figure 17(a). The occurence of these peaks appears to be a function of velocity, with a minimum at 50 kts and a maximum at 80 kts. At 80 kts (figure 17(b)) the humps have about equal or higher levels than the tone levels, particularly near the fifth through eighth harmonics. Although the humps are evident in the microphone 3 data, higher harmonics of the fundamental frequency are not evident.

The higher harmonics for microphone 1 are typically several dB higher than those of microphone 2, as shown in figure 18 for 50 and 60 knots. As already shown by the $LT1_T$ and $LT4_T$ measurements, this again suggests a stronger radiation in the thrusting direction. The higher harmonics at microphones 2 and 4 (figure 18) are not as distinct as

those at locations 1 and 3 (figure 17). Harmonic content above the fifth harmonic (about 2500 Hz) is not present at locations 2 and 4, whereas harmonic content up to 5 kHz was observed at locations 1 and 3. Above about 2 kHz, the signals at locations 2 and 4 appear to be broadband noise (figure 18) and follow a steady decay with increasing frequency. The higher frequency broadband noise is approximately 5 dB higher at microphone 4 than at microphone 2 between 800 to 3000 Hz.

The high amplitude humps seen in the microphone 1 data (figure 17), repeating at a frequency of about 500 Hz, are also present at locations 2 and 4 although less distinctly than in the microphone 1 data. The humps in the microphone 2 and 4 data occur with the same oscillation period (about 500 Hz) but are slightly offset from those seen in data from locations 1 and 3. To illustrate this offset, figure 19 presents the signal from microphone 1 and 2 plotted together. The hump amplitudes at microphones 2 and 4 also decay much faster than those at locations 1 and 3 (see figure 19(b)), and are typically important only out to about 4500 Hz (as compared to at least 7000 Hz at locations 1 and 3).

Higher harmonic content is observed at locations 5 through 9, with a broadening of the tones occurring at about the fifth harmonic (2500 Hz, see figure 20). The high amplitude humps seen in the spectra of microphones 1 through 4 are also present in the spectra from microphones 5, 7 and 9. The repetition of the humps, their amplitude and frequency range are all similar to that of the spectra from microphones 1 and 3. The levels of the first five harmonics at microphone 9 are typically higher than those at microphone 5, by several decibels (figure 20). This again indicates a stronger radiation pattern in the thrusting direction (as seen at locations 1, 2, 3 and 4) than in the non-thrusting direction.

A scalloped or humped spectrum can often be attributed to an acoustic reflection. A ripple of 500 Hz in the spectrum corresponds to a reflection delay time of .002 sec, and the reflected path length would be about 2.3 feet longer than the direct path. From the acoustic impulse data (table 5), there are no obvious reflections at a delay time of .002 sec. Further, from the geometry of the test set-up, there are no reflective surfaces which would produce an echo with such a path length or delay time.

The source of this peculiar humped spectral shape has not been firmly established. However, data from a Lynx helicopter flight test (refs. 1 and 3) measured at a microphone location similar to microphone 3, with the same rotor rotation direction, are remarkably similar to these data. The model-scaled frequency ranges in which this spectral broadening occurs is also the same for both data sets. While the results presented here are for a isolated tail rotor, the flight data also includes the main rotor signal, indicating that this shape is independent of the main rotor.

The same humped spectral shape has also been observed in both hover and forward flight acoustic data of a full-scale S-76 helicopter. For the hover data, the spectral humps were associated with the main rotor harmonics. For the fly-over data, they were attributed to the tail rotor harmonics.

A recent analytical study (ref. 25) which used the same data as presented here has indicated that these spectral peaks can be attributed to the effects of the fuselage wake, and has been termed "unsteady thickness noise." The general location and amplitude of the humps for the in-plane measurements were predicted well; further unpublished results have shown the slight shift in hump center frequencies noted in figure 19. This shift is

attributed to the difference in retarded times from the turbulence interaction locations to each of the two different measurement locations.

For the present data, the effect of the fuselage wake was investigated by comparing the spectrum from the high tail position with that from the low tail position for the same tunnel speed and tail rotor thrust. For the high tail position, the tail rotor is mostly out of the fuselage wake, whereas for the low tail position, the tail rotor is mostly submerged in the fuselage wake. The spectra from microphones 1, 4 and 9 are used for the comparison. For most of the test cases, the spectral humps from the low tail position are about 5 dB higher than the high tail position for frequencies greater than about 2500 Hz. An example of this trend is shown in figure 21(a) for microphone 1. This trend is also clearly seen in the spectra from microphones 4 and 9, see figures 21(b) and 21(c), although not as distinctly. The same general result was also shown in reference 16 using 1/12-th octave band spectra of the same data.

Tail rotor broadband noise LTB. The broadband noise level was calculated by summing the energy between 560 Hz and 4600 Hz, excluding the harmonic and subharmonic levels. These levels are given in table 11. For comparison purposes, the levels are corrected for spherical spreading by adding 20 times the logarithm of the ratio of the microphone's distance to the tail rotor hub to a reference distance. The reference distance is the radial distance from microphone 4 to the tail rotor hub.

The broadband noise levels are the highest at the out-of-plane locations in the thrusting direction. This is seen by the high broadband noise levels measured at locations 4 and 10 ($\theta_T = 60^\circ$ and 30° respectively). The next highest broadband noise levels are found at microphone location 2, also out-of-plane ($\theta_T = -60^\circ$), but not in the thrusting direction. The lowest levels were measured at microphone 7, the most in-plane of the locations ($\theta_T = 2^\circ$). The wing microphone levels increase as the polar angle increases out of the rotor plane. The highest wing microphone levels are seen at microphones 8 and 9 (polar angles $\theta_T = 9^\circ$ and $16,^\circ$ respectively) and in the thrusting direction. The levels at microphone 5 ($\theta_T = -12,^\circ$ not on the thrusting side) are not as high as those at microphone 8.

The data clearly shows that the broadband noise is at a minimum in the plane of the tail rotor, and that the noise levels increase for the out-of-plane locations, to a maximum for those locations in the rotor thrusting direction. In general, the broadband levels increase at each measurement location with increasing tunnel speed.

Comparison of tail rotor discrete noise LTD with broadband noise LTB. The tail rotor discrete levels were determined by summing the harmonic and subharmonic levels between 560 Hz and 4600 Hz. The levels are corrected for spherical spreading and are presented in table 12. In general the broadband noise is greater than the tone noise for microphones 2, 3, 4, 6 and 10 for the majority of the test conditions. The difference between the broadband noise and the tone noise is up to 7 dB, with an average of 4 dB. The only locations where the tone noise is typically greater than the broadband noise were microphones 1, 8 and 9. All three of these microphone locations are out-of-plane ($\theta_T = 10^\circ, 9^\circ$ and 16°, respectively) and on the thrusting side.

Combined Main Rotor/Tail Rotor Results

The acoustic levels produced by the combined main and tail rotors are compared with the levels produced by the isolated main rotor and isolated tail rotor. The three configurations are compared based on the OASPL, LM1, LM4, LT1 and LT4 values. The comparison is presented in terms of the arithmetic differences in decibels between the combined and isolated configurations. Tables 13 through 17 present the differences in the OASPL, LM1, LM4, LT1 and LT4 respectively.

Recall that while the performance data for each rotor configuration are valid in their own right, there are a limited number of test conditions where the tail rotor thrust for the combined configuration is sufficiently close (±5 per cent) to the tail rotor thrust of the isolated tail rotor for comparison. These cases are marked with an asterisk in the tables. The combined configuration and isolated main rotor data may be compared with confidence at all test conditions.

Overall sound pressure level OASPL for MT, M and T configurations. In general the main rotor contributes more to the OASPL of the combined configuration than does the tail rotor. This is seen in table 13 where the value of $OASPL_{MT}$-$OASPL_{M}$ is typically small and the value of $OASPL_{MT}$-$OASPL_{T}$ is typically several decibels. The largest $OASPL_{MT}$-$OASPL_{T}$ occurs at the wing microphones, indicating a strong main rotor dominance in the $OASPL_{MT}$ at those locations. The smallest value of $OASPL_{MT}$-$OASPL_{T}$ is at microphones 1 and 4, which indicates that this is where the tail rotor signal has the greatest influence on the OASPL.

The $OASPL_{MT}$ of microphone 10 is also dominated by the $OASPL_{M}$. At the higher velocity cases, the $OASPL_{M}$ is even higher than the $OASPL_{MT}$, as shown by a negative $OASPL_{MT}$-$OASPL_{M}$. This trend is also seen at the other microphones (5 through 9) and sometimes at microphones 1 and 10. No correlation with test condition is obvious to explain this.

Change in harmonic levels from isolated to combined configuration. Table 14 shows that for microphones 1, and 5 through 10, the LM1 is often lower when both rotors are present ($LM1_{MT} < LM1_{M}$). Table 15 shows that for microphones 1, and 5 through 9, the LM4 is often lower when both rotors are present ($LM4_{MT} < LM4_{M}$). Table 16 shows that for most microphones, and a large percentage of the test conditions, the LT1 is lower when both rotors are present ($LT1_{MT} < LT1_{T}$). Table 17 shows that for microphones 1, 4 and 10, the LT4 is lower with both rotors present ($LT4_{MT} < LT4_{T}$). The other microphones exhibit a sometime lower, sometime higher LT4 with both rotors present.

Relative importance of LM4 and LT4 to OASPL. An estimate of the relative importance of the main rotor and tail rotor harmonics to the total signal is determined by comparing the LM4 and LT4 with the OASPL of the combined main rotor/tail rotor signal. Percentages are formed by computing ratios of the squared pressures of $LM4_{MT}$ and $LT4_{MT}$ to that of the $OASPL_{MT}$ and multiplying by 100. These percentages are presented in table 18. The percentages show that the first 4 main rotor harmonics generally contribute considerably more acoustic energy (30 to 60 percent) than the first 4 tail rotor harmonics (about 10 percent) for almost all microphone locations and test conditions.

Tail rotor broadband noise LTB. For microphones 1 and 9 the isolated tail rotor broadband noise levels are compared to those of the combined main rotor and tail rotor. For microphone 1 the isolated tail rotor humps (figure 22(a)) are of the same amplitude as the combined configuration (figure 22(b)). For microphone 9 the isolated tail rotor signal (figure 23(a)) is of the same or greater amplitude than the corresponding combined rotor signal (figure 23(b)). As for microphone 1, the tail rotor humps are not evident in the combined rotor signal.

Spectral characteristics of main and tail rotor contributions to total signal. The narrowband spectra of the combined configuration were compared with those of the isolated main and the isolated tail rotor. The general results will be discussed for microphones 1, 2, 3, 4, 7 and 10.

Microphone 1 (under main rotor advancing side). The midfrequency spectral range is dominated by main rotor BVI harmonics for the positive α_{TPP} cases (descent), as shown for a typical descent condition in figure 24(a). At negative α_{TPP} (level flight or ascent), when main rotor BVI is not strong, the tail rotor harmonics dominate the spectra, as shown for a typical ascent condition in figure 24(b). For all α_{TPP}, at higher frequencies, the tail rotor broadband humps dominate the spectra. For a given α_{TPP}, the broadband humps have higher levels for the low tail rotor position than for the high tail rotor position. This can be seen by comparing the spectrum of figure 24(a) (low tail rotor position, highest "hump" level about 85 dB) with the spectrum in figure 25 (high tail rotor position, highest "hump" level about 80 dB). This is the same result as was found for the isolated tail rotor.

The first four tail rotor harmonics have higher levels for the high tail rotor position than for the low position. These harmonics and the broadband humps have lower levels in the combined configuration than in isolation. An example is shown in figure 25 where the spectra from both the combined and isolated tail rotor configurations are plotted.

Microphone 2 (downstream of main rotor retreating side). As for microphone 1, the main rotor BVI harmonics bury the tail rotor harmonics at high BVI conditions (positive α_{TPP}). The tail rotor harmonics dominate at low BVI conditions (negative α_{TPP}). The main rotor BVI content at this location is attributed to interactions on the retreating side. At the higher frequencies, the tail rotor broadband humps have much higher levels (nearly 10 dB) than the main rotor content. This is shown in the isolated main rotor spectrum of figure 26, a low main rotor BVI condition. This broadband content is slightly influenced by position behind the main rotor (low or high), and in general is not altered by the presence of the main rotor. The broadband part of the spectra from the isolated tail rotor and combined rotor configurations are almost identical, as shown in figure 26.

As was seen for microphone 1, the first four tail rotor harmonics have higher levels for the high tail rotor position than for the low position.

Microphone 3 (under main rotor retreating side). The main rotor fundamental frequency is the dominant component at this location. It is on the order of 10 dB higher than any other harmonic. There are very few higher harmonics and little evidence of midfrequency BVI harmonics. Typical spectra from the combined rotors and isolated main rotor are shown in figure 27. The main rotor fundamental is at least 30 dB higher than the broadband noise and 15 dB higher than the first few tail rotor harmonics. Both the tail rotor harmonics and broadband noise components are 10 to 15 dB higher than the isolated

main rotor signal. In summary, the main rotor noise dominates the lowest frequencies and the tail rotor noise dominates the higher frequencies, but at a much lower level (15 to 30 dB down).

Figures 28(a) and (b) display spectra from both the combined rotors and isolated tail rotor configurations, for a low and high tail rotor position, respectively. In general, for the low tail rotor position (figure 28(a)), the broadband humps are lower in the combined rotor configuration than in the isolated tail rotor configuration. For the high tail rotor position (figure 28(b)), the broadband humps are about the same in both rotor configurations. This suggests than in the low tail position the main rotor wake interacts with the tail rotor and tends to decrease the levels of the tail rotor harmonics and broadband humps.

The advance ratio also plays a role when the main rotor wake interacts with the tail rotor. At all the advance ratios considered, the sum of the first four tail rotor harmonics is highest for the high tail position than for the low tail position. At the higher advance ratios of .140 and .186, the broadband noise and humps are also highest for the high tail position. At the lower advance ratio of .115, the broadband noise and humps are highest for the low tail position. Apparently the tail rotor is less influenced by the main rotor wake in the high position at high advance ratios and in the low position at low advance ratios.

The character of the broadband humps is also dependent on the advance ratio. For the spectra from the combined rotor configuration, at the lower advance ratios, $\mu \leq .14$, the broadband humps are more defined for the low tail rotor position than the high tail rotor position, see figure 29(a). At the higher advance ratio of .186, the broadband humps are more defined for the high tail rotor position, see figure 29(b). Note that the broadband humps in the isolated tail rotor spectra for the same operating conditions are about equally defined, compare the isolated tail rotor signals in figures 28(a) and (b). Thus the effect of the main rotor wake can be seen by comparing the combined rotor data. In general the tail rotor signal is least affected by the main rotor wake in the high position at high advance ratios and in the low position at low advance ratios.

Microphone 4 (downstream of the main rotor advancing side). This location measures very little midfrequency main rotor BVI. The tail rotor harmonics dominate the main rotor signal at low frequencies, and the tail rotor broadband noise dominates the higher frequencies, see figure 30. The broadband noise spectra here are not as humped as at other locations, see the data of location 1 for the same test condition, figure 24(b). The tail rotor broadband noise and first harmonic from the isolated tail rotor configuration are up to 10 dB higher than those from the combined rotors. This is independent of the tail rotor position behind the main rotor (low or high). Thus the presence of the main rotor decreases the tail rotor broadband content and first tail rotor harmonic. A typical example of this is shown in figure 31, showing the spectra from both the isolated tail rotor and combined rotor configuration.

Microphone 7 (upstream, in the flight path). At this location, as well as at the other traversing array microphones which are upstream and somewhat out of the main rotor plane, the signal is almost totally dominated by the main rotor signal, at all frequencies. Figure 32(a) presents spectra from the isolated main rotor and combined rotor configurations, while figure 32(b) presents spectra from the isolated tail rotor and combined config-

urations. The spectra of the isolated main rotor and the combined rotor configuration are almost identical at all frequencies. The spectra from the isolated tail rotor configuration is up to 10 dB lower than that spectrum from the combined rotor configuration.

The main rotor midfrequency content is stronger than the tail rotor harmonics at both conditions of low (figure 32) and high (figure 33) main rotor BVI. The main rotor broadband noise is also stronger than the tail rotor broadband noise.

Microphone 10 (upstream, nearly in the main rotor plane). The midfrequencies at this location is dominated by the main rotor BVI at high BVI conditions, and dominated by the tail rotor harmonics at low BVI conditions. This is independent of tail position (high or low). Typical spectra for the low tail rotor position are shown in figures 34 and 35, at a high and low main rotor BVI condition respectively.

Summary and Conclusions

Acoustic data from a model scale main rotor and tail rotor noise experiment in the NASA Langley 14 by 22 Foot Subsonic Tunnel are presented. Results are presented for the main rotor and tail rotor in isolation, and for the two rotors operating together for a range of moderate flight speed conditions.

The following conclusions were reached from the isolated main rotor acoustic data:

(1) A comparison of the main rotor spectra measured at the same tip-path-plane angle, but with and without longitudinal flapping, showed significant differences (up to 5 dB) in the midfrequency harmonic content.

(2) The level of the main rotor fundamental frequency and the sum of the first four harmonics are several dB higher directly under and downstream of the retreating side than at a symmetric position under the advancing side. At the low to moderate speeds tested, these low frequencies are attributed to loading noise.

(3) Higher levels of the midfrequency harmonics are measured directly under the advancing side than at a symmetric position under the retreating side. This content is attributed to advancing side BVI.

(4) Higher levels of the midfrequency harmonics are measured under and downstream of the retreating side than at a symmetric position under the advancing side. This harmonic content is attributed to retreating side BVI.

The following conclusions were reached regarding the isolated tail rotor acoustic data:

(1) The tail rotor overall sound level generally increases with velocity. This increase is attributed to increasing thickness noise with velocity.

(2) The tail rotor overall sound level and low frequency harmonic levels are higher when measured in the thrusting direction than at a symmetric position in the non-thrusting direction. This increase is attributed to the directivity of loading noise.

(3) The higher harmonics eventually broaden into broadband noise "humps" which are attributed to fuselage wake turbulence.

(4) The onset of the harmonic broadening occurs at a lower frequency for the out-of-plane locations than at other locations.

(5) The center frequencies of the harmonic humps occur at same frequencies at all the in-plane microphones but at slightly higher frequencies at the out-of-plane microphones.

(6) The broadband noise is lowest at in-plane locations and increases as locations move out-of-plane, and is highest in the thrusting direction.

The following conclusions were reached from the combined main rotor/tail rotor acoustic data:

(1) The overall acoustic levels at all measurement locations were dominated by the first four main rotor harmonics. The first four tail rotor harmonic levels are a small contribution to the overall sound levels.

(2) Acoustic measurements made directly under the advancing side, directly under the retreating side, and downstream of the advancing side, exhibited the largest contribution of the tail rotor noise to the overall noise levels.

(3) The main and tail rotor harmonic levels, as well as the tail rotor broadband noise, are often lower than those measured for each rotor in isolation.

(4) The main rotor harmonics and main rotor BVI dominate the spectrum for locations upstream along the flight path.

(5) The tail rotor harmonics and tail rotor broadband noise dominate the spectrum at locations downstream and to the sides of the vehicle.

(6) For a location directly under the advancing side, in descent modes, the acoustic signal is dominated by main rotor BVI. In level flight, the main and tail rotor signals are about equal. At high frequencies, at all flight conditions, the acoustic signal is dominated by tail rotor broadband noise.

(7) For a location directly under the retreating side, at all flight conditions, the acoustic signal is completely dominated by tail rotor harmonics and tail rotor broadband noise.

References

1. Wills, C. R.; and Leverton, J. W.: Reversed Direction Tail Rotor Lynx Burble Noise Investigation–Test Report. Westland Helicopters, AA1115, June 1975.

2. Leverton, J. W.; Pollard, J. S.; and Wills, C. R.: Main Rotor Wake/Tail Rotor Interaction. Vertica, 1977, Vol. 1, pp. 213-221.

3. Leverton, J. W.: Reduction of Helicopter Noise by the Use of a Quiet Tail Rotor. Paper No. 24, Sixth European Rotorcraft and Powered Lift Forum, Bristol, England, 1980.

4. Laudien, E.: Main and Tail Rotor Interaction Noise During Hover and Low Speed Conditions. Paper No. 18, Second European Rotorcraft and Powered Lift Aircraft Forum, September 20-22, 1976, Buckeburg, Federal Republic of Germany.

5. Balcerak, J. C.: Parametric Study of the Noise Produced by the Interaction of the Main Rotor Wake with the Tail Rotor. NASA CR-145001, 1976.

6. White, R. P.; Balcerak, J. C.; and Pegg, R. J.: A Parametric Model Study of the Noise Generated by the Aerodynamic Interaction of the Tail Rotor with the Wake of the Main Rotor. Presented at the 1976 Annual Forum of the American Helicopter Society.

7. Pegg, R. J.; and Shidler, P. A.: Exploratory Wind Tunnel Investigation of the Effect of the Main Rotor Wake on Tail Rotor Noise. NASA CP-2052, 1978.

8. Schlinker, R. H.; and Amiet, R. K.: Tail Rotor Blade-Vortex Interaction Noise. AIAA 83-0720.

9. George, A. R.; and Chou, S.-T.: A Comparative Study of Tail Rotor Noise Mechanisms. Presented at the 41st Annual Forum of the American Helicopter Society, Fort

Worth, Texas, May 15-17, 1985.

10. Chou, S.-T.; and George, A. R.: Progress in Tail Rotor Analysis. Presented at the 42nd Annual Forum of the American Helicopter Society, Arlington, Virginia, June 2-4, 1986.

11. Hoad, Danny R.; Elliott, Joe W.; and Orie, Nettie M.: Rotor Performance Characteristics From an Aeroacoustic Helicopter Wind-Tunnel Test Program. NASA TM-87661, 1986.

12. Martin, R. M.; and Connor, A. B.: Wind-Tunnel Acoustic Results of Two Rotor Models With Several Tip Designs. NASA TM-87698, 1986.

13. Martin, R. M.; Elliott, J. W.; and Hoad, D. R.: Comparison of Experimental and Analytical Predictions of Rotor Blade-Vortex Interactions using Model Scale Acoustic Data. AIAA-84-2269.

14. Shenoy, K. R.: The Role of Scale Models in the Design of "Low BVI Noise" Rotorcraft. Presented at the 41st Annual Forum of the American Helicopter Society, May, 1985.

15. Jacobs, E.W. and Shenoy, K.R.: Acoustic Characteristics of Tail Rotors and the Effects of Empennage Interactions. Presented at the 43rd Annual Forum of the American Helicopter Society, May, 1987.

16. Fitzgerald, J. and Kohlhepp, F.: Research Investigation of Helicopter Main/Tail Rotor Interaction Noise. NASA CR-4143, May, 1988.

17. Hayden, R. E.; and Wilby, J. F. : Sources, Paths and Concepts for Reductions of Noise in the Test Section of the NASA Langley 4- by 7-m Wind Tunnel. NASA CR-172446-2, September, 1984.

18. Yu, J. C.; and Abrahamson, A. L.: Acoustic Treatment of the NASA 4- by 7-M Wind Tunnel: a Feasibility Study. NASA TP-2563, 1986.

19. Jepson, D.; Moffitt, R.; Hilzinger, K.; and Bissell, J.: Analysis and Correlation of Test Data From an Advanced Technology Rotor System. NASA CR-3714, August 1983.

20. Heyson, Harry H.: Use of Superposition of Digital Computers to Obtain Wind-Tunnel Interference Factors for Arbitrary Configurations with Particular Reference to V/STOL Models. NASA TR-302, 1969.

21. Martin, R. M.; and Burley, C. L.: Evaluation of the Power Cepstrum Technique with Application to Model Rotor Acoustic Data. NASA TP-2586, 1986.

22. Miles, J.H.; Stevens, G. H.; and Leininger, G.G.; Analysis and Correction of Ground Reflection Effects in Measured Narrowband Sound Spectra Using Cepstral Techniques. NASA TM X-71810, 1975.

23. Syed, A.A.; Brown, J. D. ; Oliver, M. J.; and Hills, S. A.: The Cepstrum: A Viable Method for the Removal of Ground Reflections. J. Sound and Vibration, Vol. 71, No. 2, July 22, 1980, pp. 299-313.

24. Martin, R.M.; Splettstoesser, W.R.; Elliott, J.W.; and Schultz, K.-J.: Advancing Side Directivity and Retreating Side Interactions of Model Rotor Blade-Vortex Interaction Noise. NASA TP-2784, 1988.

25. Glegg, S.L.A.: The Prediction of Helicopter Tail Rotor Noise on the Flight Path. AIAA-87-2747, 11th AIAA Aeroacoustics Conference, Sunnyvale, CA, October 19-21, 1987.

Table 1. Test Matrix

MR C_T	V, kts	μ	α_{tpp}, deg.	α_s, deg.	MT T_{TR},lb	T T_{TR},lb	TR pos.	Comments
.0070	50	.115	5.0	9.0	15.6	13.6	low	moderate MR BVI
			4.9*	1.0	13.7	12.9	high	moderate MR BVI
			-2.1*	2.0	19.2	20.2	low	low MR BVI
			-2.0*	-6.0	17.6	18.1	high	low MR BVI
	60	.140	6.1*	10.0	10.3	11.6	low	high MR BVI
			5.7	2.0	8.9	10.9	high	high MR BVI
			-1.8*	2.0	16.2	17.5	low	low MR BVI
			-1.9	-6.0	16.5	19.0	high	low MR BVI
	70	.161	-1.9*	2.0	17.1	19.1	low	low MR BVI
			-2.0*	-6.0	15.4	17.3	high	low MR BVI
	80	.186	2.0*	6.0	10.9	11.2	low	high MR BVI
			2.1	-2.0	11.2	14.2	high	high MR BVI
			-2.0*	2.0	14.4	15.8	low	low MR BVI
			-2.0	-6.0	19.9	5.7	high	low MR BVI
.0085	50	.115	4.9	1.0	22.5	18.4	high	compare with .0070 data
			-2.1*	-6.0	27.1	26.1	high	
.0075	50	.115	-2.0	0.4	†	20.5	N/A	typical level flight
.0071	70	.161	-2.5	0.9	14.1	16.4		
.0074	80	.186	-3.0	1.1	18.0	21.0		
.0072	50	.115	4.1	5.7	15.1	13.6		typical descent
.0073	60	.140	4.1*	5.8	12.1	12.0		**
.0074	60	.140	2.8	0.5	†	15.9		
.0072	70	.161	3.6	6.2	9.8	11.0		

* conditions where tail rotor thrust of MT and T configurations most closely match

** traversing microphone array set at x=7.3 ft instead of 8.3 ft

† not available

Table 2. Microphone locations
in Cartesian coordinates
for main rotor at zero pitch.

Microphone	x, ft	y, ft	z, ft
1	0.	-1.29	-3.37
2	-4.86	5.99	-3.49
3	0.13	1.29	-3.39
4	-5.80	-6.28	-3.44
5	8.31	2.84	-5.67
6	↓	1.00	↓
7	↓	-0.84	↓
8	↓	-2.68	↓
9	↓	-4.52	↓
10	10.39	-9.38	-0.03
TR hub	-5.67	-0.22	-0.58
MR hub	0.	0.	0.

Table 3. Change in radial distance r, polar angle θ and azimuth angle ψ with respect to main rotor hub at zero fuselage pitch.

α_s,	Microphone number									
deg.	1	2	3	4	5	6	7	8	9	10
						r, ft				
-6	3.61	9.49	3.63	10.17	11.56	11.25	11.23	11.52	12.08	14.06
-5	3.61	9.49	3.63	10.16	11.57	11.26	11.25	11.53	12.09	14.08
-4	3.61	9.48	3.63	10.15	11.58	11.27	11.26	11.55	12.11	14.09
-3	3.61	9.47	3.63	10.14	11.60	11.29	11.27	11.56	12.12	14.10
-2	3.61	9.46	3.63	10.13	11.61	11.30	11.29	11.57	12.13	14.11
-1	3.61	9.45	3.63	10.12	11.62	11.31	11.30	11.58	12.14	14.13
0	3.61	9.44	3.63	10.11	11.63	11.33	11.31	11.60	12.15	14.14
1	3.61	9.44	3.63	10.10	11.65	11.34	11.33	11.61	12.16	14.15
2	3.61	9.43	3.63	10.09	11.66	11.35	11.34	11.62	12.18	14.16
3	3.61	9.42	3.63	10.08	11.67	11.36	11.35	11.63	12.19	14.18
4	3.61	9.41	3.63	10.07	11.68	11.37	11.36	11.64	12.20	14.19
5	3.61	9.40	3.63	10.06	11.69	11.39	11.37	11.65	12.21	14.20
6	3.61	9.39	3.63	10.05	11.70	11.40	11.38	11.67	12.22	14.21
7	3.61	9.38	3.63	10.04	11.71	11.41	11.40	11.68	12.23	14.23
8	3.61	9.37	3.63	10.03	11.73	11.42	11.41	11.69	12.24	14.24
9	3.61	9.36	3.63	10.02	11.74	11.43	11.42	11.70	12.25	14.25
10	3.61	9.35	3.63	10.01	11.75	11.44	11.43	11.71	12.26	14.26
						θ, deg				
-6	69.	39.	69.	36.	36.	37.	37.	36.	34.	4.
-5	69.	38.	69.	35.	36.	38.	38.	37.	35.	4.
-4	69.	38.	69.	35.	37.	39.	39.	38.	36.	5.
-3	69.	37.	69.	34.	38.	40.	40.	38.	36.	6.
-2	69.	36.	69.	34.	39.	40.	41.	39.	37.	7.
-1	69.	36.	69.	33.	40.	41.	41.	40.	38.	7.
0	69.	35.	69.	32.	41.	42.	42.	41.	39.	8.
1	69.	35.	69.	32.	42.	43.	43.	42.	40.	9.
2	69.	34.	69.	31.	43.	44.	44.	43.	41.	10.
3	69.	33.	69.	30.	44.	45.	45.	44.	41.	10.
4	69.	33.	69.	30.	45.	46.	46.	45.	42.	11.
5	69.	32.	69.	29.	45.	47.	47.	46.	43.	12.
6	69.	32.	69.	28.	46.	48.	48.	47.	44.	12.
7	69.	31.	69.	28.	47.	49.	49.	47.	45.	13.
8	69.	30.	69.	27.	48.	50.	50.	48.	45.	14.
9	69.	30.	69.	26.	49.	51.	51.	49.	46.	15.
10	69.	29.	69.	26.	50.	52.	52.	50.	47.	15.
						ψ, deg				
-6	90.	306.	264.	50.	198.	186.	175.	163.	153.	138.
-5	90.	307.	264.	49.	198.	186.	175.	163.	153.	138.
-4	90.	307.	264.	49.	198.	187.	175.	163.	153.	138.
-3	90.	308.	264.	48.	198.	187.	174.	163.	152.	138.
-2	90.	308.	264.	48.	198.	187.	174.	163.	152.	138.
-1	90.	309.	264.	48.	199.	187.	174.	162.	152.	138.
0	90.	309.	264.	47.	199.	187.	174.	162.	151.	138.
1	90.	309.	264.	47.	199.	187.	174.	162.	151.	138.
2	90.	310.	264.	47.	199.	187.	174.	162.	151.	138.
3	90.	310.	264.	46.	200.	187.	174.	161.	150.	138.
4	90.	311.	264.	46.	200.	187.	174.	161.	150.	138.
5	90.	311.	264.	46.	200.	187.	174.	161.	150.	138.
6	90.	312.	264.	45.	201.	188.	174.	161.	149.	137.
7	90.	312.	264.	45.	201.	188.	174.	160.	149.	137.
8	90.	312.	264.	45.	201.	188.	173.	160.	148.	137.
9	90.	313.	264.	44.	202.	188.	173.	159.	148.	137.
10	90.	313.	264.	44.	202.	188.	173.	159.	147.	137.

Table 4. Change in radial distance r, polar angle θ and azimuth angle ψ with respect to tail rotor hub at zero fuselage pitch.

α_s, deg.	Microphone number 1	2	3	4	5	6	7	8	9	10
					r, ft					
-6	6.41	7.17	6.62	6.98	15.33	15.07	15.04	15.22	15.63	18.43
-5	6.41	7.12	6.62	6.93	15.31	15.05	15.01	15.20	15.61	18.44
-4	6.41	7.08	6.62	6.88	15.29	15.03	14.99	15.18	15.58	18.45
-3	6.41	7.03	6.62	6.83	15.26	15.00	14.97	15.16	15.56	18.47
-2	6.41	6.99	6.62	6.79	15.24	14.98	14.94	15.13	15.54	18.48
-1	6.41	6.95	6.62	6.75	15.22	14.95	14.92	15.11	15.51	18.49
0	6.41	6.91	6.62	6.70	15.19	14.93	14.89	15.08	15.49	18.50
1	6.41	6.87	6.62	6.66	15.16	14.90	14.86	15.05	15.46	18.51
2	6.41	6.83	6.62	6.62	15.13	14.87	14.83	15.02	15.43	18.51
3	6.41	6.79	6.62	6.58	15.10	14.84	14.80	14.99	15.40	18.52
4	6.41	6.75	6.62	6.54	15.07	14.81	14.77	14.96	15.37	18.53
5	6.41	6.71	6.62	6.51	15.04	14.78	14.74	14.93	15.34	18.53
6	6.41	6.68	6.62	6.47	15.01	14.75	14.71	14.90	15.31	18.53
7	6.41	6.64	6.62	6.44	14.98	14.71	14.67	14.87	15.28	18.54
8	6.41	6.61	6.62	6.40	14.94	14.68	14.64	14.83	15.24	18.54
9	6.41	6.58	6.62	6.37	14.91	14.64	14.60	14.80	15.21	18.54
10	6.41	6.55	6.62	6.34	14.87	14.60	14.57	14.76	15.17	18.54
					θ, deg					
-6.	10.	-60.	-13.	60.	-12.	-5.	2.	9.	16.	30.
-5.	10.	-61.	-13.	61.	-12.	-5.	2.	9.	16.	30.
-4.	10.	-61.	-13.	62.	-12.	-5.	2.	9.	16.	30.
-3.	10.	-62.	-13.	62.	-12.	-5.	2.	9.	16.	30.
-2.	10.	-63.	-13.	63.	-12.	-5.	2.	9.	16.	30.
-1.	10.	-63.	-13.	64.	-12.	-5.	2.	9.	16.	30.
0.	10.	-64.	-13.	65.	-12.	-5.	2.	9.	16.	30.
1.	10.	-65.	-13.	65.	-12.	-5.	2.	9.	16.	30.
2.	10.	-65.	-13.	66.	-12.	-5.	2.	9.	16.	30.
3.	10.	-66.	-13.	67.	-12.	-5.	2.	9.	16.	30.
4.	10.	-67.	-13.	68.	-12.	-5.	2.	9.	16.	30.
5.	10.	-68.	-13.	69.	-12.	-5.	2.	9.	16.	30.
6.	10.	-68.	-13.	69.	-12.	-5.	2.	10.	16.	30.
7.	10.	-69.	-13.	70.	-12.	-5.	2.	10.	16.	30.
8.	10.	-70.	-13.	71.	-12.	-5.	2.	10.	16.	30.
9.	10.	-71.	-13.	72.	-12.	-5.	2.	10.	16.	30.
10.	10.	-72.	-13.	73.	-12.	-5.	2.	10.	16.	30.
					ψ, deg					
-6.	206.	342.	206.	357.	196.	196.	196.	196.	196.	174.
-5.	206.	343.	206.	358.	197.	197.	197.	197.	197.	175.
-4.	206.	343.	206.	359.	197.	197.	197.	197.	197.	175.
-3.	206.	343.	206.	360.	198.	198.	198.	198.	198.	176.
-2.	206.	344.	206.	1.	199.	199.	199.	199.	199.	177.
-1.	206.	344.	206.	2.	199.	199.	199.	199.	199.	177.
0.	206.	344.	206.	3.	200.	200.	200.	200.	200.	178.
1.	206.	345.	206.	4.	201.	201.	201.	201.	201.	179.
2.	206.	345.	206.	5.	201.	201.	201.	201.	201.	179.
3.	206.	346.	206.	6.	202.	202.	202.	202.	202.	180.
4.	206.	346.	206.	7.	203.	203.	203.	203.	203.	181.
5.	206.	346.	206.	8.	203.	203.	203.	203.	203.	181.
6.	206.	346.	206.	9.	204.	204.	204.	204.	204.	182.
7.	206.	347.	206.	10.	204.	204.	204.	204.	204.	183.
8.	206.	347.	206.	11.	205.	205.	205.	205.	205.	183.
9.	206.	347.	206.	13.	206.	206.	206.	206.	206.	184.
10.	206.	348.	206.	14.	206.	206.	206.	206.	206.	185.

Table 5. Estimated acoustic reflection amplitudes and delay times for each microphone.

Microphone number	Delay time, sec.	Relative Amplitude of the reflection	dB below direct wave
1	.006151	*	*
2	.005813		
3	.006036		
4	.005950		
5	.001988	0.44	7.1
6	.002030	0.55	5.2
7	.002070	0.58	4.7
8	.002003	0.71	3.0
9	.001951	0.62	4.2
10	.004310	0.31	10.2

* not available from data as recorded

Table 6. Overall sound pressure level (OASPL) in dB for combined configuration (MT), isolated main rotor (M) and isolated tail rotor (T).

$C_{T_{MR}}$	V, kts	α_{tpp}, deg.	α_s, deg.	MT T_{TR},lb	T T_{TR},lb	TR pos.	config.	Microphone number 1	2	3	4	5	6	7	8	9	10
.0070	50	5	9	15.6	13.6	low	MT	117.	114.	116.	112.	106.	111.	109.	109.	110.	110.
							M	117.	111.	115.	111.	107.	109.	109.	109.	110.	109.
							T	111.	107.	104.	108.	92.	97.	97.	95.	97.	101.
			1*	13.6	12.9	high	MT	117.	114.	118.	111.	105.	110.	107.	108.	109.	109.
							M	116.	112.	118.	109.	104.	106.	106.	107.	109.	107.
							T	110.	106.	108.	108.	95.	96.	98.	97.	99.	100.
		-2	2*	19.2	20.2	low	MT	115.	114.	120.	114.	107.	111.	107.	109.	111.	109.
							M	114.	113.	119.	113.	107.	108.	107.	108.	110.	107.
							T	111.	109.	110.	111.	98.	98.	98.	99.	99.	102.
			-6*	17.6	18.1	high	MT	113.	114.	120.	113.	109.	112.	108.	108.	110.	110.
							M	112.	113.	120.	111.	109.	110.	109.	108.	110.	107.
							T	110.	105.	109.	107.	98.	97.	99.	99.	100.	100.
	60	6	10*	10.3	11.6	low	MT	117.	112.	114.	112.	107.	113.	110.	111.	111.	113.
							M	118.	110.	112.	111.	108.	110.	110.	111.	111.	111.
							T	112.	107.	104.	108.	95.	97.	99.	96.	98.	102.
			2	8.9	10.9	high	MT	117.	113.	116.	111.	105.	111.	109.	110.	110.	110.
							M	118.	112.	115.	108.	105.	108.	109.	110.	110.	110.
							T	113.	111.	111.	111.	100.	100.	101.	101.	103.	104.
		-2	2*	16.2	17.5	low	MT	115.	114.	119.	113.	105.	109.	106.	108.	110.	109.
							M	114.	113.	118.	110.	102.	105.	105.	107.	109.	107.
							T	112.	109.	110.	111.	99.	100.	100.	100.	100.	103.
			-6	16.5	19.0	high	MT	114.	114.	120.	112.	107.	111.	106.	107.	108.	109.
							M	114.	112.	119.	108.	106.	107.	107.	107.	109.	106.
							T	111.	107.	109.	108.	100.	99.	101.	101.	101.	102.
	70	-2	2*	17.1	19.1	low	MT	116.	112.	117.	112.	104.	107.	107.	109.	110.	110.
							M	115.	110.	116.	110.	106.	108.	107.	109.	110.	108.
							T	114.	110.	111.	112.	99.	101.	100.	101.	102.	104.
			-6*	15.4	17.3	high	MT	115.	114.	118.	113.	105.	107.	106.	107.	109.	108.
							M	115.	110.	116.	108.	105.	107.	107.	109.	110.	108.
							T	112.	108.	110.	109.	100.	99.	101.	102.	102.	103.
	80	2	6*	10.9	11.2	low	MT	120.	113.	114.	113.	109.	111.	111.	113.	114.	112.
							M	119.	113.	112.	111.	108.	111.	111.	113.	113.	112.
							T	113.	110.	108.	111.	99.	102.	102.	101.	103.	104.
			-2	11.2	14.2	high	MT	120.	113.	117.	111.	109.	111.	112.	113.	113.	112.
							M	120.	113.	116.	110.	109.	111.	111.	113.	113.	112.
							T	114.	109.	111.	111.	100.	101.	101.	102.	104.	105.
		-2	2*	14.4	15.8	low	MT	118.	112.	116.	112.	108.	110.	110.	112.	113.	109.
							M	117.	116.	115.	110.	107.	109.	110.	112.	113.	110.
							T	115.	110.	111.	112.	99.	102.	101.	102.	104.	105.
			-6	19.9	5.7	high	MT	116.	114.	118.	113.	107.	108.	108.	109.	110.	108.
							M	116.	111.	116.	107.	107.	109.	109.	110.	111.	109.
							T	114.	109.	112.	111.	100.	101.	101.	103.	104.	105.
.0085	50	5	1	22.5	18.4	high	MT	118.	116.	121.	113.	109.	113.	110.	111.	113.	112.
							M	117.	113.	121.	111.	110.	111.	110.	111.	113.	108.
							T	111.	108.	111.	110.	98.	98.	98.	99.	100.	101.
		-2	-6*	27.1	26.1	high	MT	112.	116.	121.	114.	112.	115.	111.	111.	112.	111.
							M	110.	114.	120.	113.	112.	113.	111.	111.	112.	109.
							T	112.	108.	111.	109.	100.	99.	100.	101.	101.	102.

* conditions where tail rotor thrust of MT and T configurations most closely match

Table 7. First main rotor harmonic level (LM1) in dB for combined configuraton (MT) and isolated main rotor (M).

$C_{T_{MR}}$	V, kts	α_{tpp}, deg.	α_s, deg.	harmonic level	Microphone number 1	2	3	4	5	6	7	8	9	10
.0070	50	5	9	$LM1_{MT}$	106.	102.	114.	105.	96.	102.	99.	95.	85.	106.
				$LM1_M$	106.	101.	112.	104.	97.	100.	100.	97.	88.	106.
			1	$LM1_{MT}$	111.	105.	116.	104.	97.	103.	99.	96.	94.	104.
				$LM1_M$	110.	104.	116.	104.	97.	99.	97.	87.	91.	103.
		-2	2	$LM1_{MT}$	108.	107.	117.	103.	102.	103.	96.	98.	101.	104.
				$LM1_M$	108.	107.	117.	102.	102.	100.	96.	97.	99.	104.
			-6	$LM1_{MT}$	106.	108.	118.	104.	105.	108.	101.	95.	99.	102.
				$LM1_M$	105.	108.	117.	104.	106.	105.	101.	96.	100.	103.
	60	6	10	$LM1_{MT}$	104.	101.	109.	104.	102.	107.	103.	100.	99.	108.
				$LM1_M$	106.	101.	108.	104.	103.	105.	104.	101.	99.	108.
			2	$LM1_{MT}$	109.	103.	112.	103.	94.	101.	100.	97.	92.	106.
				$LM1_M$	111.	104.	111.	102.	95.	99.	101.	98.	95.	106.
		-2	2	$LM1_{MT}$	108.	105.	117.	102.	99.	99.	91.	99.	102.	102.
				$LM1_M$	109.	104.	116.	101.	91.	85.	82.	98.	99.	102.
			-6	$LM1_{MT}$	108.	105.	117.	103.	104.	107.	99.	93.	97.	100.
				$LM1_M$	110.	104.	117.	101.	101.	101.	98.	85.	95.	99.
	70	-2	2	$LM1_{MT}$	107.	102.	114.	102.	83.	87.	92.	98.	99.	104.
				$LM1_M$	107.	102.	114.	101.	84.	89.	92.	100.	100.	104.
			-6	$LM1_{MT}$	108.	103.	116.	103.	100.	101.	95.	84.	94.	100.
				$LM1_M$	111.	103.	114.	102.	94.	99.	99.	93.	85.	103.
	80	2	6	$LM1_{MT}$	108.	98.	110.	102.	103.	105.	104.	104.	103.	107.
				$LM1_M$	109.	101.	108.	102.	104.	106.	105.	104.	103.	109.
			-2	$LM1_{MT}$	109.	101.	113.	102.	92.	98.	100.	99.	96.	106.
				$LM1_M$	111.	101.	112.	103.	98.	102.	103.	103.	102.	109.
		-2	2	$LM1_{MT}$	102.	101.	113.	102.	94.	98.	98.	101.	103.	104.
				$LM1_M$	101.	106.	113.	101.	96.	99.	99.	103.	103.	105.
			-6	$LM1_{MT}$	108.	103.	115.	102.	100.	101.	95.	90.	93.	100.
				$LM1_M$	109.	102.	114.	101.	91.	96.	95.	93.	90.	105.
.0085	50	5	1	$LM1_{MT}$	111.	107.	118.	106.	103.	106.	101.	96.	99.	103.
				$LM1_M$	110.	107.	119.	104.	106.	106.	103.	98.	102.	101.
		-2	-6	$LM1_{MT}$	103.	110.	118.	105.	109.	111.	104.	97.	100.	105.
				$LM1_M$	103.	109.	118.	104.	109.	109.	104.	96.	99.	105.

Table 8. Sum of first 4 main rotor harmonic levels (LM4) in dB for both rotors (MT) and isolated main rotor (M).

$C_{T_{Mn}}$	V, kts	α_{tpp}, deg.	α_s, deg.	harmonic level	Microphone number 1	2	3	4	5	6	7	8	9	10
.0070	50	5	9	$LM4_{MT}$	113.	109.	114.	108.	102.	107.	104.	104.	106.	107.
				$LM4_M$	114.	108.	113.	108.	102.	104.	105.	105.	106.	107.
			1	$LM4_{MT}$	114.	110.	116.	107.	101.	106.	103.	103.	105.	105.
				$LM4_M$	113.	109.	116.	107.	101.	102.	102.	102.	105.	104.
		-2	2	$LM4_{MT}$	111.	111.	118.	111.	104.	108.	104.	105.	107.	106.
				$LM4_M$	112.	111.	117.	111.	105.	106.	104.	105.	107.	105.
			-6	$LM4_{MT}$	108.	111.	118.	110.	106.	110.	104.	103.	106.	106.
				$LM4_M$	108.	110.	118.	109.	107.	107.	105.	104.	106.	105.
	60	6	10	$LM4_{MT}$	111.	103.	110.	107.	103.	108.	105.	104.	103.	109.
				$LM4_M$	111.	102.	109.	107.	104.	105.	105.	104.	103.	108.
			2	$LM4_{MT}$	112.	107.	113.	105.	96.	103.	102.	102.	102.	107.
				$LM4_M$	113.	107.	112.	104.	98.	102.	103.	102.	102.	107.
		-2	2	$LM4_{MT}$	110.	111.	117.	109.	102.	106.	102.	104.	106.	105.
				$LM4_M$	111.	110.	116.	108.	99.	101.	98.	104.	105.	105.
			-6	$LM4_{MT}$	109.	110.	117.	107.	105.	108.	101.	100.	103.	104.
				$LM4_M$	111.	110.	117.	106.	103.	104.	102.	102.	104.	103.
	70	-2	2	$LM4_{MT}$	111.	108.	114.	108.	98.	102.	102.	104.	106.	106.
				$LM4_M$	111.	108.	114.	107.	96.	103.	102.	105.	106.	106.
			-6	$LM4_{MT}$	109.	109.	116.	107.	102.	103.	100.	98.	104.	103.
				$LM4_M$	113.	107.	115.	106.	99.	103.	103.	104.	106.	105.
	80	2	6	$LM4_{MT}$	113.	107.	111.	107.	104.	106.	106.	107.	107.	108.
				$LM4_M$	112.	107.	109.	107.	104.	107.	106.	106.	106.	110.
			-2	$LM4_{MT}$	113.	106.	114.	105.	98.	102.	104.	104.	103.	108.
				$LM4_M$	115.	105.	113.	106.	101.	104.	106.	106.	105.	109.
		-2	2	$LM4_{MT}$	111.	108.	114.	107.	100.	101.	102.	105.	107.	106.
				$LM4_M$	111.	113.	113.	107.	99.	102.	103.	106.	107.	107.
			-6	$LM4_{MT}$	109.	108.	116.	106.	102.	103.	101.	102.	104.	104.
				$LM4_M$	111.	108.	114.	104.	98.	100.	100.	101.	102.	107.
.0085	50	5	1	$LM4_{MT}$	114.	112.	119.	109.	105.	109.	105.	105.	107.	107.
				$LM4_M$	114.	111.	119.	109.	107.	108.	106.	105.	108.	104.
		-2	-6	$LM4_{MT}$	106.	112.	119.	111.	109.	113.	108.	108.	109.	107.
				$LM4_M$	106.	112.	118.	111.	110.	111.	108.	108.	109.	107.

Table 9. First tail rotor harmonic level (LT1) in dB
for combined configuration (MT) and isolated tail rotor (T).

$C_{T_{MR}}$	V, kts	α_{tpp}, deg.	α_s, deg.	MT T_{TR},lb.	T T_{TR},lb.	harmonic level	Microphone number 1	2	3	4	5	6	7	8	9	10
.0070	50	5	9	15.6	13.6	$LT1_{MT}$	99.	97.	95.	85.	84.	94.	91.	86.	86.	94.
						$LT1_T$	102.	97.	96.	96.	77.	93.	87.	76.	87.	94.
			1*	13.6	12.9	$LT1_{MT}$	100.	96.	100.	94.	89.	95.	90.	98.	99.	92.
						$LT1_T$	104.	97.	99.	101.	87.	92.	93.	85.	93.	92.
		-2	2*	19.2	20.2	$LT1_{MT}$	98.	97.	99.	92.	89.	96.	88.	86.	83.	92.
						$LT1_T$	104.	99.	101.	102.	89.	94.	92.	86.	92.	87.
			-6*	17.6	18.1	$LT1_{MT}$	101.	96.	103.	91.	92.	94.	92.	91.	88.	98.
						$LT1_T$	105.	96.	102.	99.	89.	93.	94.	90.	93.	93.
	60	6	10*	10.3	11.6	$LT1_{MT}$	100.	98.	93.	96.	81.	95.	93.	88.	90.	96.
						$LT1_T$	102.	95.	95.	93.	81.	92.	91.	87.	90.	95.
			2	8.9	10.9	$LT1_{MT}$	102.	95.	99.	95.	86.	94.	89.	89.	88.	92.
						$LT1_T$	105.	96.	99.	99.	87.	94.	95.	92.	95.	96.
		-2	2*	16.2	17.5	$LT1_{MT}$	102.	95.	99.	91.	85.	95.	89.	89.	92.	95.
						$LT1_T$	104.	98.	100.	100.	93.	96.	95.	91.	92.	95.
			-6	16.5	19.0	$LT1_{MT}$	102.	92.	102.	88.	90.	93.	92.	92.	91.	99.
						$LT1_T$	106.	98.	100.	96.	94.	95.	95.	94.	95.	97.
	70	-2	2*	17.1	19.1	$LT1_{MT}$	104.	94.	98.	95.	85.	95.	91.	90.	91.	95.
						$LT1_T$	106.	100.	99.	102.	90.	96.	94.	90.	93.	96.
			-6*	15.4	17.3	$LT1_{MT}$	102.	91.	100.	94.	88.	88.	91.	85.	89.	97.
						$LT1_T$	106.	100.	99.	99.	90.	93.	95.	93.	95.	97.
	80	2	6*	10.9	11.2	$LT1_{MT}$	104.	96.	99.	97.	81.	89.	93.	90.	89.	97.
						$LT1_T$	107.	97.	100.	99.	87.	94.	94.	91.	96.	99.
			-2	11.2	14.2	$LT1_{MT}$	105.	95.	97.	96.	83.	96.	94.	91.	96.	97.
						$LT1_T$	106.	99.	99.	100.	82.	95.	94.	92.	95.	97.
		-2	2*	14.4	15.8	$LT1_{MT}$	106.	91.	100.	95.	81.	95.	93.	90.	93.	96.
						$LT1_T$	107.	100.	101.	102.	86.	96.	95.	92.	95.	97.
			-6	19.9	5.7	$LT1_{MT}$	104.	94.	99.	93.	85.	89.	94.	85.	90.	98.
						$LT1_T$	108.	100.	101.	99.	88.	94.	96.	93.	95.	97.
.0085	50	5	1	22.5	18.4	$LT1_{MT}$	99.	98.	102.	98.	92.	97.	90.	92.	88.	95.
						$LT1_T$	104.	99.	101.	103.	88.	94.	92.	88.	93.	88.
		-2	-6*	27.1	26.1	$LT1_{MT}$	101.	97.	104.	93.	92.	95.	92.	90.	90.	99.
						$LT1_T$	106.	100.	105.	100.	92.	94.	95.	90.	94.	92.

* conditions where tail rotor thrust of MT and T configurations most closely match

Table 10. Sum of first four tail rotor harmonic levels (LT4) in dB for combined configuration (MT) and isolated tail rotor (T).

$C_{T_{MR}}$	V, kts	α_{tpp}, deg.	α_s, deg.	MT T_{TR},lb.	T T_{TR},lb.	harmonic level	Microphone number 1	2	3	4	5	6	7	8	9	10
.0070	50	5	9	15.6	13.6	$LT4_{MT}$	103.	100.	98.	93.	90.	97.	94.	92.	96.	95.
						$LT4_T$	104.	100.	98.	98.	85.	93.	91.	87.	92.	95.
			1*	13.6	12.9	$LT4_{MT}$	105.	99.	103.	96.	92.	97.	93.	99.	100.	93.
						$LT4_T$	106.	98.	101.	102.	89.	93.	94.	91.	95.	94.
		-2	2*	19.2	20.2	$LT4_{MT}$	101.	100.	101.	98.	90.	97.	90.	92.	91.	93.
						$LT4_T$	106.	101.	102.	104.	92.	95.	93.	92.	94.	94.
			-6*	17.6	18.1	$LT4_{MT}$	105.	100.	105.	95.	94.	97.	94.	97.	95.	99.
						$LT4_T$	106.	97.	103.	100.	91.	93.	95.	95.	96.	94.
	60	6	10*	10.3	11.6	$LT4_{MT}$	106.	101.	100.	100.	89.	100.	100.	100.	102.	100.
						$LT4_T$	105.	98.	98.	96.	90.	93.	94.	89.	93.	96.
			2	8.9	10.9	$LT4_{MT}$	105.	101.	102.	98.	90.	97.	95.	99.	101.	96.
						$LT4_T$	107.	99.	103.	100.	92.	95.	96.	95.	98.	97.
		-2	2*	16.2	17.5	$LT4_{MT}$	104.	98.	101.	96.	87.	97.	91.	92.	94.	95.
						$LT4_T$	107.	100.	101.	102.	94.	96.	95.	94.	95.	98.
			-6	16.5	19.0	$LT4_{MT}$	105.	99.	104.	95.	92.	94.	93.	97.	95.	99.
						$LT4_T$	107.	100.	102.	99.	95.	96.	96.	97.	97.	98.
	70	-2	2*	17.1	19.1	$LT4_{MT}$	106.	96.	102.	97.	90.	96.	94.	94.	96.	97.
						$LT4_T$	108.	102.	101.	103.	92.	97.	95.	94.	96.	98.
			-6*	15.4	17.3	$LT4_{MT}$	105.	100.	103.	98.	91.	92.	94.	94.	95.	98.
						$LT4_T$	108.	100.	102.	101.	93.	94.	96.	97.	97.	98.
	80	2	6*	10.9	11.2	$LT4_{MT}$	109.	99.	102.	99.	95.	98.	98.	102.	103.	99.
						$LT4_T$	108.	101.	101.	100.	89.	96.	96.	93.	97.	98.
			-2	11.2	14.2	$LT4_{MT}$	108.	100.	103.	99.	99.	97.	100.	102.	103.	98.
						$LT4_T$	110.	99.	102.	100.	90.	94.	96.	96.	99.	100.
		-2	2*	14.4	15.8	$LT4_{MT}$	109.	97.	104.	98.	98.	99.	99.	100.	100.	97.
						$LT4_T$	110.	101.	102.	102.	90.	96.	96.	94.	98.	99.
			-6	19.9	5.7	$LT4_{MT}$	106.	100.	102.	100.	91.	94.	97.	96.	96.	98.
						$LT4_T$	110.	101.	104.	102.	91.	95.	96.	98.	98.	99.
.0085	50	5	1	22.5	18.4	$LT4_{MT}$	105.	100.	104.	99.	94.	98.	96.	96.	98.	97.
						$LT4_T$	106.	100.	102.	104.	93.	94.	93.	92.	95.	94.
		-2	-6*	27.1	26.1	$LT4_{MT}$	104.	103.	105.	100.	95.	98.	95.	97.	95.	100.
						$LT4_T$	107.	101.	105.	102.	93.	95.	96.	96.	97.	94.

* conditions where tail rotor thrust of MT and T configuration most closely match

Table 11. Broadband levels between 560 Hz and 4600 Hz in dB (LTB_T) from the isolated tail rotor condition (T), corrected for spherical spreading

V, kts	α_s, deg.	T_{TR},lb	TR pos.	Microphone number 1	2	3	4	5	6	7	8	9	10
50	9	13.6	low	104.7	104.4	99.8	106.4	95.7	95.7	96.4	98.0	98.7	104.9
	1	12.9	high	101.8	103.9	103.1	105.4	97.8	96.2	96.0	99.1	99.3	104.1
	2	20.2	low	103.8	106.0	104.6	107.5	99.0	98.0	97.5	100.5	101.0	105.8
	-6	18.1	high	99.6	102.5	101.4	103.8	97.6	95.1	95.4	99.0	99.6	103.5
60	10	11.6	low	105.5	105.5	104.6	107.1	99.0	98.8	99.8	100.7	101.7	105.9
	2	10.9	high	105.7	104.7	98.8	107.0	97.0	97.6	99.1	99.1	99.7	105.8
	2	17.5	low	105.7	106.6	105.6	108.2	99.8	99.7	99.5	101.4	102.0	106.4
	-6	19.0	high	101.3	103.7	102.6	105.5	98.4	97.4	98.4	99.2	100.2	104.8
70	2	19.1	low	107.4	107.2	106.1	109.1	100.4	101.4	99.8	102.4	103.3	107.2
	-6	17.3	high	103.1	104.1	103.8	106.2	99.7	99.7	99.2	100.2	101.1	105.7
80	6	15.8	low	106.4	106.2	106.3	108.3	101.0	102.6	101.2	102.7	103.6	107.3
	-2	14.2	high	105.9	106.6	101.9	108.8	100.1	102.6	101.4	102.3	103.0	107.5
	2	11.2	low	108.0	107.4	105.9	109.3	101.2	103.2	101.4	103.4	104.5	107.3
	-6	5.7	high	105.0	105.7	105.8	107.6	101.2	102.1	100.7	102.4	103.3	107.1
50	1	18.4	high	103.5	105.7	104.9	107.1	99.7	97.9	97.3	100.6	100.9	105.2
	-6	26.1		102.2	104.6	104.2	106.2	100.0	97.6	96.9	101.5	101.8	106.3
50	.4	20.5	N/A	103.3	106.0	105.0	107.4	100.1	98.3	97.3	101.0	101.4	105.5
70	.9	16.4		106.2	106.3	105.6	108.3	100.0	100.8	99.1	101.7	102.6	106.5
80	1.1	21.0		109.1	108.3	107.5	110.1	102.0	103.7	101.8	104.2	105.2	107.9
50	5.7	13.6		103.3	104.5	101.3	106.4	97.6	96.3	96.4	99.7	100.8	105.0
60	5.8	12.0		104.0	104.7	101.1	106.7	96.8	97.1	98.8	98.8	99.4	105.5
60	.5	15.9		104.4	105.3	104.9	107.1	98.9	99.0	99.3	100.6	101.2	105.8
70	6.2	11.0		104.9	105.3	101.0	107.6	97.8	100.1	99.1	100.6	101.1	106.7

Table 12. Tone levels between 560 Hz and 4600 Hz (LTD_T) in dB from isolated tail rotor condition (T), corrected for spherical spreading.

V, kts	α_s, deg.	T_{TR},lb	TR pos.	Microphone number 1	2	3	4	5	6	7	8	9	10
50	9	13.6	low	103.4	100.5	98.1	99.8	95.2	94.6	97.8	97.5	100.8	100.6
	1	12.9	high	103.4	98.0	100.1	99.0	97.1	93.0	94.6	100.0	101.5	103.2
	2	20.2	low	103.4	101.0	100.0	103.0	100.0	92.5	95.0	101.3	100.7	105.3
	-6	18.1	high	102.6	96.7	99.5	99.3	97.2	94.9	96.6	103.0	102.3	101.1
60	10	11.6	low	107.3	106.5	106.1	101.9	103.1	100.7	99.8	103.1	105.4	107.8
	2	10.9	high	104.9	99.7	98.8	100.0	99.5	96.8	100.2	95.9	100.7	102.2
	2	17.5	low	105.6	102.5	100.4	103.0	99.0	94.3	97.4	101.3	102.0	106.3
	-6	19.0	high	104.0	100.1	102.6	102.0	100.0	99.4	98.5	103.7	103.7	101.4
70	2	19.1	low	106.9	102.9	101.0	103.7	99.6	98.5	98.8	101.5	103.5	105.6
	-6	17.3	high	106.2	100.2	103.3	102.3	100.4	96.9	99.4	105.0	103.3	103.1
80	6	11.2	low	108.7	102.4	103.7	102.4	99.8	98.9	101.0	104.9	106.7	106.8
	-2	14.2	high	107.3	103.3	101.7	102.3	100.1	101.1	101.1	99.2	101.5	104.6
	2	15.8	low	109.0	102.7	102.2	103.3	99.6	98.6	100.1	100.8	105.3	106.9
	-6	5.7	high	107.0	101.1	103.8	103.7	100.6	99.3	99.6	106.4	105.1	104.9
50	1	18.4	high	103.5	99.7	100.5	102.4	101.4	94.0	95.1	100.6	100.7	105.2
	-6	26.1		104.8	100.1	100.8	102.3	97.9	97.5	97.9	104.8	103.8	104.8
50	.4	20.5	N/A	103.1	100.4	100.2	103.5	101.5	93.4	94.3	100.3	101.4	105.2
70	.9	16.4		107.3	102.1	102.1	102.3	99.1	97.7	98.2	101.4	104.3	106.1
80	1.1	21.0		108.8	102.7	102.6	104.6	99.5	100.7	100.0	102.2	105.5	107.7
50	5.7	13.6		102.5	100.4	97.1	99.9	95.7	91.2	96.1	101.6	102.1	103.8
60	5.8	12.0		102.5	99.8	98.0	99.5	97.5	94.4	97.9	97.7	99.4	102.9
60	.5	15.9		105.5	102.2	101.3	101.4	98.4	95.8	97.5	102.2	102.9	105.7
70	6.2	11.0		105.8	102.4	101.5	101.1	99.3	99.7	101.9	96.6	102.0	103.8

Table 13. Difference between overall sound pressure level in dB of combined configuration (MT) with isolated main rotor (MT-M) and with isolated tail rotor (MT-T)

$C_{T_{MR}}$	V_t, kts,	α_{tpp}, deg.	α_s, deg.	MT T_{TR},lb	T T_{TR},lb	rotor config.	Microphone number 1	2	3	4	5	6	7	8	9	10
.0070	50	5	9	15.6	13.6	MT-M	0.0	2.6	1.6	1.5	-0.3	2.5	-0.1	-0.1	0.0	1.3
						MT-T	6.7	6.5	11.9	4.2	13.9	14.4	12.2	14.5	13.4	9.9
			1*	13.6	12.9	MT-M	1.0	2.5	0.3	1.9	1.0	4.5	1.6	1.6	0.6	1.9
						MT-T	7.3	7.8	10.4	3.0	9.8	13.8	9.1	11.1	10.4	9.0
		-2	2*	19.2	20.2	MT-M	0.1	1.5	0.6	1.7	0.1	3.4	0.0	0.7	0.4	1.7
						MT-T	3.5	5.7	9.2	3.8	9.2	12.9	8.9	10.1	11.2	7.5
			-6*	17.6	18.1	MT-M	1.5	1.2	0.5	1.4	-0.2	2.5	-0.3	0.0	-0.1	2.1
						MT-T	3.2	8.7	11.6	5.7	11.3	15.3	9.3	9.0	10.0	9.4
	60	6	10*	10.3	11.6	MT-M	-0.5	2.1	1.3	1.3	-0.7	2.9	0.2	0.0	0.1	1.4
						MT-T	5.8	5.4	9.8	3.9	11.9	15.7	11.2	15.2	12.8	10.9
			2	8.9	10.9	MT-M	-0.5	1.6	1.6	3.0	-0.4	2.7	-0.3	-0.1	-0.2	0.6
						MT-T	4.9	2.4	5.3	0.1	5.2	11.2	7.7	8.9	7.0	6.1
		-2	2*	16.2	17.5	MT-M	0.6	1.5	0.8	2.5	2.6	4.4	1.1	0.8	1.1	1.7
						MT-T	2.6	4.8	8.5	2.0	5.7	9.0	6.0	8.0	9.6	5.7
			-6	16.5	19.0	MT-M	-0.1	1.7	0.8	3.6	1.4	3.6	-0.8	-0.4	-1.0	2.4
						MT-T	3.1	6.7	10.3	3.3	7.1	11.5	5.5	5.9	6.6	6.3
	70	-2	2*	17.1	19.1	MT-M	0.4	1.8	0.8	2.1	-1.6	-0.3	0.0	-0.4	0.0	1.3
						MT-T	1.8	1.8	5.7	0.3	4.8	6.0	6.4	8.1	8.4	5.7
			-6*	15.4	17.3	MT-M	-0.5	3.7	2.0	4.3	0.7	-0.2	-1.4	-1.6	-1.1	0.3
						MT-T	2.7	5.9	8.6	3.4	5.8	7.7	5.0	5.6	6.8	4.8
	80	2	6*	10.9	11.2	MT-M	1.1	-0.3	1.8	1.4	0.3	0.0	0.2	0.1	0.4	-0.7
						MT-T	7.1	3.1	6.0	1.9	10.0	9.2	9.6	12.1	10.7	7.6
			-2	11.2	14.2	MT-M	-0.4	0.5	0.5	1.6	0.3	0.1	0.3	-0.1	0.1	-0.4
						MT-T	5.7	4.2	5.2	0.9	9.2	9.7	10.5	10.9	9.3	6.5
		-2	2*	14.4	15.8	MT-M	0.6	-4.2	1.3	2.4	0.6	0.7	0.0	-0.6	0.0	-0.2
						MT-T	2.7	1.9	5.1	0.4	8.5	8.0	8.6	9.9	8.9	4.7
			-6	19.9	5.7	MT-M	-0.1	3.3	2.1	6.2	0.0	-0.4	-1.2	-1.0	-0.6	-0.7
						MT-T	2.4	5.0	6.5	2.5	6.7	7.1	6.5	6.3	6.5	3.8
.0085	50	5	1	22.5	18.4	MT-M	0.9	2.5	0.2	1.7	-1.0	2.2	0.0	0.7	0.2	3.6
						MT-T	7.3	7.3	10.5	2.8	10.7	14.9	11.9	12.3	13.2	10.8
		-2	-6*	27.1	26.1	MT-M	2.2	1.5	0.7	1.1	-0.6	2.6	0.1	0.0	0.0	1.4
						MT-T	0.7	7.8	9.8	4.8	11.8	16.7	10.8	10.1	10.9	8.6

* conditions where tail rotor thrust of MT and T configuration most closely match

Table 14. Differences between first main rotor harmonic levels: level for both rotors ($LM1_{MT}$) minus level for isolated main rotor ($LM1_M$).

				$LM1_{MT}$ - $LM1_M$, dB									
$C_{T_{MR}}$	V, kts	α_{tpp}, deg.	α_s, deg.	Microphone number 1	2	3	4	5	6	7	8	9	10
.0070	50	5	9	-0.5	0.4	1.1	0.4	-1.1	2.2	-0.8	-2.0	-2.6	0.1
↓	↓	↓	1	1.4	0.3	-0.3	0.4	-0.5	4.2	2.6	8.1	2.5	1.0
		-2	2	-0.6	0.1	0.3	1.6	-0.3	2.5	0.8	1.4	2.0	0.1
	↓	↓	-6	0.8	0.1	0.3	0.7	-0.4	2.6	-0.4	-1.9	-1.1	-0.4
	60	6	10	-1.8	0.2	1.2	0.0	-1.5	1.9	-0.5	-0.1	-0.5	0.6
	↓	↓	2	-1.6	-0.8	1.3	0.6	-1.8	1.4	-1.5	-1.0	-2.5	-0.5
		-2	2	-1.2	1.2	0.4	0.6	7.8	14.3	9.4	0.7	2.9	-0.1
	↓	↓	-6	-2.5	1.2	0.3	1.3	2.8	5.4	0.7	8.0	2.2	0.4
	70	-2	2	-0.2	0.0	0.3	0.8	-1.4	-1.8	0.4	-2.3	-0.9	-0.2
	↓	↓	-6	-2.7	0.3	1.6	1.0	6.2	2.3	-3.7	-8.8	9.1	-3.5
	80	2	6	-0.9	-2.8	1.8	0.2	-0.7	-1.1	-1.1	-0.4	0.0	-2.1
	↓	↓	-2	-2.6	0.0	1.3	-1.2	-6.2	-4.2	-3.4	-3.8	-5.4	-2.3
		-2	2	0.7	-5.5	0.8	0.6	-1.8	-1.8	-1.0	-1.7	-0.2	-1.4
↓	↓	↓	-6	-1.7	1.4	1.8	0.8	8.8	4.7	0.3	-3.0	2.9	-4.6
.0085	50	5	1	0.3	0.6	-0.4	1.4	-3.0	0.0	-2.1	-2.1	-2.9	2.4
↓	↓	-2	-6	0.0	1.5	0.1	0.8	-0.8	2.3	0.1	1.4	1.4	0.1

Table 15. Difference between sum of first 4 main rotor harmonic levels: level for both rotors ($LM4_{MT}$) minus level for isolated main rotor ($LM4_{M}$).

				$LM4_{MT}$ - $LM4_{M}$, dB									
				Microphone number									
$C_{T_{MR}}$	V, kts	α_{tpp}, deg.	α_s, deg.	1	2	3	4	5	6	7	8	9	10
.0070	50	5	9	-0.3	1.3	1.2	0.2	-0.2	2.6	-0.2	-0.4	-0.1	0.5
↓	↓	↓	1	0.4	1.3	-0.3	0.1	-0.2	3.9	1.1	0.7	0.3	1.0
		-2	2	-0.9	0.3	0.3	0.4	-0.2	2.9	-0.5	0.1	0.0	0.8
		↓	-6	0.3	0.3	0.3	0.5	-0.2	2.5	-0.4	-0.5	-0.2	1.0
	60	6	10	-0.4	1.1	1.1	0.0	-1.2	2.4	-0.3	0.0	0.4	0.6
	↓	↓	2	-1.1	0.4	1.2	0.7	-1.3	1.7	-0.7	-0.1	0.2	0.1
		-2	2	-1.0	0.4	0.5	0.8	3.4	4.2	3.1	0.4	1.1	0.6
		↓	-6	-2.5	-0.2	0.3	1.4	1.8	3.9	-0.9	-1.5	-0.7	0.7
	70	-2	2	-0.9	0.3	0.2	0.2	1.9	-0.4	0.1	-0.9	-0.3	0.3
	↓	↓	-6	-3.4	1.5	1.3	1.2	2.4	-0.2	-2.9	-5.7	-1.8	-1.7
	80	2	6	-1.7	1.6	0.2	-1.1	-2.6	-1.8	-1.9	-2.1	-1.9	-1.4
	↓	↓	-2	0.7	0.2	1.8	0.5	-0.6	-1.0	-0.5	0.2	0.9	-1.7
		-2	2	-0.6	-5.2	0.7	0.6	0.3	-0.2	-0.2	-0.9	0.2	-1.1
		↓	-6	-2.0	0.7	1.8	2.4	4.4	3.3	1.0	1.1	1.6	-3.0
.0085	50	5	1	0.0	1.7	-0.3	0.1	-2.0	1.1	-1.0	-0.6	-0.9	2.3
↓	↓	-2	-6	-0.2	0.6	0.4	-0.2	-1.0	2.4	-0.4	-0.5	-0.2	0.4

Table 16. Differences between first tail rotor harmonic levels: level for both rotors ($LT1_{MT}$) minus level for isolated tail rotor ($LT1_T$).

						$LT1_{MT}$ - $LT1_T$, dB									
						Microphone number									
$C_{T_{MR}}$	V, kts	α_{tpp}, deg.	α_s, deg.	MT T_{TR},lb	T T_{TR},lb	1	2	3	4	5	6	7	8	9	10
.0070	50	5	9	15.6	13.6	-2.7	-0.3	-1.0	-11.0	7.5	0.9	3.2	10.2	-0.2	0.8
		↓	1*	13.6	12.9	-4.5	-1.0	1.2	-7.3	2.4	2.5	-2.9	13.1	6.2	0.6
		-2	2*	19.2	20.2	-6.2	-2.2	-2.0	-10.3	0.8	1.6	-4.8	-0.5	-8.8	4.8
	↓	↓	-6*	17.6	18.1	-3.8	-0.3	0.6	-7.6	2.4	1.3	-1.9	0.8	-5.2	5.5
	60	6	10*	10.3	11.6	-1.8	2.5	-1.9	2.7	-0.7	3.0	1.8	1.3	-0.3	1.1
		↓	2	8.9	10.9	-2.9	-0.7	0.1	-4.3	-1.0	0.1	-6.2	-3.7	-6.7	-3.7
		-2	2*	16.2	17.5	-2.2	-3.0	-0.7	-9.2	-8.1	-1.3	-5.6	-2.7	-0.7	0.6
	↓	↓	-6	16.5	19.0	-3.7	-6.2	1.4	-7.4	-4.6	-1.5	-3.6	-2.0	-3.7	2.0
	70	-2	2*	17.1	19.1	-2.1	-6.9	-1.4	-6.6	-5.9	-1.7	-2.8	-0.5	-2.6	-0.8
	↓	↓	-6*	15.4	17.3	-4.0	-8.7	1.7	-4.9	-1.8	-5.3	-3.8	-7.6	-5.7	0.0
	80	2	6*	10.9	11.2	-0.6	-4.2	-2.7	-3.5	0.7	0.7	-0.8	-0.8	0.5	0.5
		↓	-2	11.2	14.2	-3.1	-1.5	-0.9	-2.2	-6.4	-4.6	-1.2	-1.5	-6.8	-2.3
		-2	2*	14.4	15.8	-0.6	-8.3	-1.1	-6.5	-5.0	-0.6	-1.3	-1.6	-2.0	-1.0
	↓	↓	-6	19.9	5.7	-3.7	-5.5	-2.5	-6.6	-2.5	-5.4	-1.6	-7.7	-5.2	0.3
.0085	50	5	1	22.5	18.4	-5.7	-1.0	0.4	-4.8	4.5	2.7	-2.2	4.4	-4.3	7.1
↓	↓	-2	-6*	27.1	26.1	-5.2	-3.3	-0.9	-6.9	-0.2	1.3	-3.1	0.0	-3.3	7.0

* conditions where tail rotor thrust of MT and T configuration most closely match

Table 17. Differences between first 4 tail rotor harmonic levels: level for both rotors ($LT4_{MT}$) minus level for isolated tail rotor ($LT4_T$).

						$LT4_{MT}$ - $LT4_T$, dB									
						Microphone number									
$C_{T_{MT}}$	V, kts	α_{tpp}, deg.	α_s, deg.	MT T_{TR},lb	T T_{TR},lb	1	2	3	4	5	6	7	8	9	10
.0070	50	5	9	15.6	13.6	-1.7	0.2	0.3	-4.4	5.4	3.6	3.7	4.9	3.5	0.8
		↓	1*	13.6	12.9	-1.1	1.4	2.9	-5.8	2.2	4.2	-1.2	8.2	4.9	-1.2
		-2	2*	19.2	20.2	-4.9	-1.3	-1.2	-6.3	-1.7	2.0	-2.9	0.1	-2.9	-1.1
		↓	-6*	17.6	18.1	-1.0	2.8	1.7	-5.1	2.5	3.2	-0.3	2.1	-0.1	4.8
	60	6	10*	10.3	11.6	1.1	2.7	1.3	4.4	-1.2	7.7	6.0	11.6	8.2	3.6
		↓	2	8.9	10.9	-2.5	2.6	-0.3	-2.2	-1.6	2.3	-0.7	4.5	3.0	-1.0
		-2	2*	16.2	17.5	-2.6	-2.2	0.7	-6.1	-6.5	0.5	-3.7	-2.3	-0.9	-2.1
		↓	-6	16.5	19.0	-1.9	-0.5	1.8	-4.5	-3.2	-1.1	-2.9	-0.2	-2.4	1.9
	70	-2	2*	17.1	19.1	-1.9	-6.0	1.3	-6.3	-2.0	-0.3	-0.9	0.2	0.1	-0.9
	↓	↓	-6*	15.4	17.3	-3.3	-0.2	1.3	-2.9	-2.0	-1.3	-2.4	-3.3	-2.0	-0.3
	80	2	6*	10.9	11.2	0.7	-2.1	0.8	-1.2	5.7	1.8	1.7	9.4	6.4	1.1
		↓	-2	11.2	14.2	-1.6	0.8	0.7	-1.6	9.0	2.6	4.3	5.9	4.2	-2.1
		-2	2*	14.4	15.8	-0.8	-4.5	1.2	-4.7	8.2	3.0	3.4	6.7	1.5	-2.0
		↓	-6	19.9	5.7	-3.4	-0.5	-1.1	-1.3	0.9	-0.4	0.8	-2.1	-2.0	-0.2
.0085	50	5	1	22.5	18.4	-0.7	-0.5	2.3	-4.9	1.1	3.7	2.6	4.1	3.0	3.2
↓	↓	-2	-6*	27.1	26.1	-3.0	1.4	-0.1	-2.8	1.4	2.8	-1.3	0.9	-1.4	5.1

* conditions where tail rotor thrust of MT and T configuration most closely match

Table 18. Percent of LM4 and LT4 relative to the OASPL of combined configuration (MT) (percent of squared pressures).

$C_{T_{MR}}$	V, kts	α_{tpp}, deg.	α_s, deg.	MT T_{TR},lb	harmonic level	Microphone number 1	2	3	4	5	6	7	8	9	10
.0070	50	5	9	15.6	LM4	40.	37.	58.	40.	35.	35.	35.	32.	38.	47.
					LT4	3.	5.	2.	1.	3.	4.	3.	2.	3.	3.
			1*	13.6	LM4	47.	43.	56.	38.	35.	39.	40.	32.	40.	45.
					LT4	6.	3.	3.	3.	4.	5.	3.	12.	11.	3.
		-2	2*	19.2	LM4	44.	46.	63.	47.	55.	52.	46.	43.	48.	48.
					LT4	4.	3.	1.	2.	2.	3.	2.	2.	1.	3.
			-6*	17.6	LM4	30.	47.	62.	51.	56.	54.	41.	30.	38.	43.
					LT4	15.	4.	3.	2.	3.	3.	4.	8.	4.	8.
	60	6	10*	10.3	LM4	22.	12.	46.	30.	39.	29.	28.	19.	17.	42.
					LT4	8.	7.	4.	6.	2.	6.	9.	8.	11.	5.
			2	8.9	LM4	26.	23.	50.	28.	14.	18.	21.	16.	17.	46.
					LT4	6.	6.	4.	5.	3.	4.	4.	8.	12.	3.
		-2	2*	16.2	LM4	36.	44.	62.	42.	51.	43.	35.	39.	44.	45.
					LT4	9.	2.	2.	2.	2.	5.	3.	2.	3.	4.
			-6	16.5	LM4	31.	39.	59.	36.	54.	50.	35.	21.	33.	35.
					LT4	13.	3.	3.	2.	3.	2.	5.	10.	5.	12.
	70	-2	2*	17.1	LM4	32.	40.	56.	37.	27.	32.	30.	32.	36.	47.
					LT4	11.	2.	3.	3.	4.	8.	5.	3.	4.	5.
			-6*	15.4	LM4	28.	33.	56.	30.	43.	38.	27.	13.	30.	35.
					LT4	10.	5.	3.	4.	3.	3.	6.	5.	4.	9.
	80	2	6*	10.9	LM4	17.	25.	45.	27.	32.	29.	29.	22.	20.	41.
					LT4	8.	4.	6.	4.	4.	5.	4.	8.	9.	5.
			-2	11.2	LM4	21.	21.	50.	22.	8.	12.	15.	11.	9.	43.
					LT4	7.	5.	4.	5.	10.	4.	7.	8.	10.	4.
		-2	2	14.4	LM4	19.	39.	55.	33.	15.	13.	17.	23.	30.	45.
					LT4	13.	3.	5.	4.	10.	9.	8.	7.	5.	6.
			-6	19.9	LM4	21.	28.	56.	20.	31.	32.	22.	17.	25.	33.
					LT4	10.	4.	3.	5.	3.	4.	9.	5.	4.	10.
.0085	50	5	1	22.5	LM4	43.	47.	59.	40.	42.	39.	31.	22.	29.	30.
					LT4	5.	3.	2.	4.	3.	3.	4.	3.	3.	4.
		-2	-6*	27.1	LM4	22.	47.	60.	47.	59.	59.	51.	44.	46.	44.
					LT4	16.	5.	3.	4.	2.	2.	2.	4.	2.	8.

* conditions where tail rotor thrust of MT and T configuration most closely match

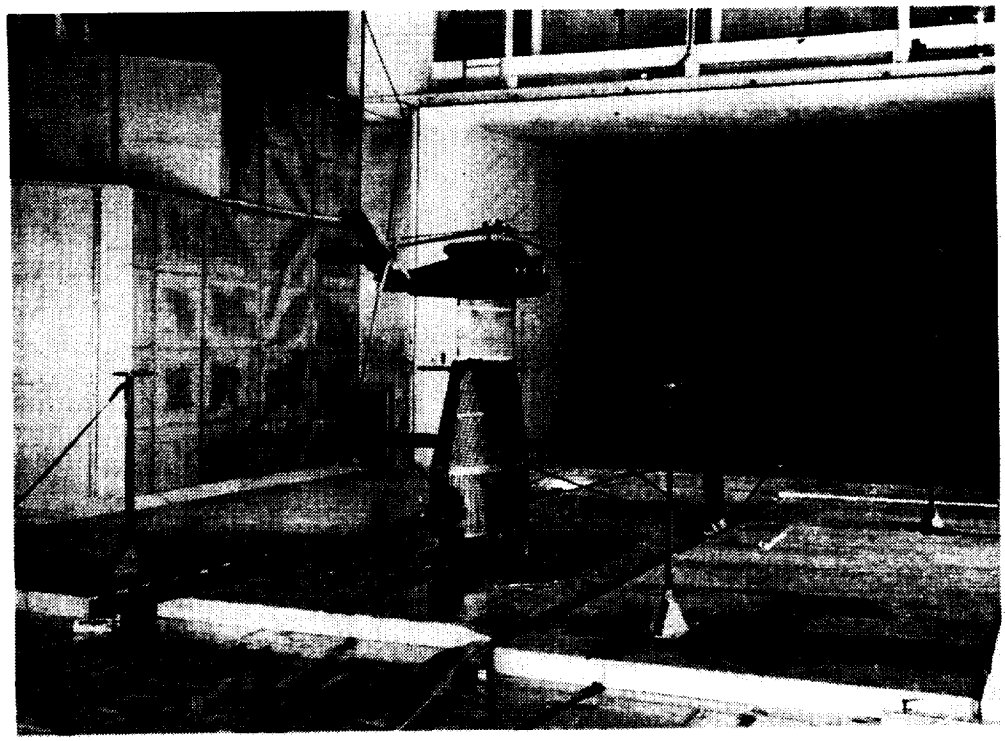

(a) view looking upstream

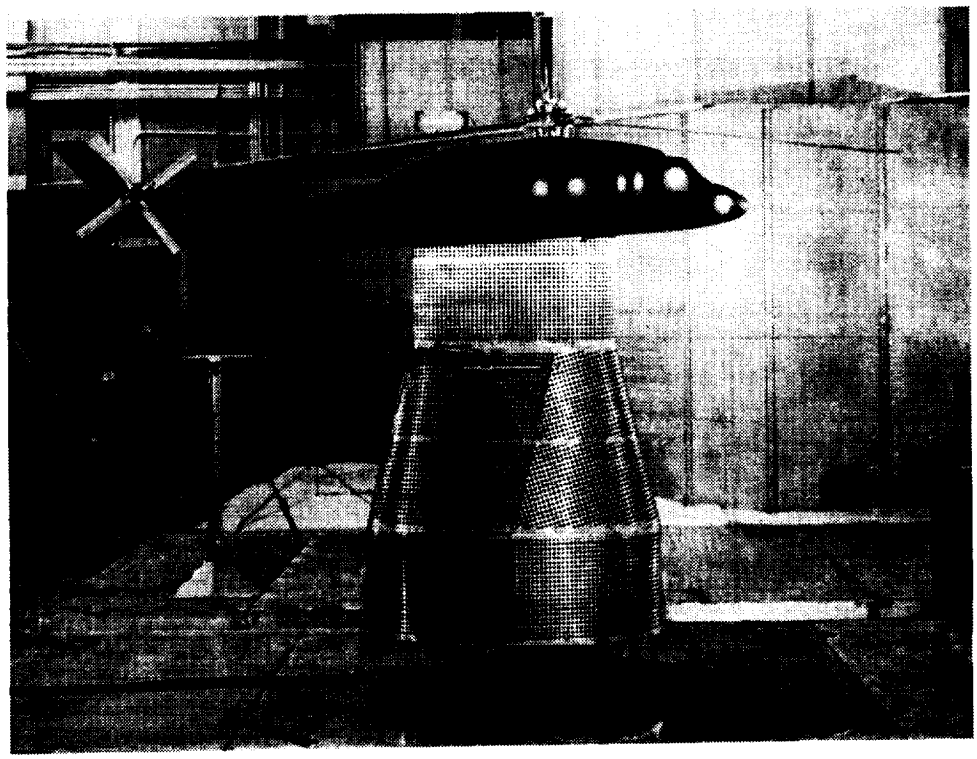

(b) Side view

Figure 1. Photographs of the model test rig and traversing microphone array installed in the open test section of the Langley 14 by 22 Foot Subsonic Tunnel.

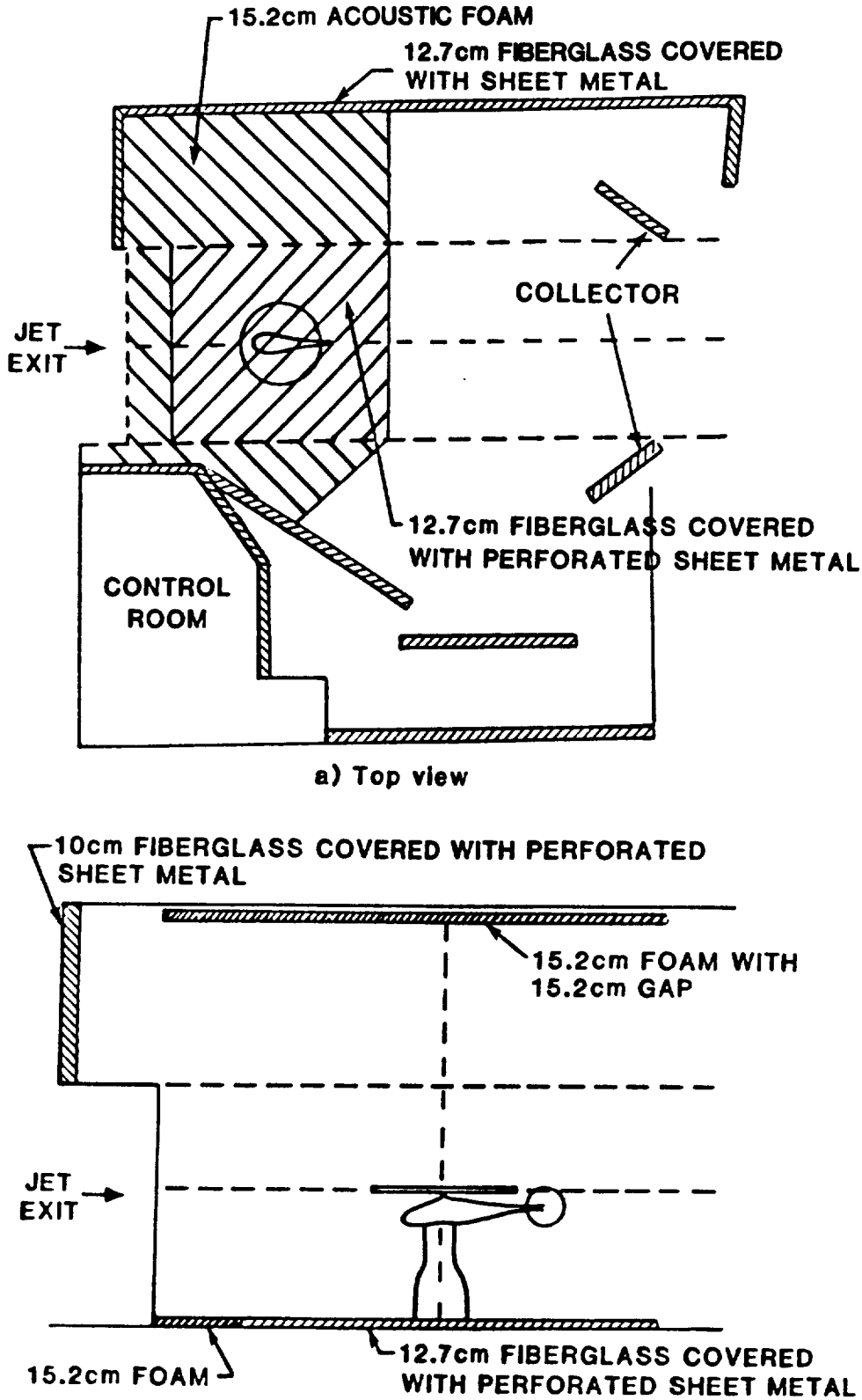

Figure 2. Schematic of the Langley 14 by 22 Foot Subsonic Tunnel open test section showing acoustic treatment.

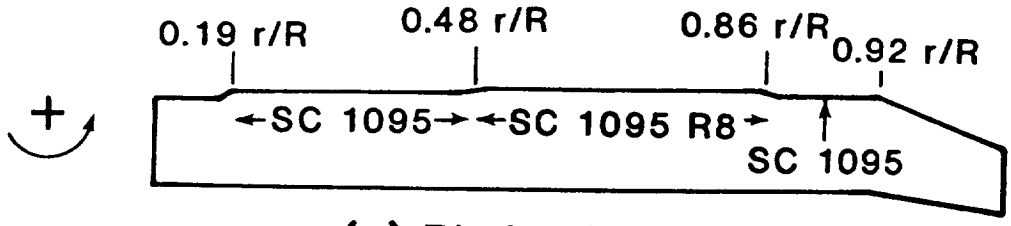

(a) Blade planform

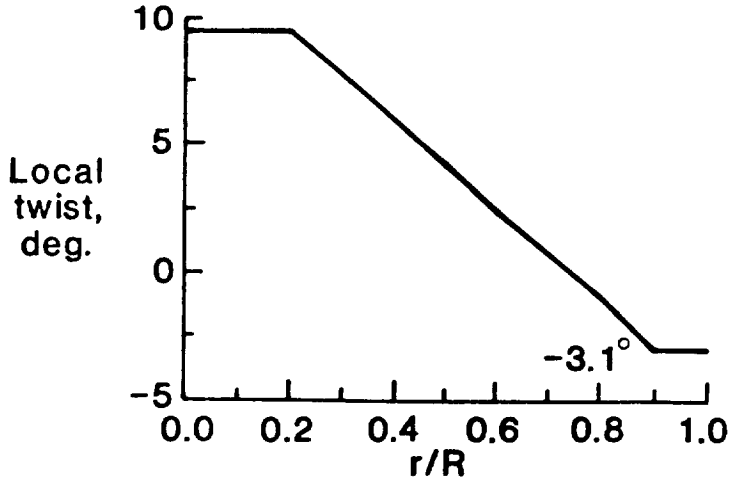

(b) Blade twist

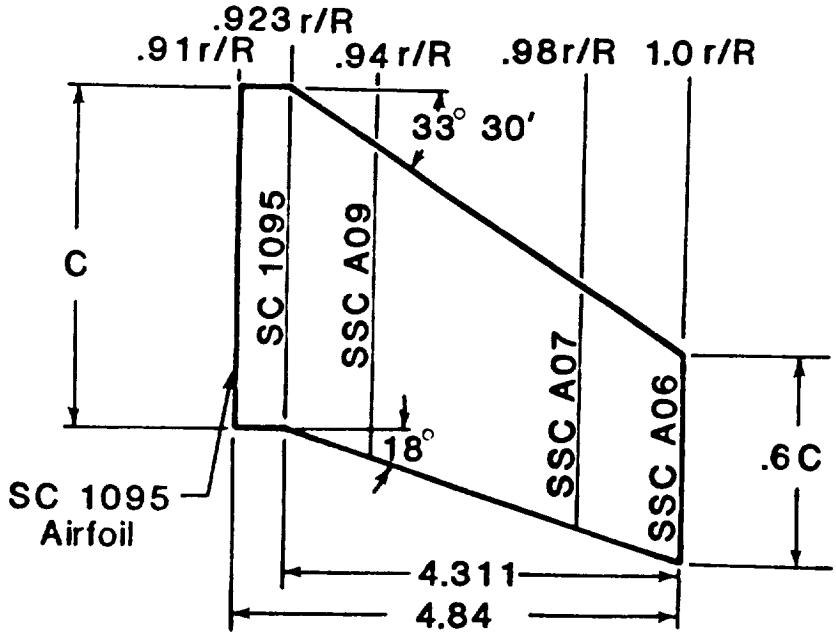

(c) Tip shape

Figure 3. Geometry of model main rotor blades.

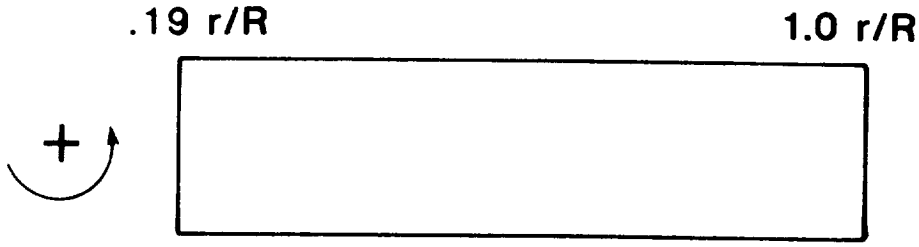

(a) Blade planform

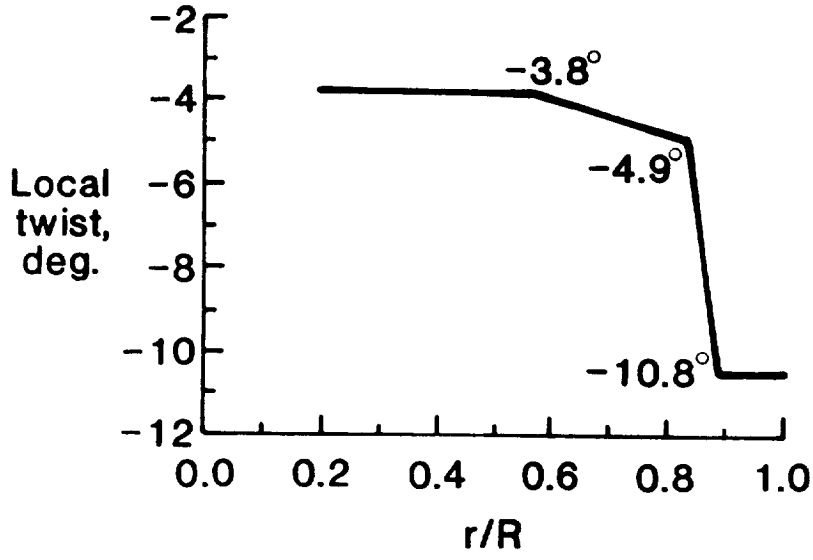

(b) Blade twist

Figure 4. Geometry of model tail rotor blades.

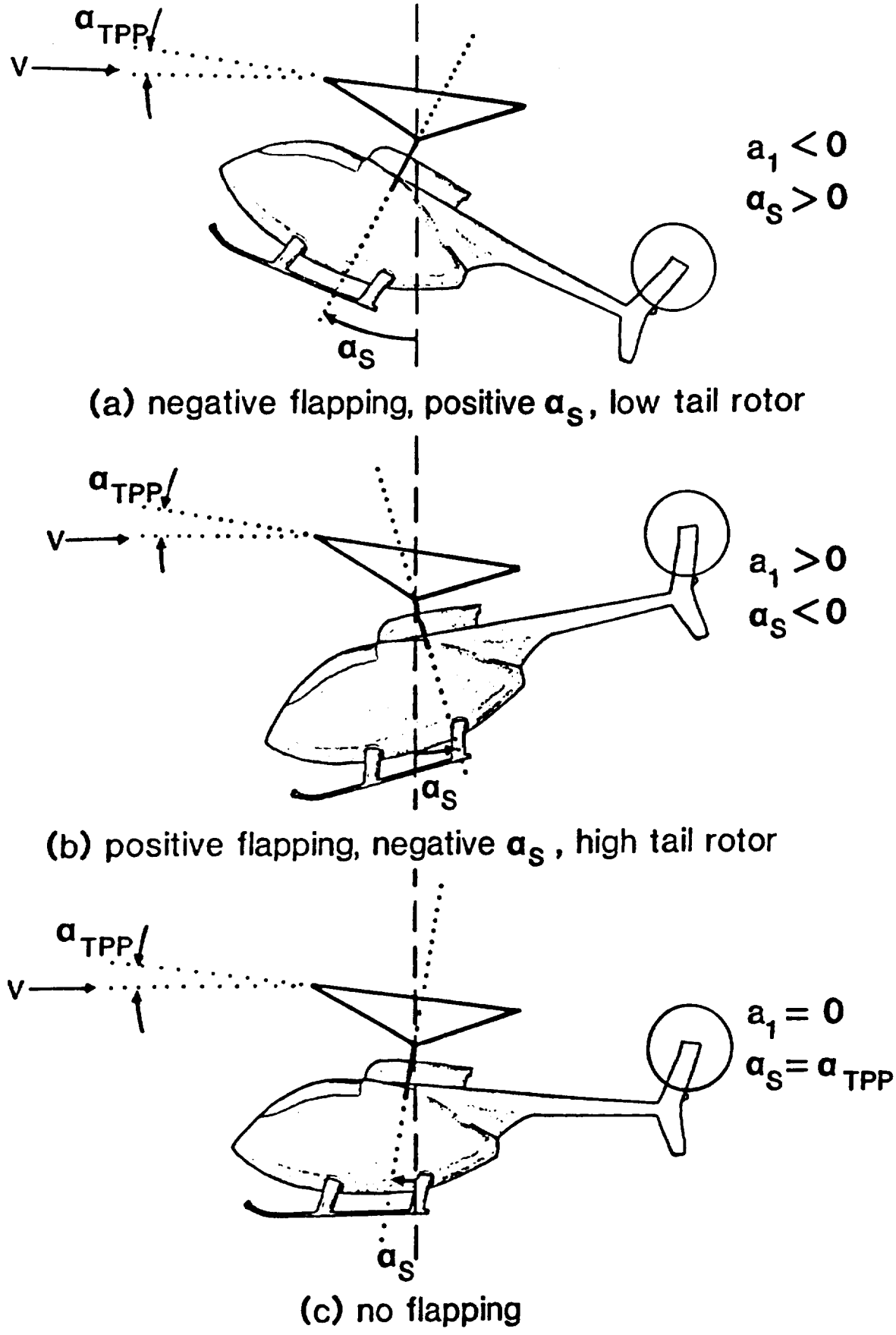

Figure 5. Geometry of rotors and fuselage for different flapping conditions at constant α_{TPP} (not to scale).

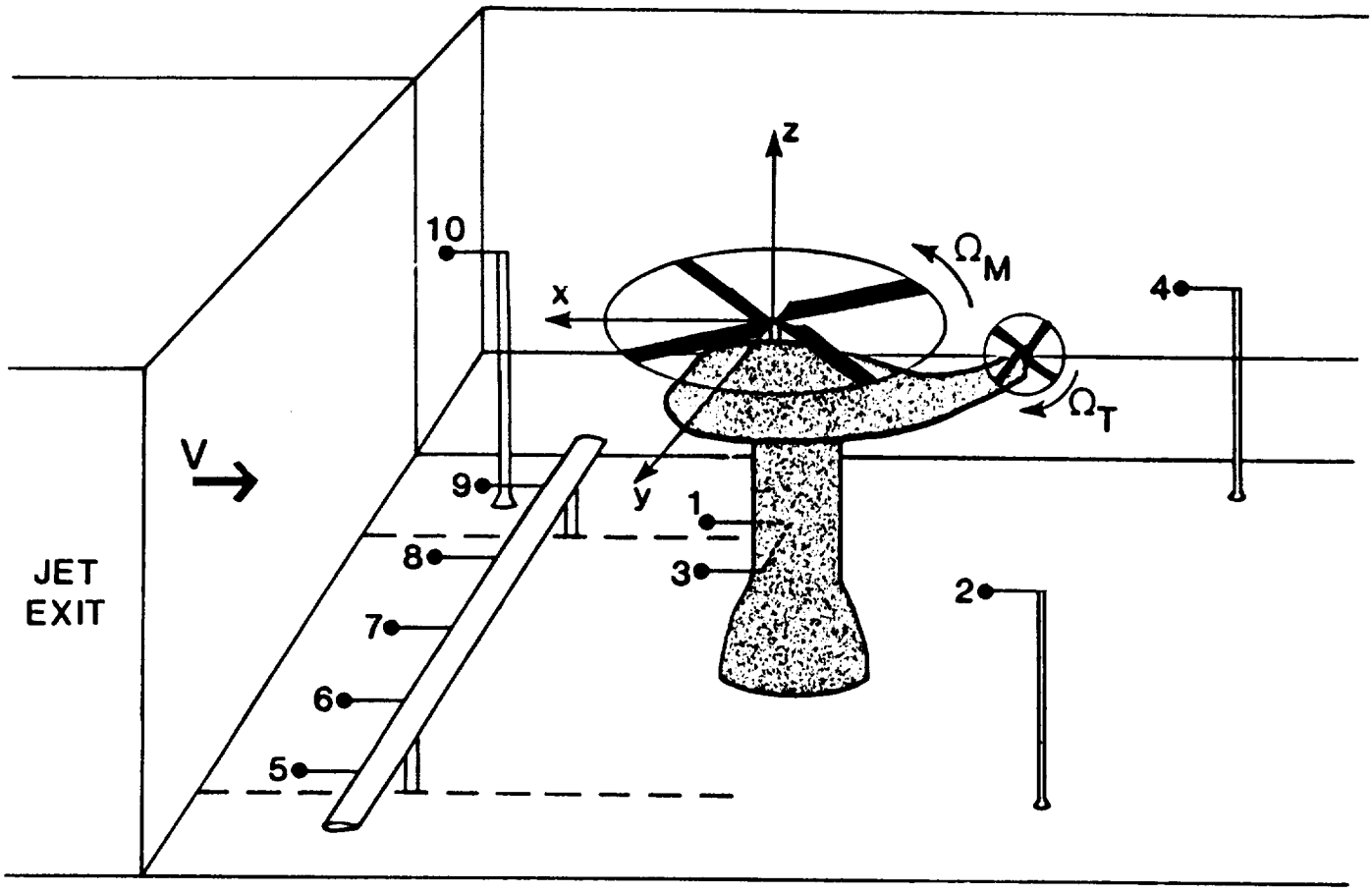

Figure 6. Schematic of experimental apparatus and microphone positions.

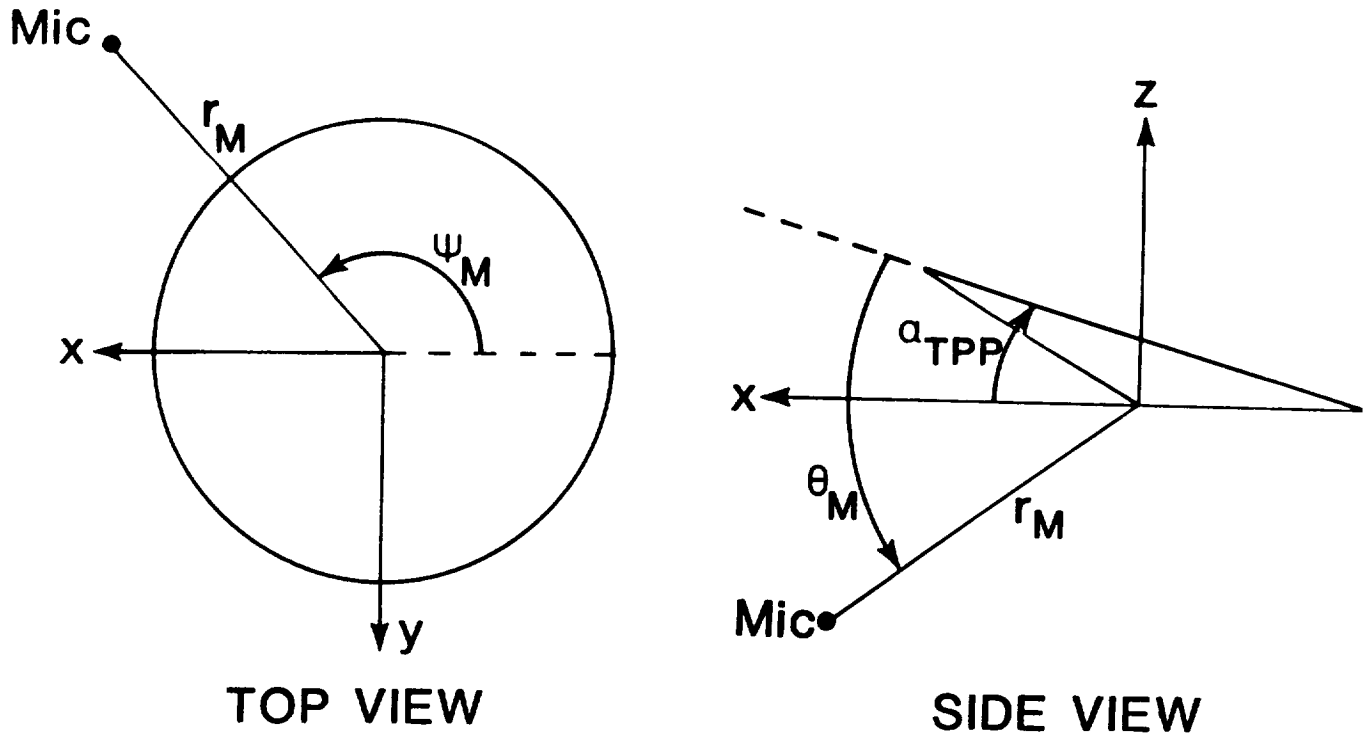

(a) coordinates relative to main rotor

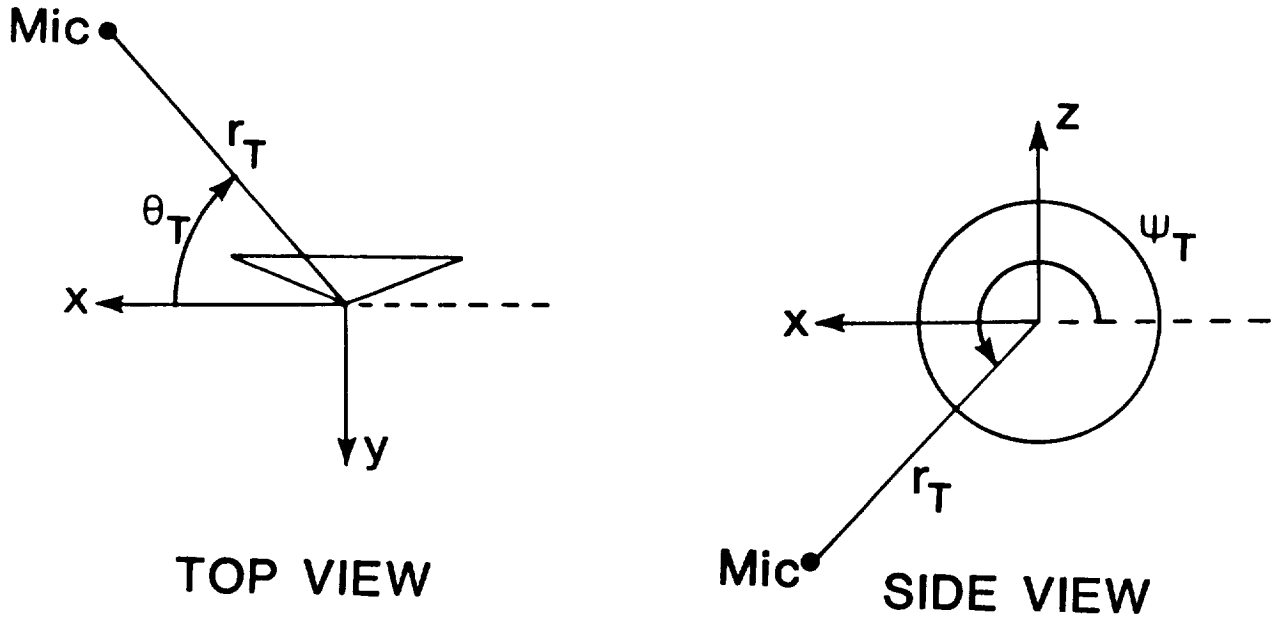

(b) coordinates relative to tail rotor

Figure 7. Measurement location coordinate systems.

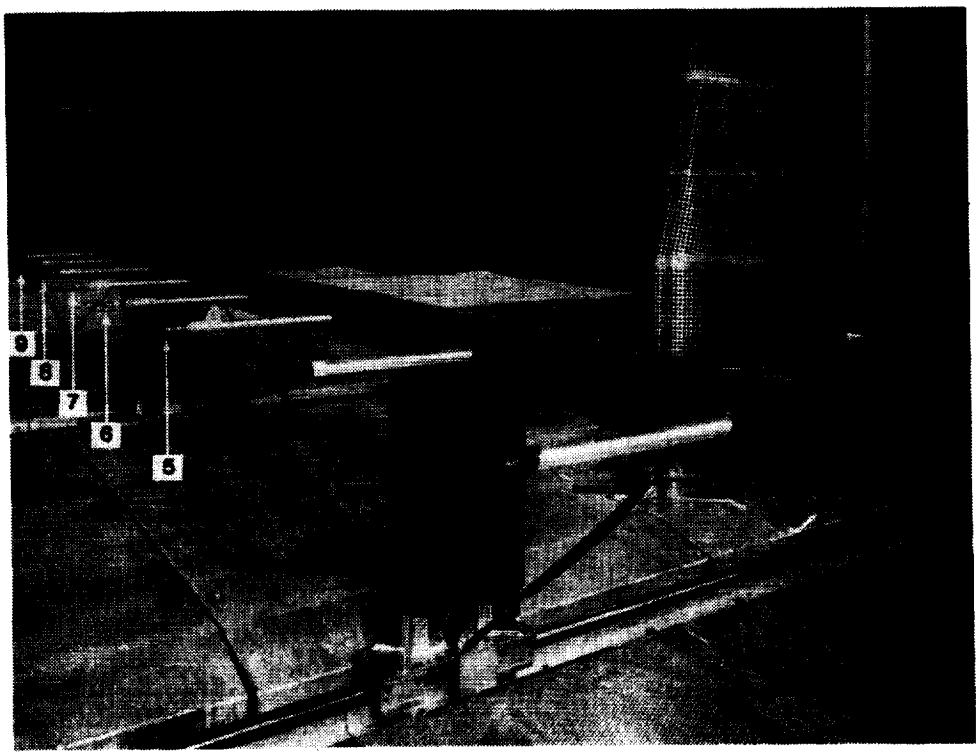

Figure 8. Photograph of the traversing microphone array.

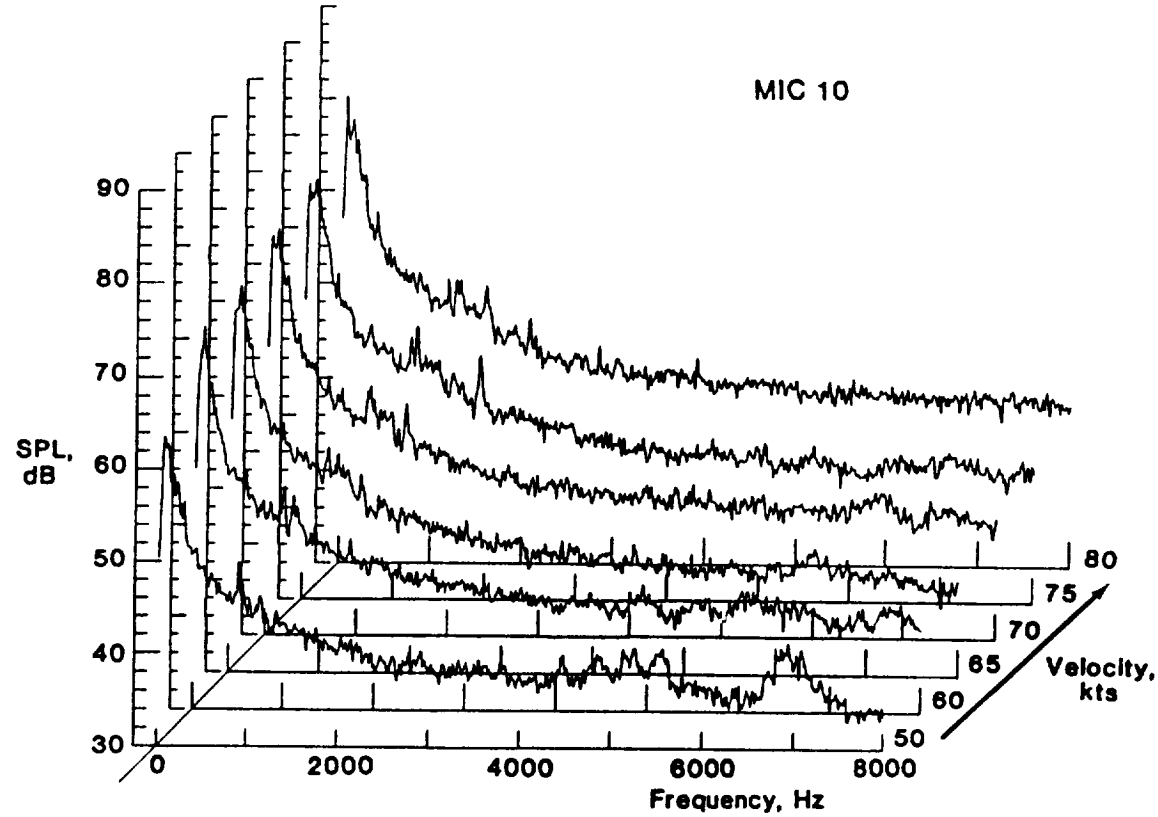

(a) Microphone 10

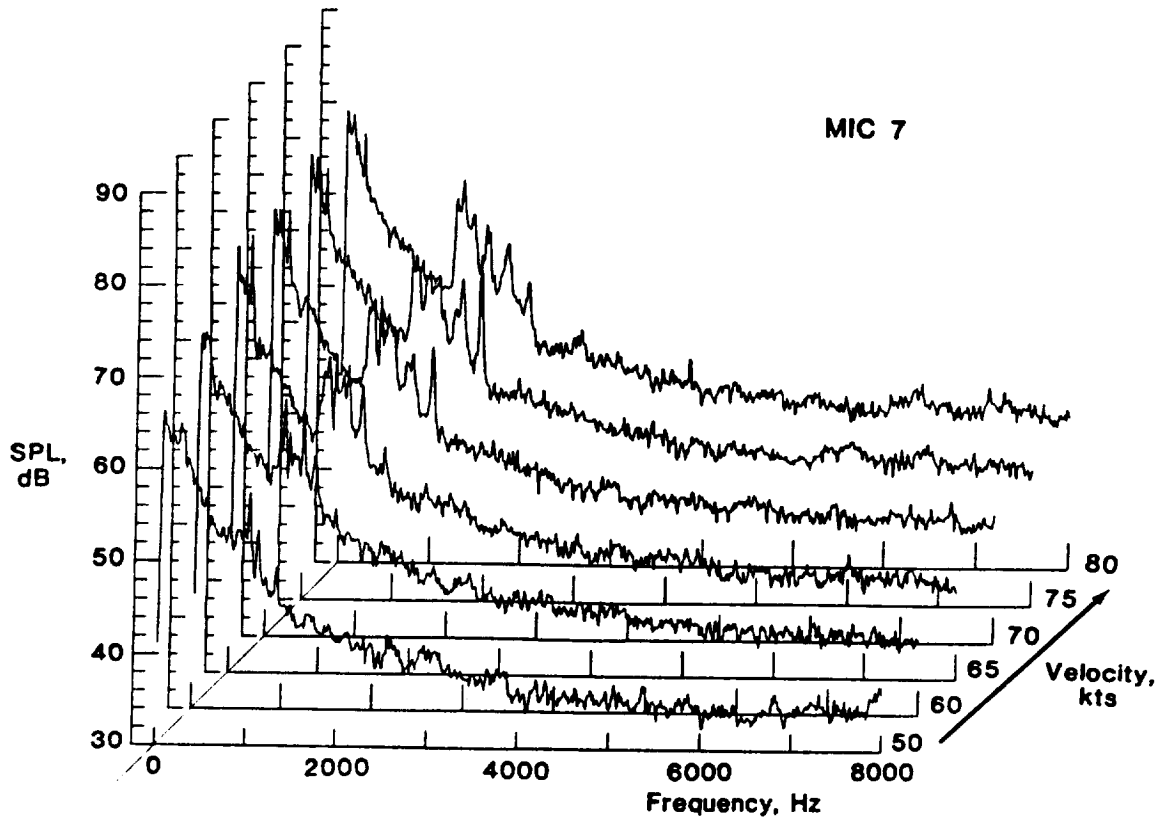

(b) Microphone 7

Figure 9. Examples of background noise spectra as a function of tunnel speed (freefield and nosecone corrections applied).

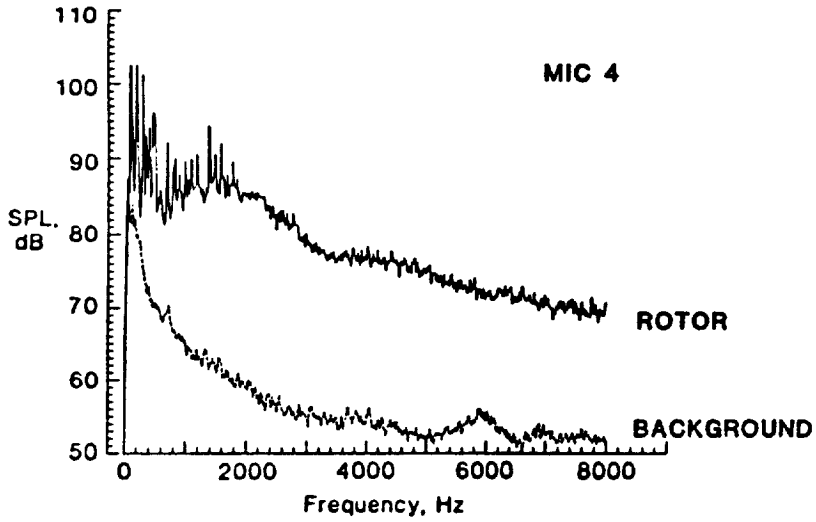

(a) Microphone 4

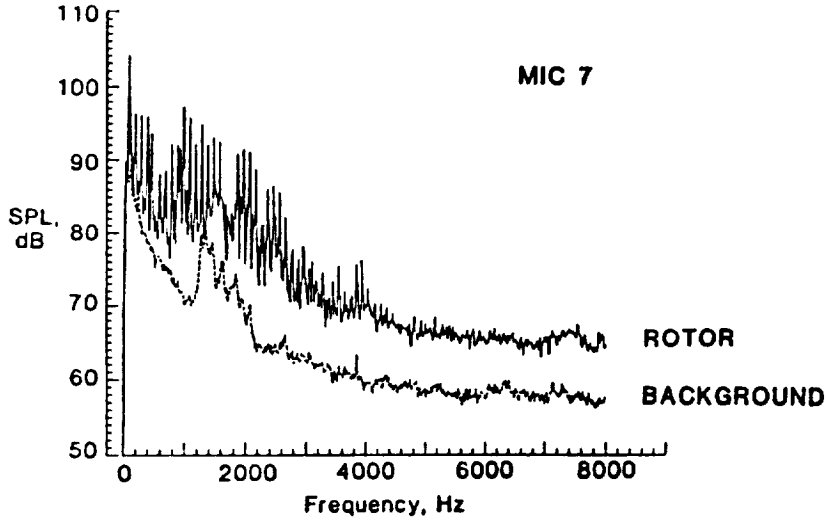

(b) Microphone 7

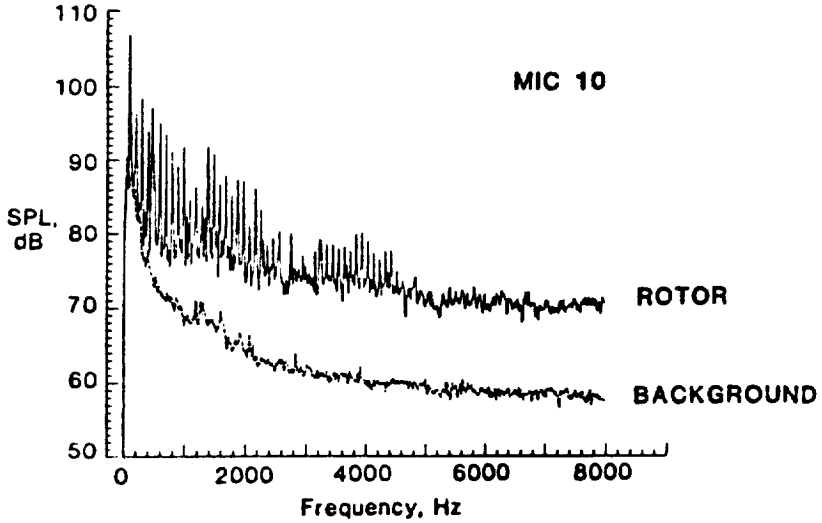

(c) Microphone 10

Figure 10. Comparison of typical rotor spectra with background noise spectra (V=80 kts, α_{TPP}=2°, α_s=6°, $C_{T\text{-}M}$=.007).

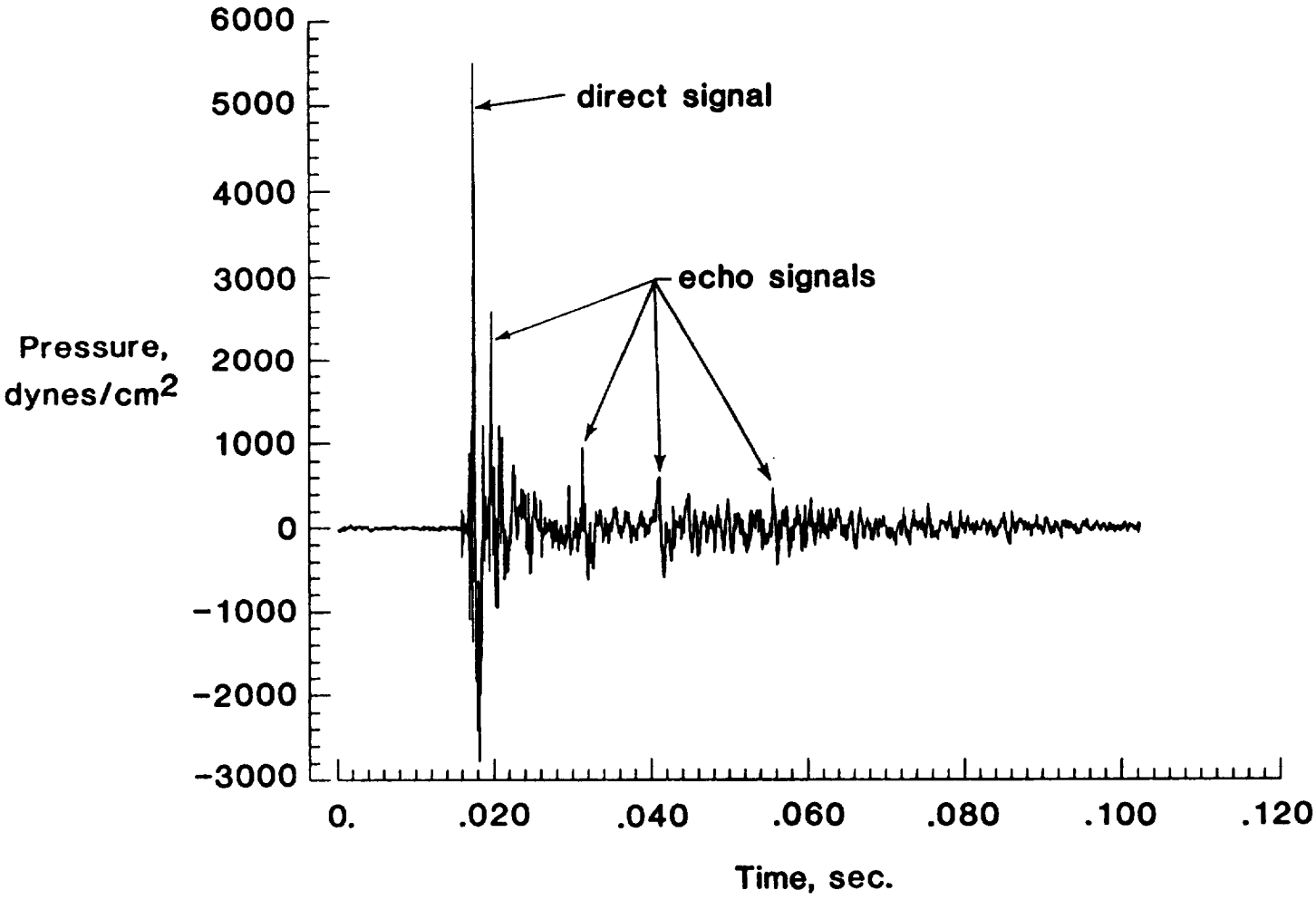

Figure 11. Impulsive noise source, V=0 kts, microphone 5.

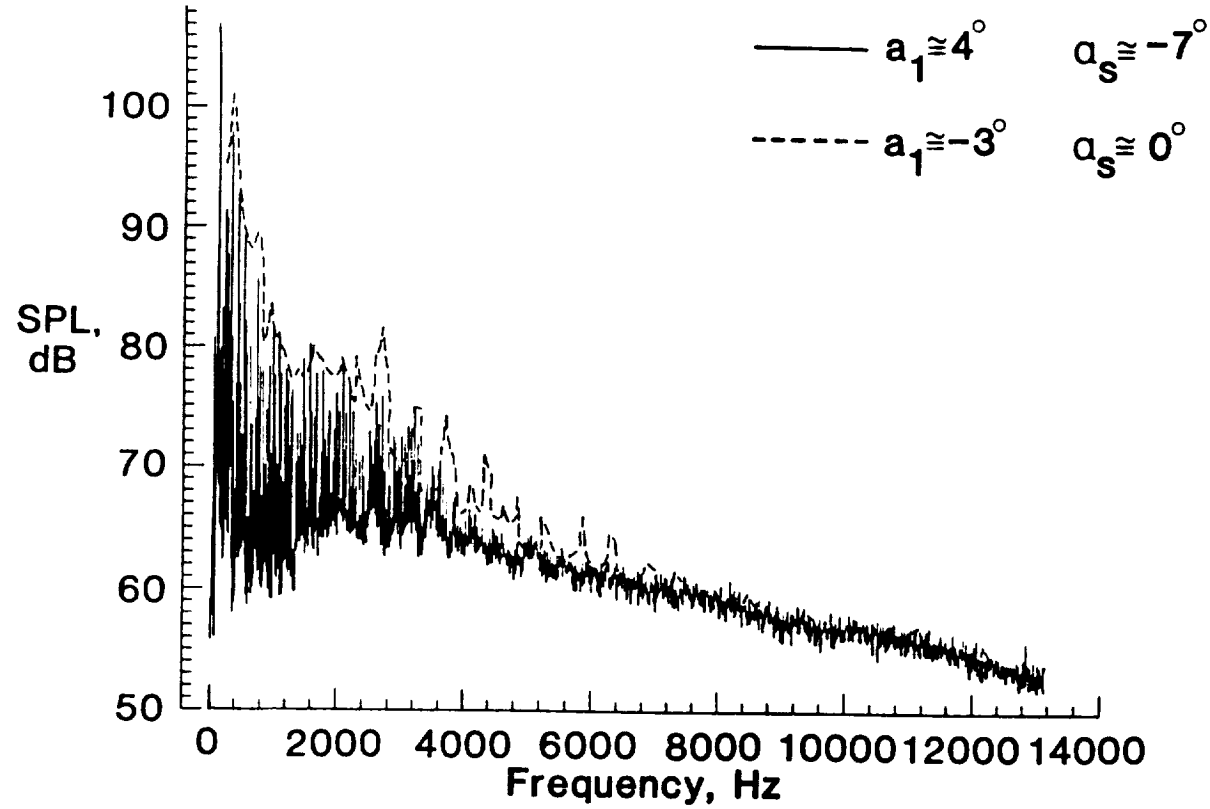

(a) Microphone 5, α_{TPP}~-3°

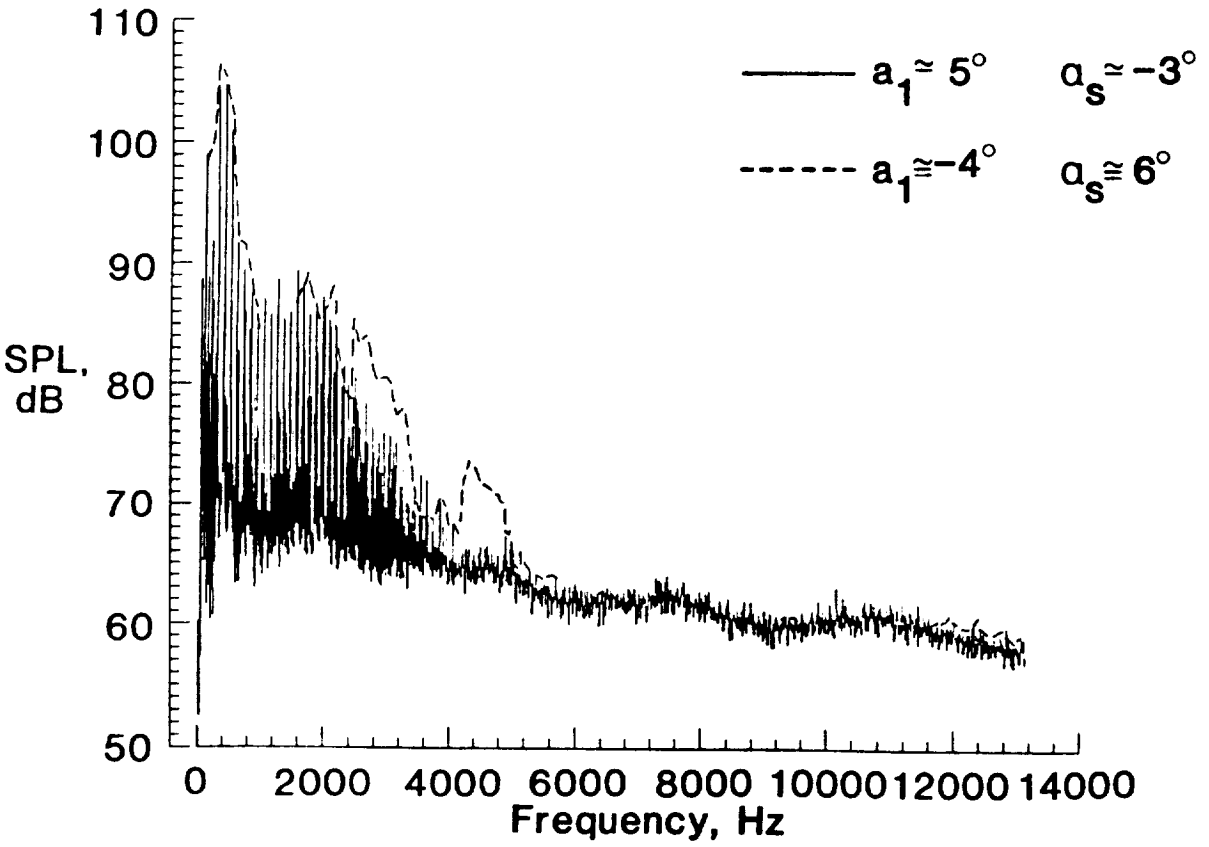

(b) Microphone 9, α_{TPP}~2°

Figure 12. Comparison of spectra for constant tip-path-plane angle α_{TPP} but with positive and negative longitudinal flapping a_1 (V=50 kts, C_{T-M}=.007).

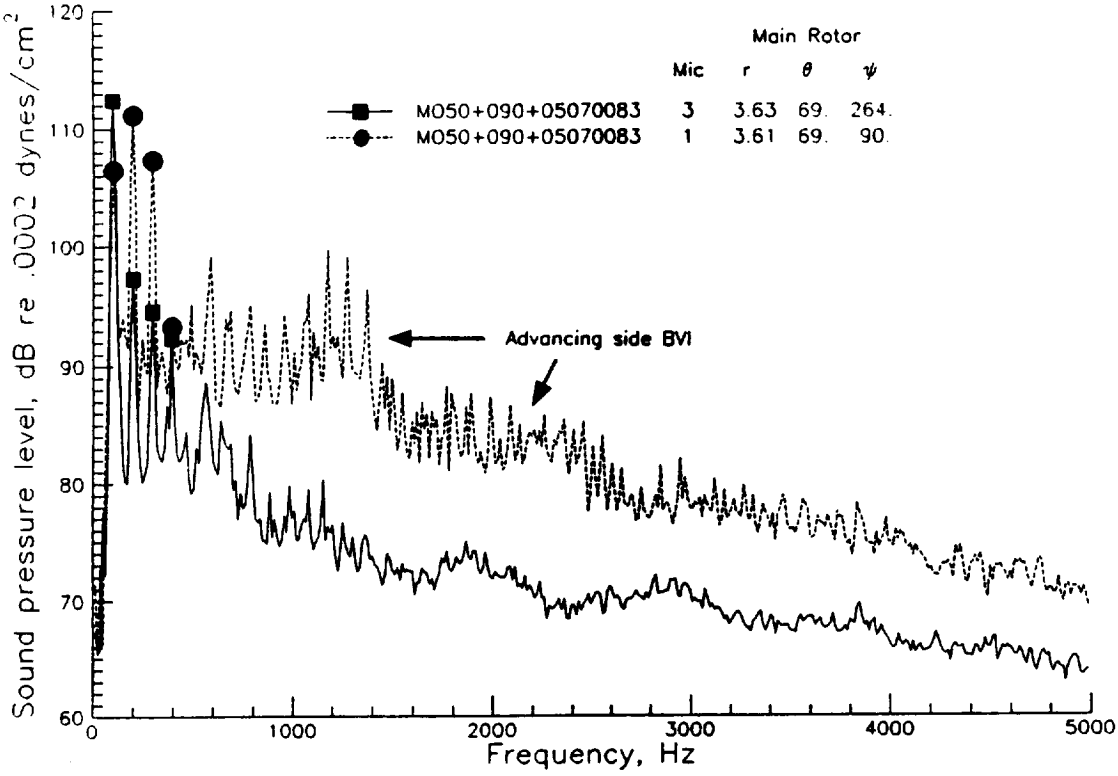

(a) V=50 kts, α_{TPP}=5°, C_{T-M}=.007

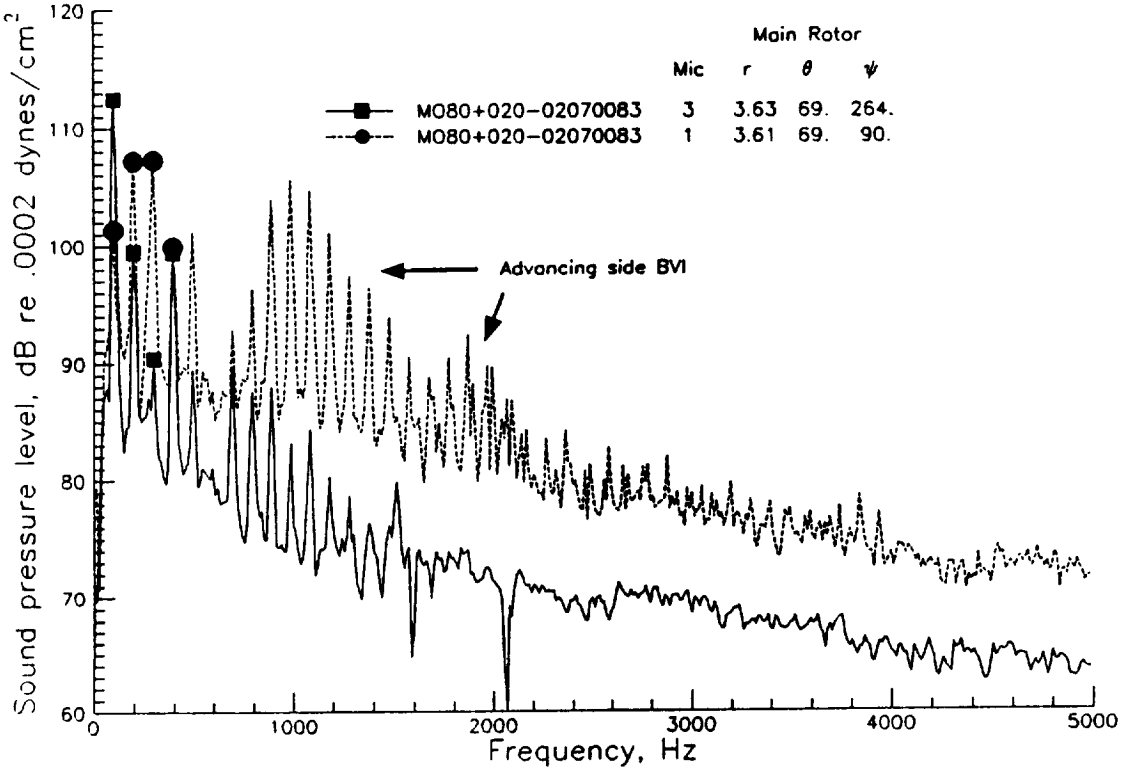

(b) V=80 kts, α_{TPP}=-2°, C_{T-M}=.007

Figure 13. Comparison of isolated main rotor data measured at microphones 1 and 3.

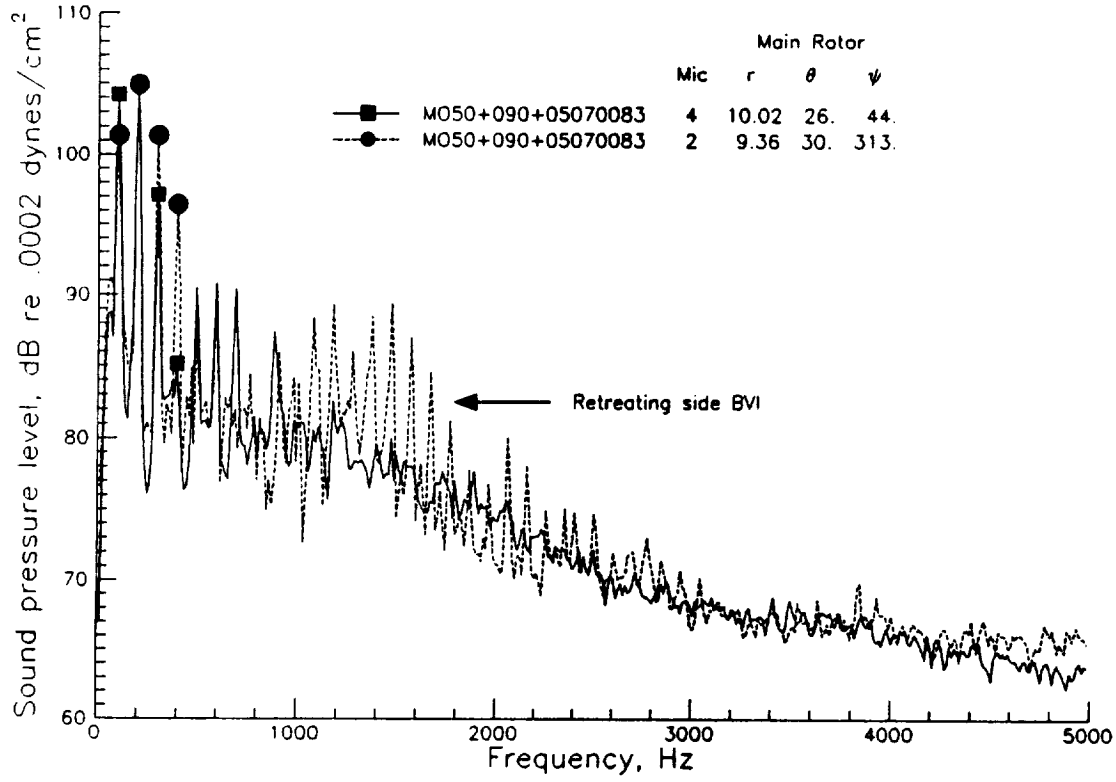

(a) V=50 kts, α_{TPP}=5°, C_{T-M}=.007

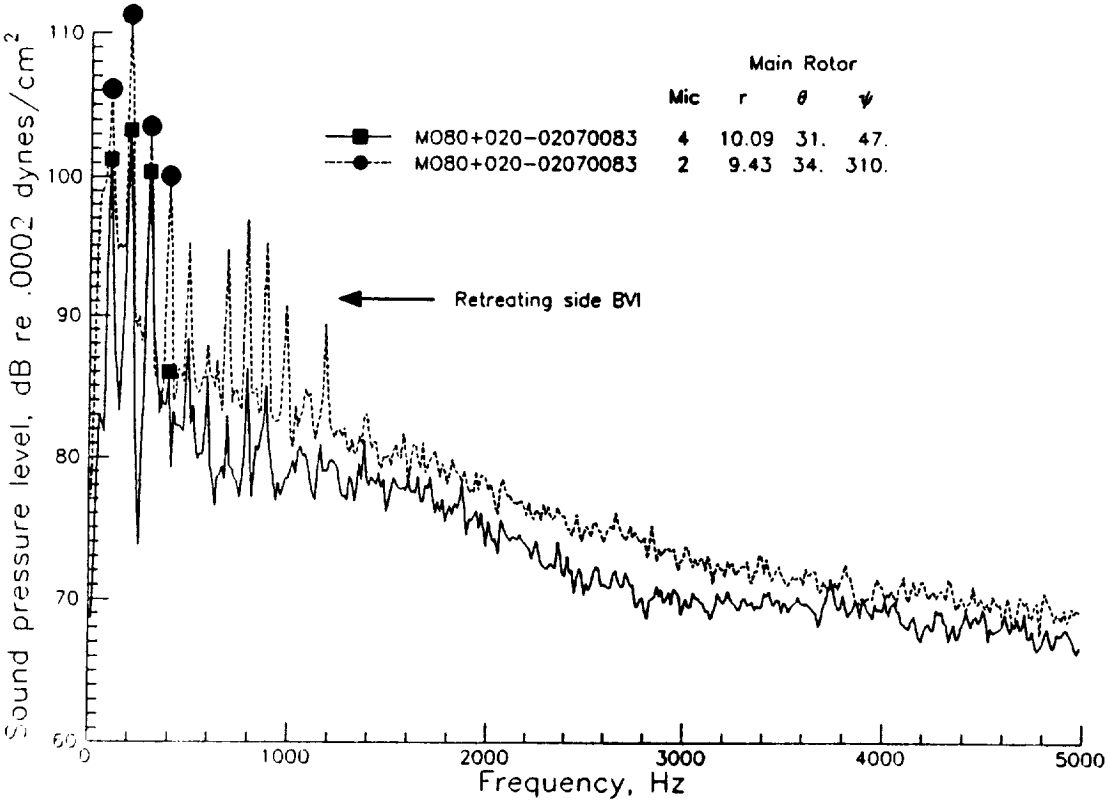

(b) V=80 kts, α_{TPP}=-2°, C_{T-M}=.007

Figure 14. Comparison of isolated main rotor data measured at microphones 2 and 4.

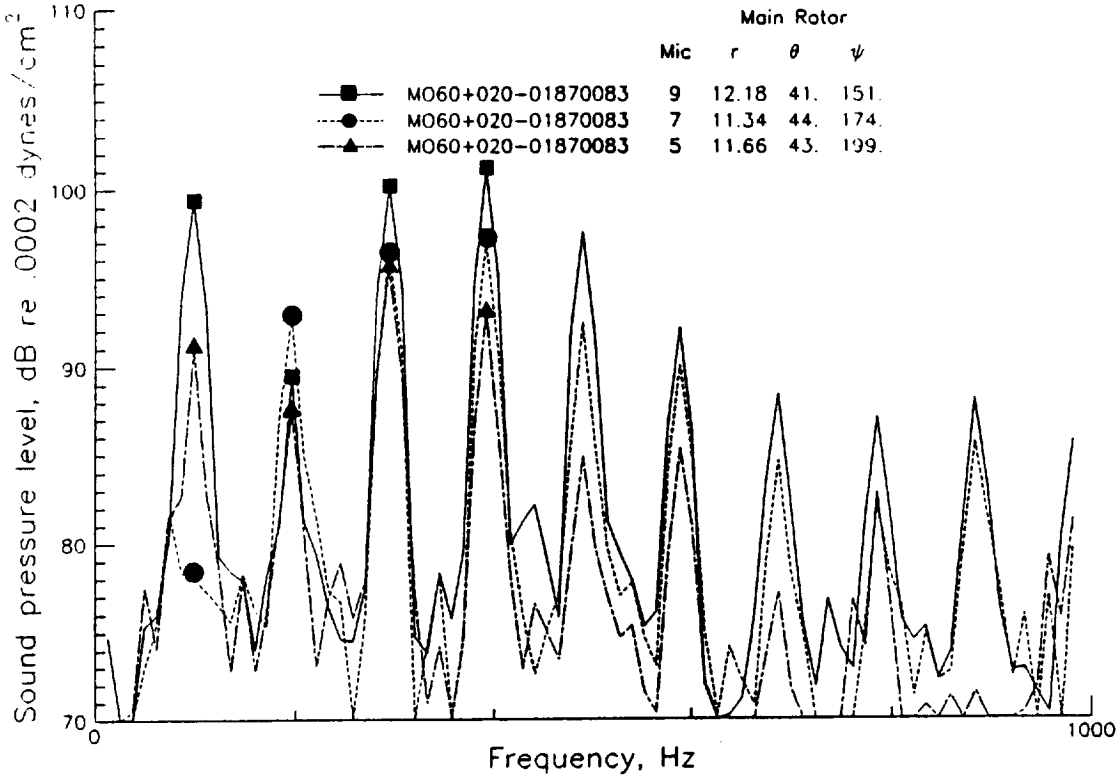

(a) V=60 kts, α_{TPP}=-2°, C_{T-M}=.007.

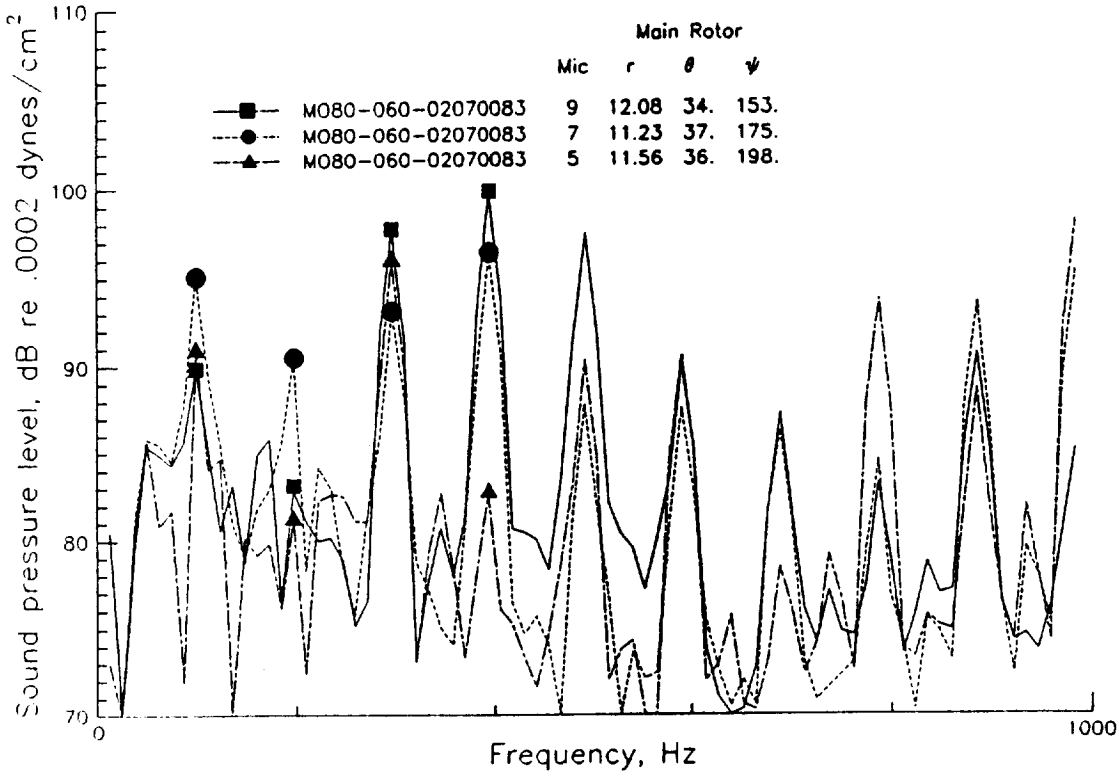

(b) V=80 kts, α_{TPP}=-2°, C_{T-M}=.007

Figure 15. Comparison of isolated main rotor data measured at microphones 5, 7 and 9.

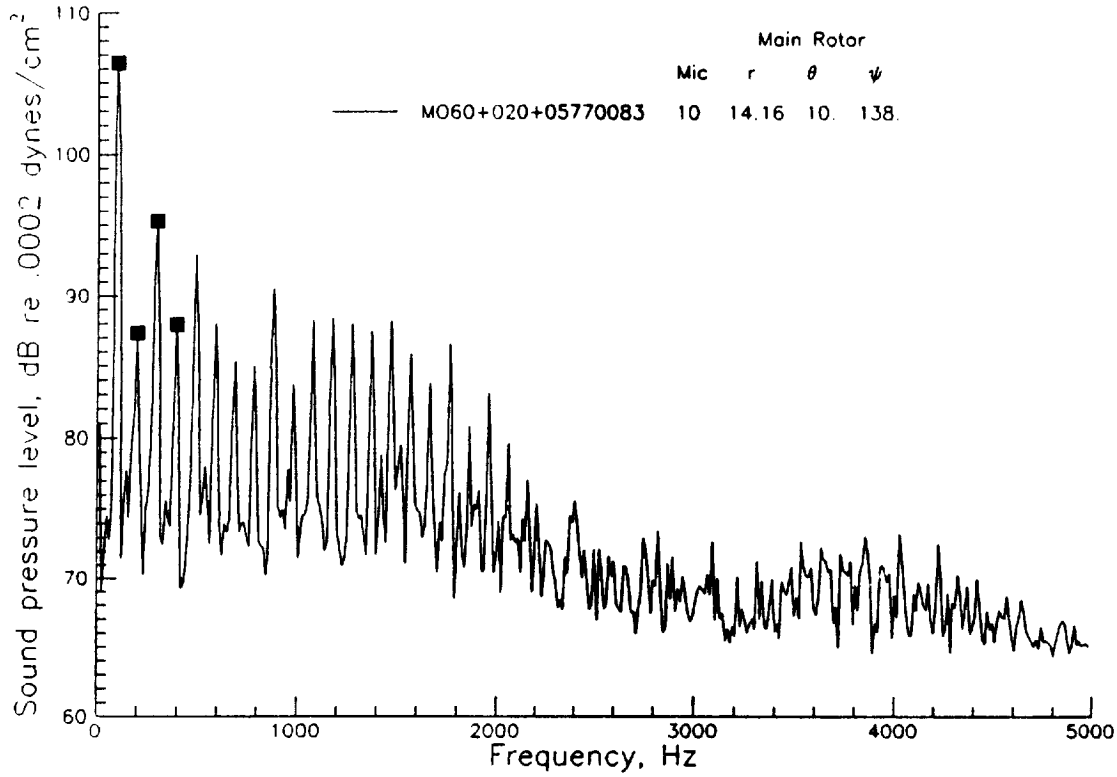

(a) α_{TPP}=5.7°

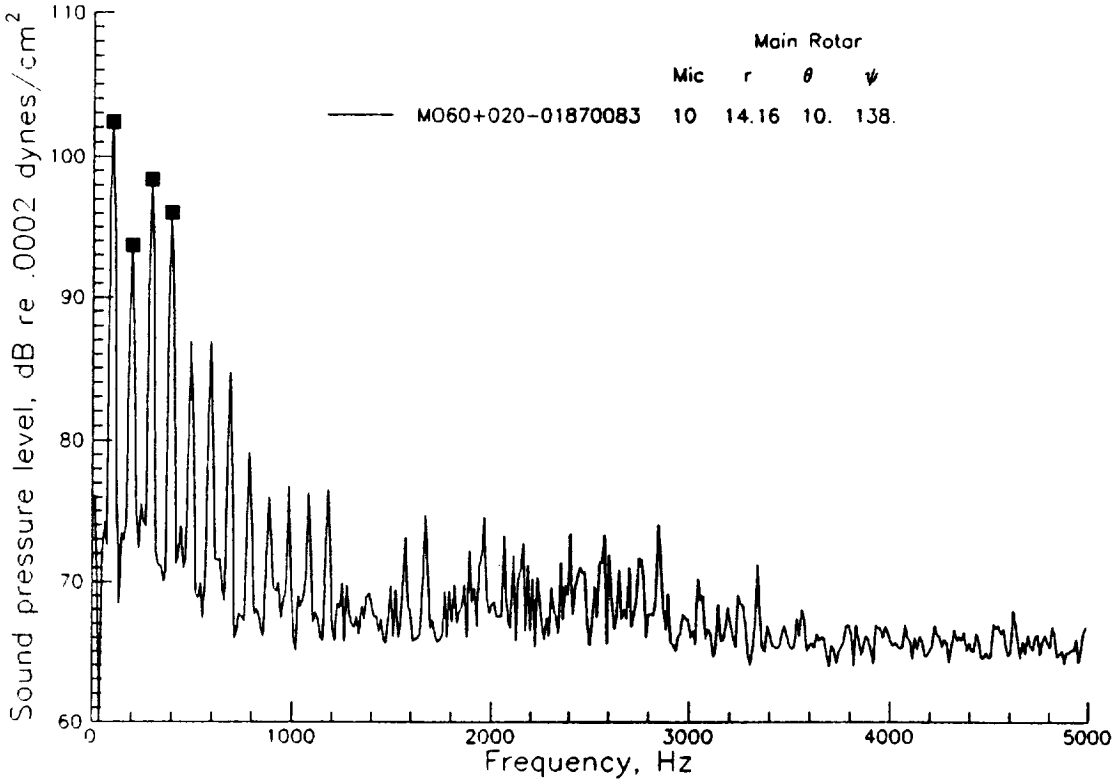

(b) α_{TPP}=-1.8°

Figure 16. Comparison of isolated main rotor harmonic levels for two different tip-path-plane angles α_{TPP} for microphone 10 (V=60 kts, α_s=2°, C_{T-M}=.007).

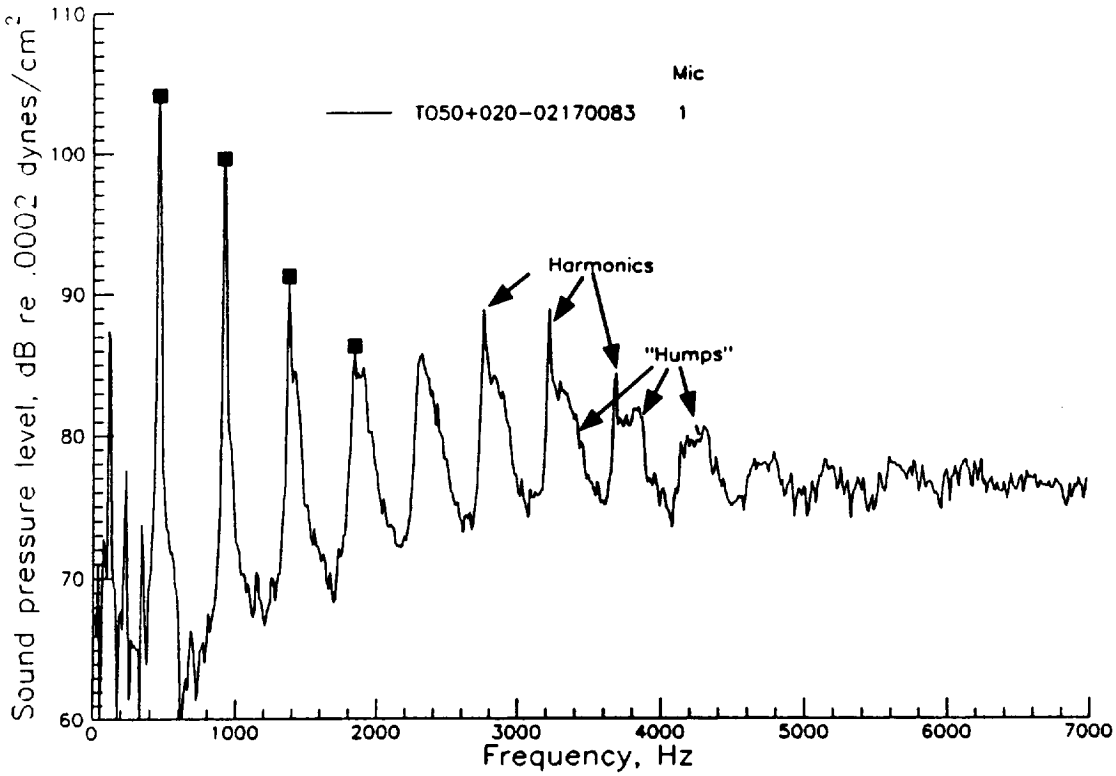

(a) V=50 kts

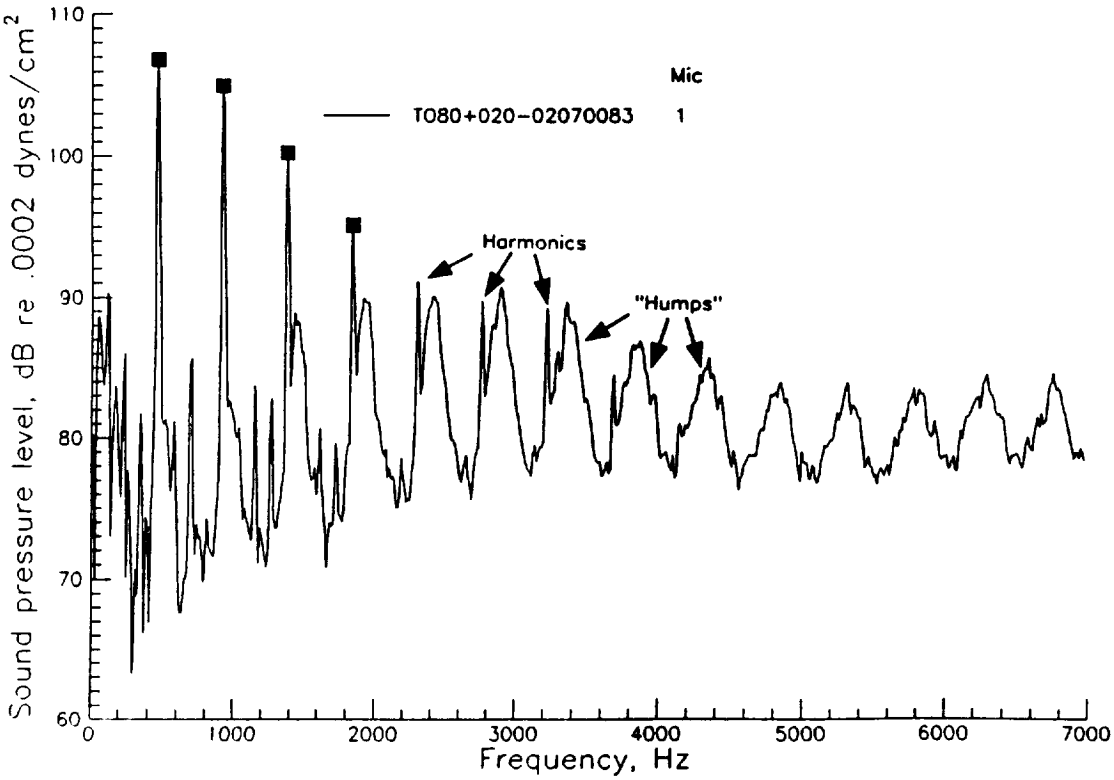

(b) V=80 kts

Figure 17. Isolated tail rotor data at microphone 1 showing harmonics and "humps" (α_{TPP}=-2°, α_S=2°).

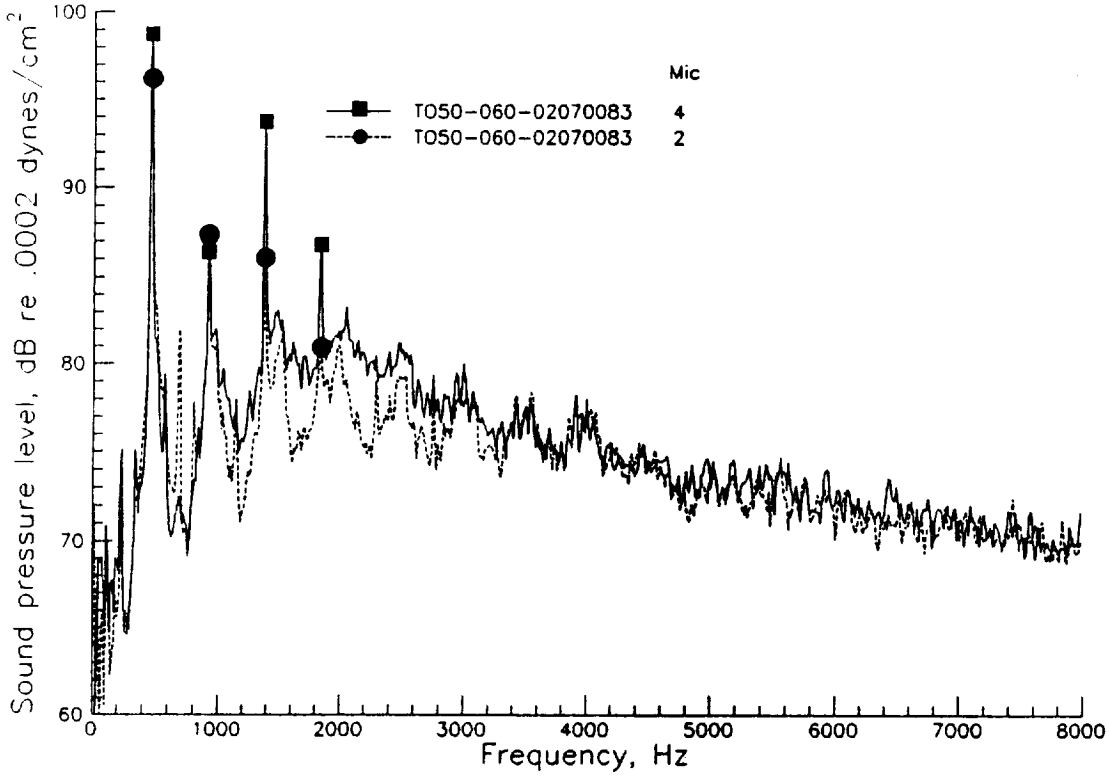

(a) V=50 kts, tail rotor thrust 18 lb

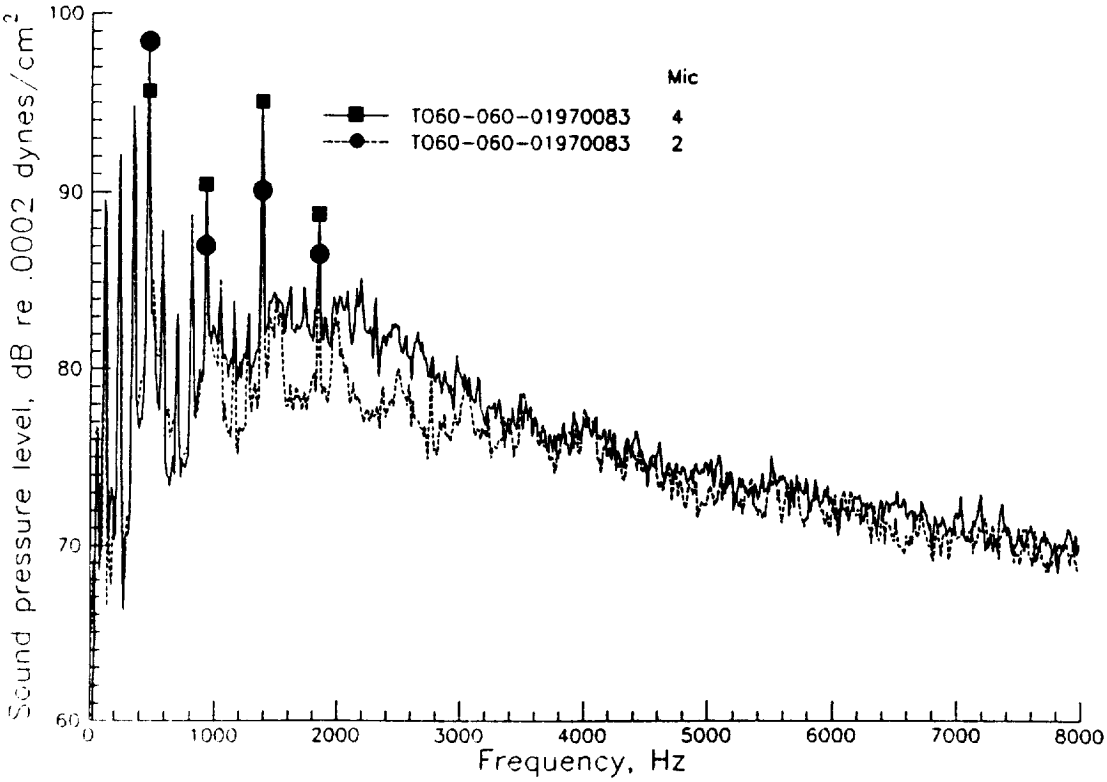

(b) V=60 kts, tail rotor thrust 19 lb

Figure 18. Isolated tail rotor data measured at microphones 2 and 4 (α_s=-6°).

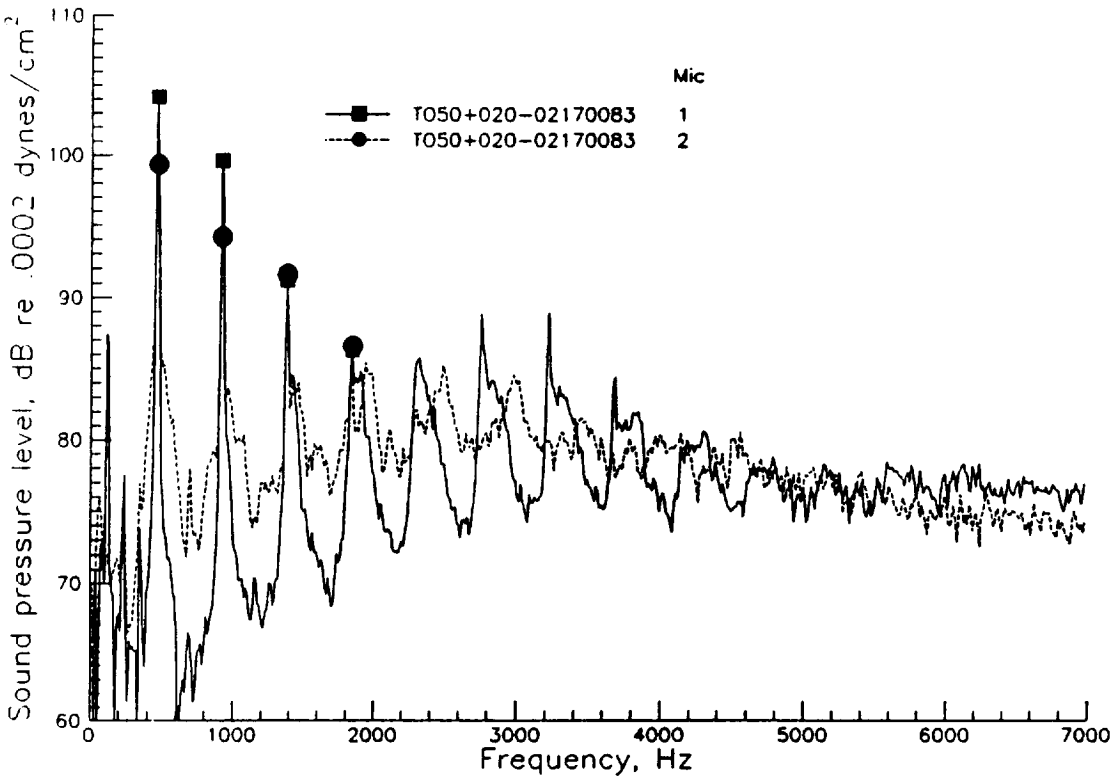

(a) V=50 kts, tail rotor thrust 20 lb

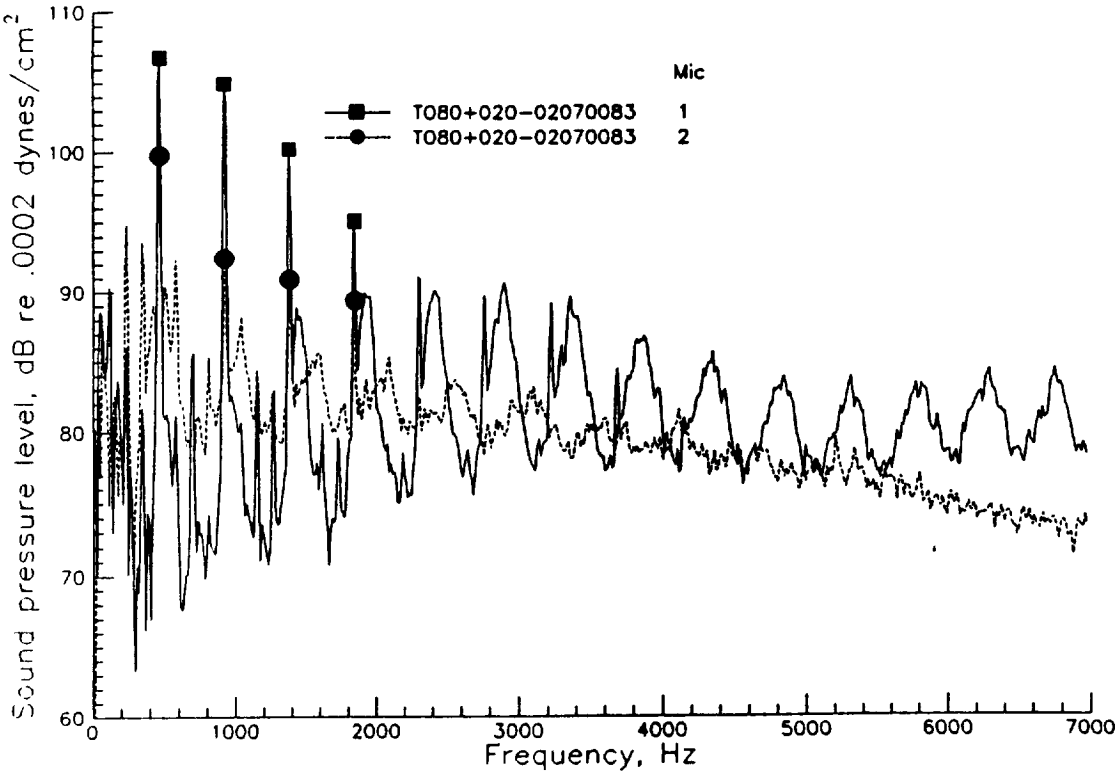

(b) V=80 kts, tail rotor thrust 16 lb

Figure 19. Comparison of isolated tail rotor "humps" measured at microphones 1 and 2 (α_S=2°).

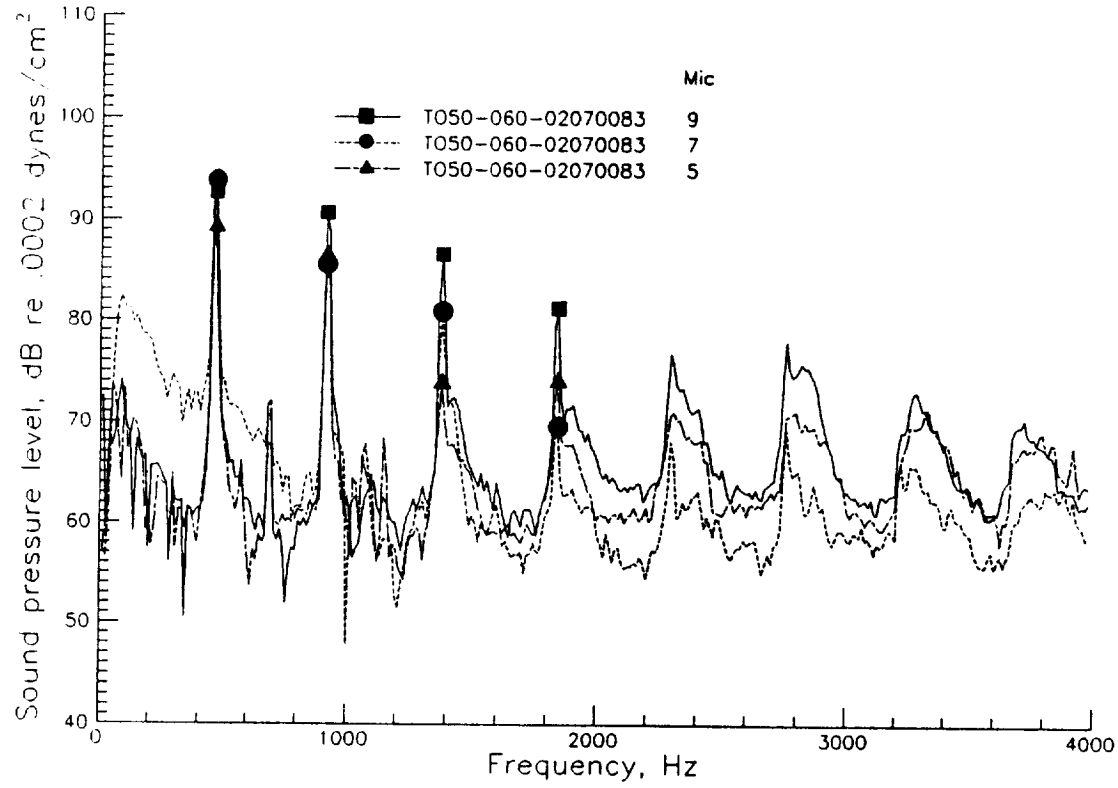

(a) V=50 kts, tail rotor thrust 18 lb

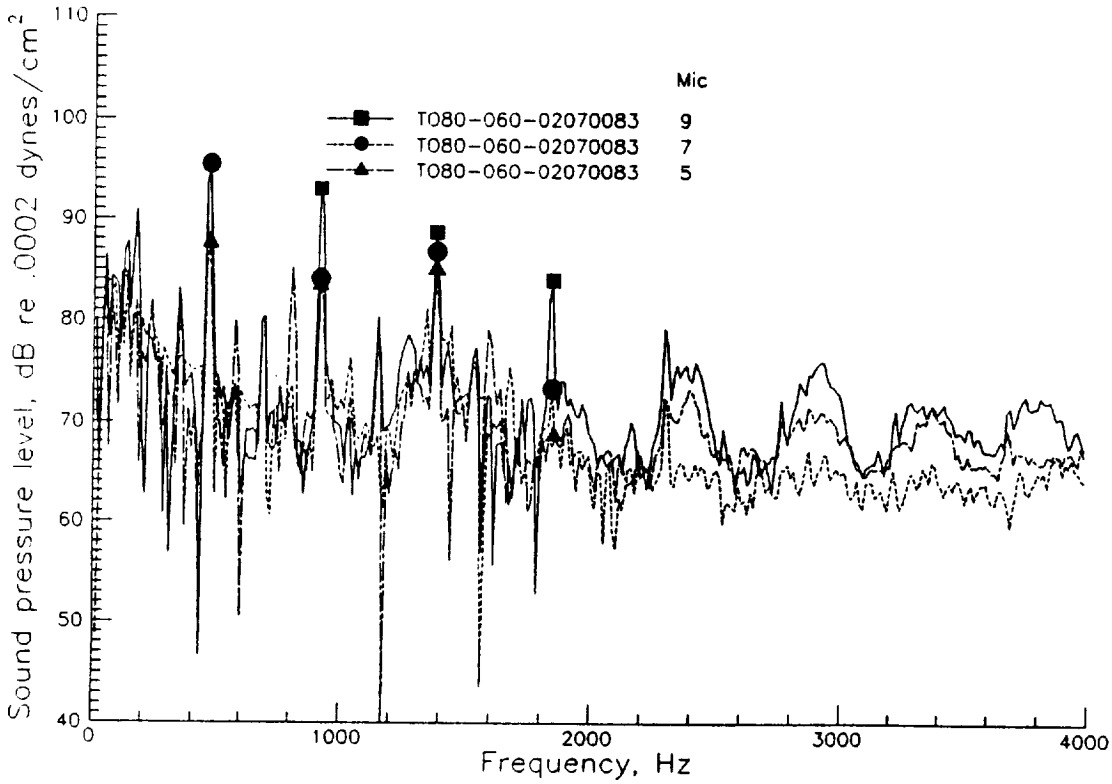

(b) V=80 kts, tail rotor thrust 5.7 lb

Figure 20. Isolated tail rotor data for microphones 5, 7 and 9 (α_s=-6°)

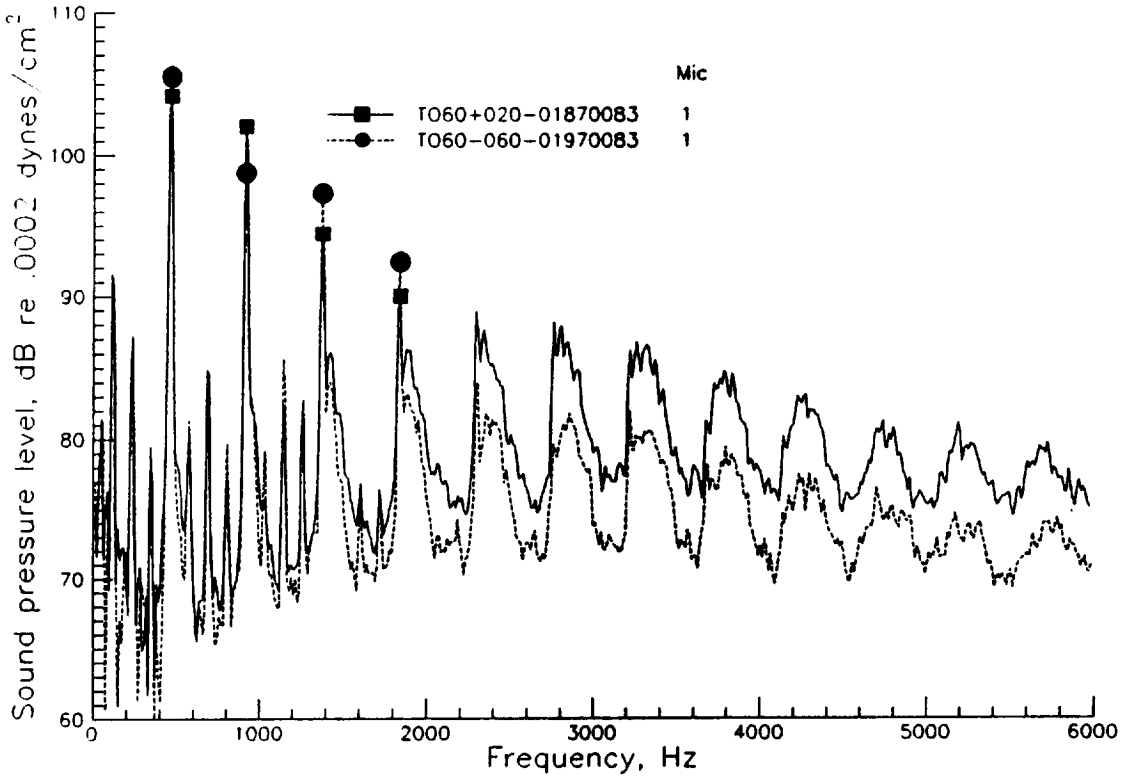

(a) Microphone 1

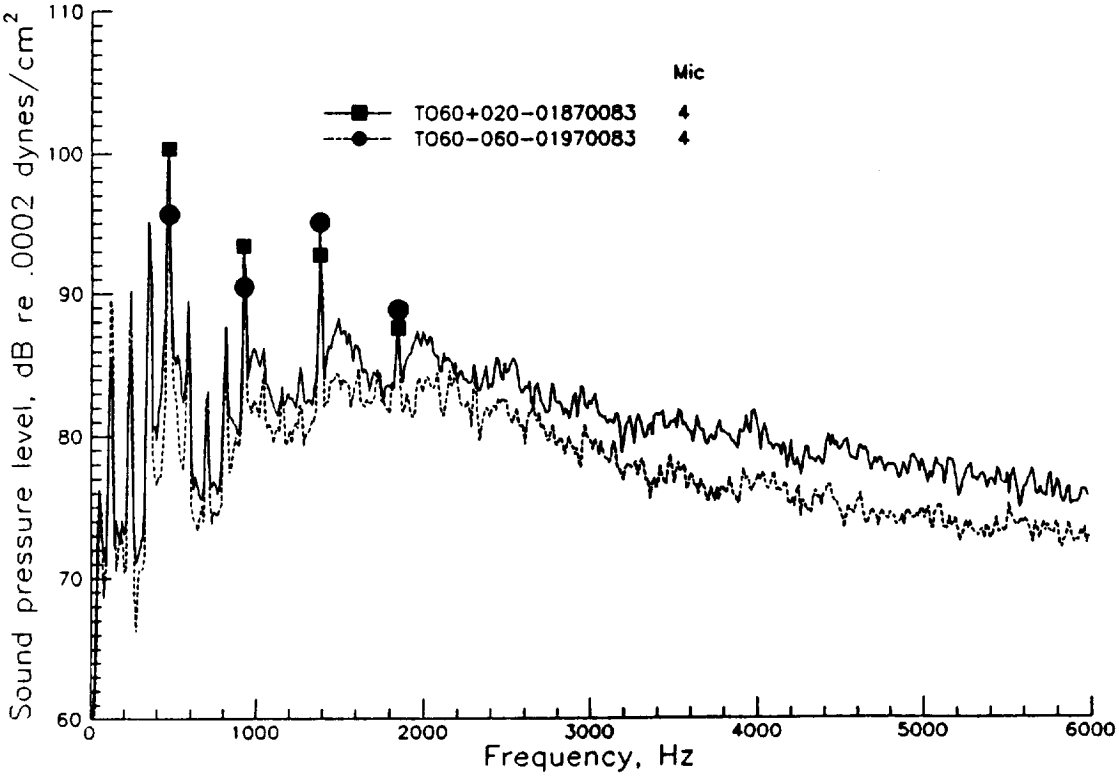

(b) Microphone 4

Figure 21. Isolated tail rotor for low (α_S=2°) and high (α_S=-6°) tail positions at three microphones locations (V=60 kts, α_{TPP}=-1.8°, C_{T-M}=.007, tail rotor thrust ~ 18 lb).

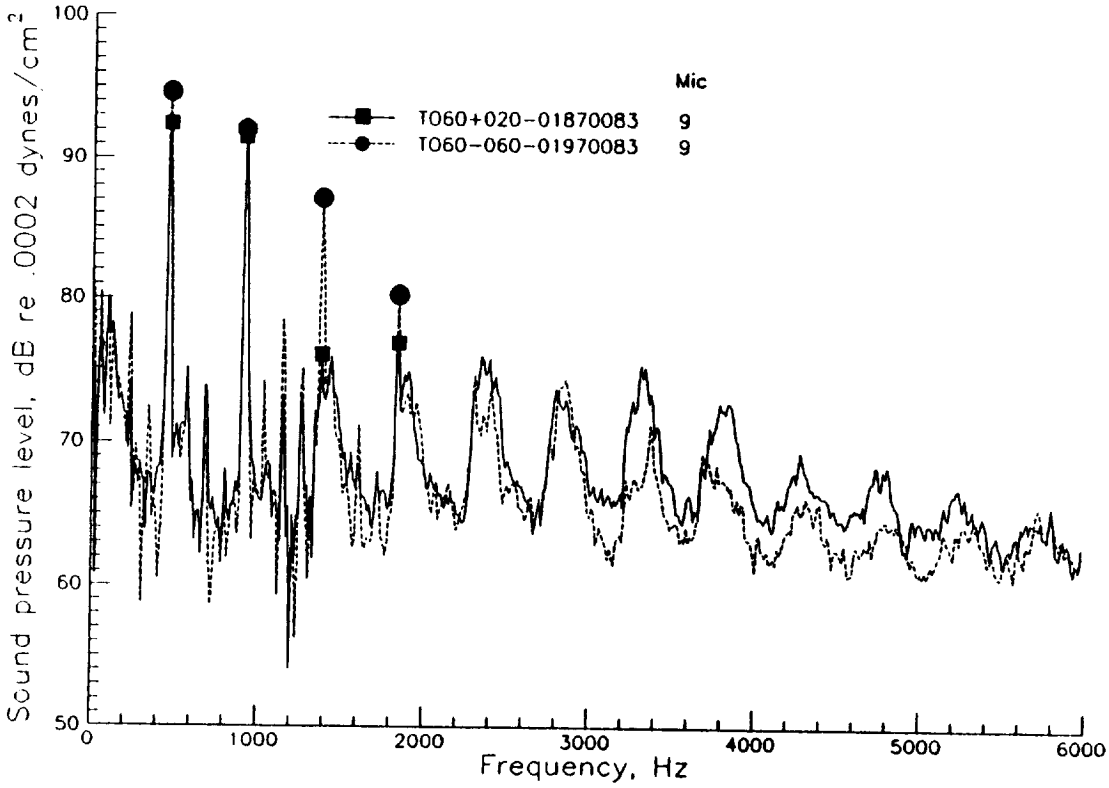

(c) Microphone 9

Figure 21 continued.

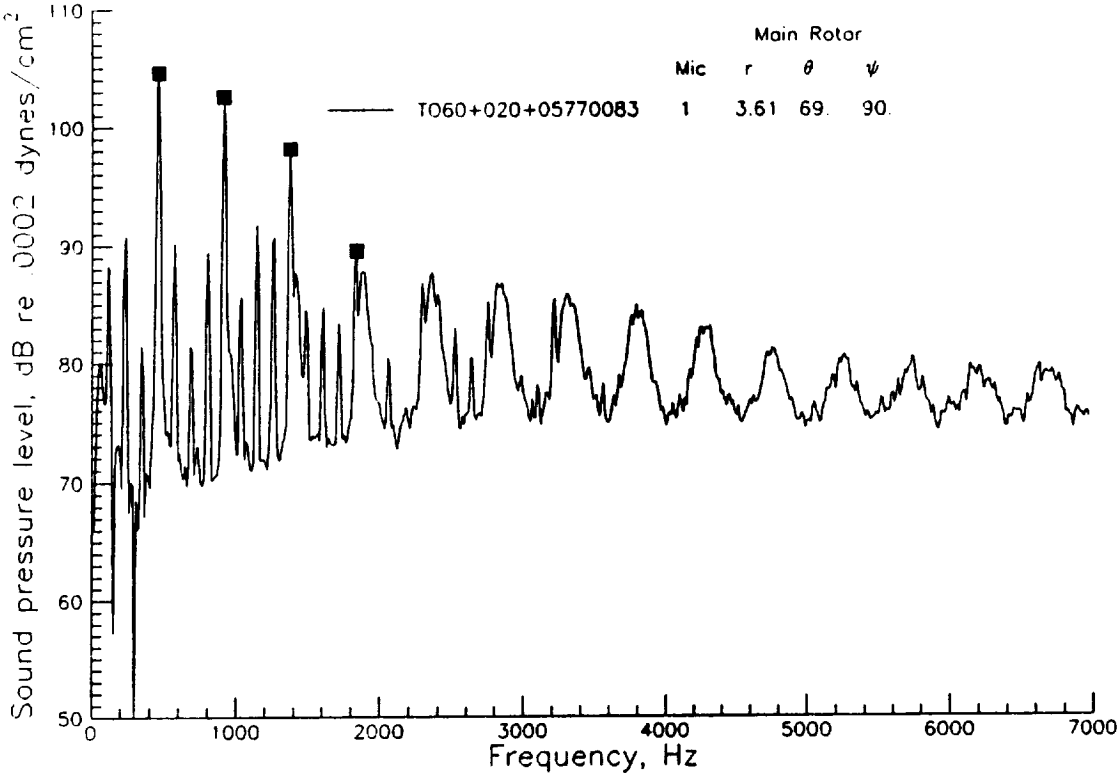

(a) isolated tail rotor

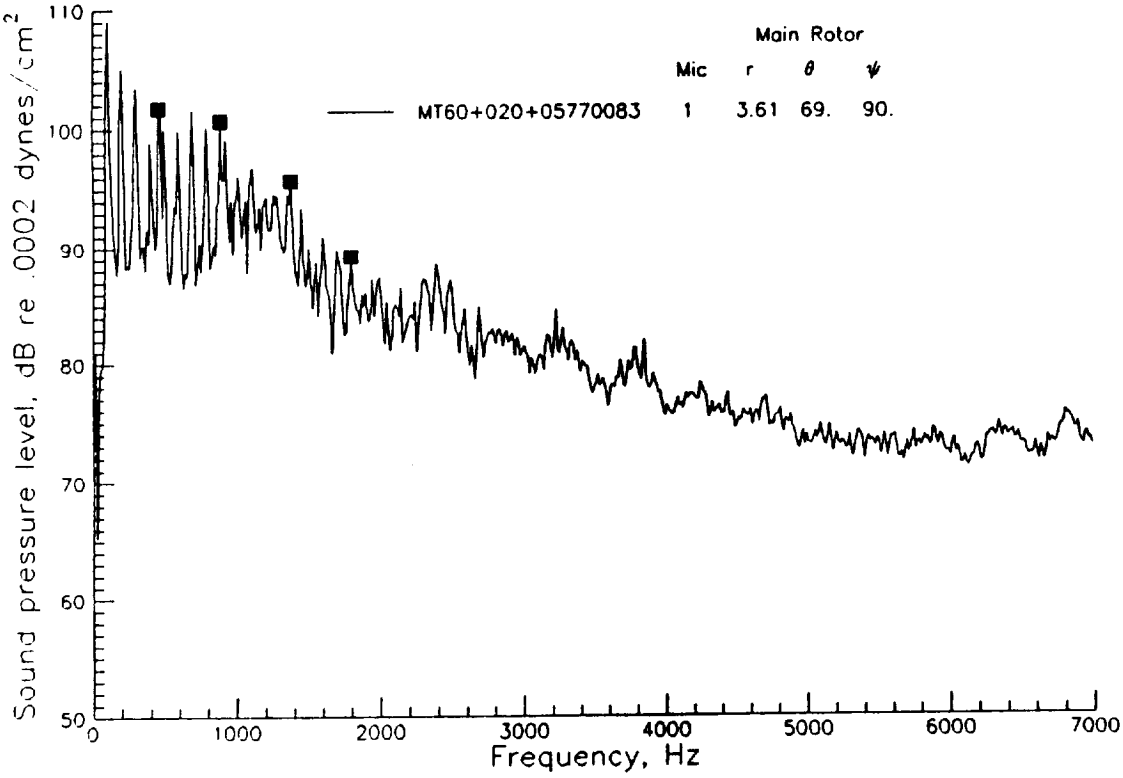

(b) main rotor and tail rotor (symbols mark tail rotor harmonics)

Figure 22. Comparison of isolated tail rotor with combined rotor configuration data at microphone 1 (V=60 kts, α_S=2°, α_{TPP}=5.7°, C_{T-M}=.007, tail rotor thrust 11 lb).

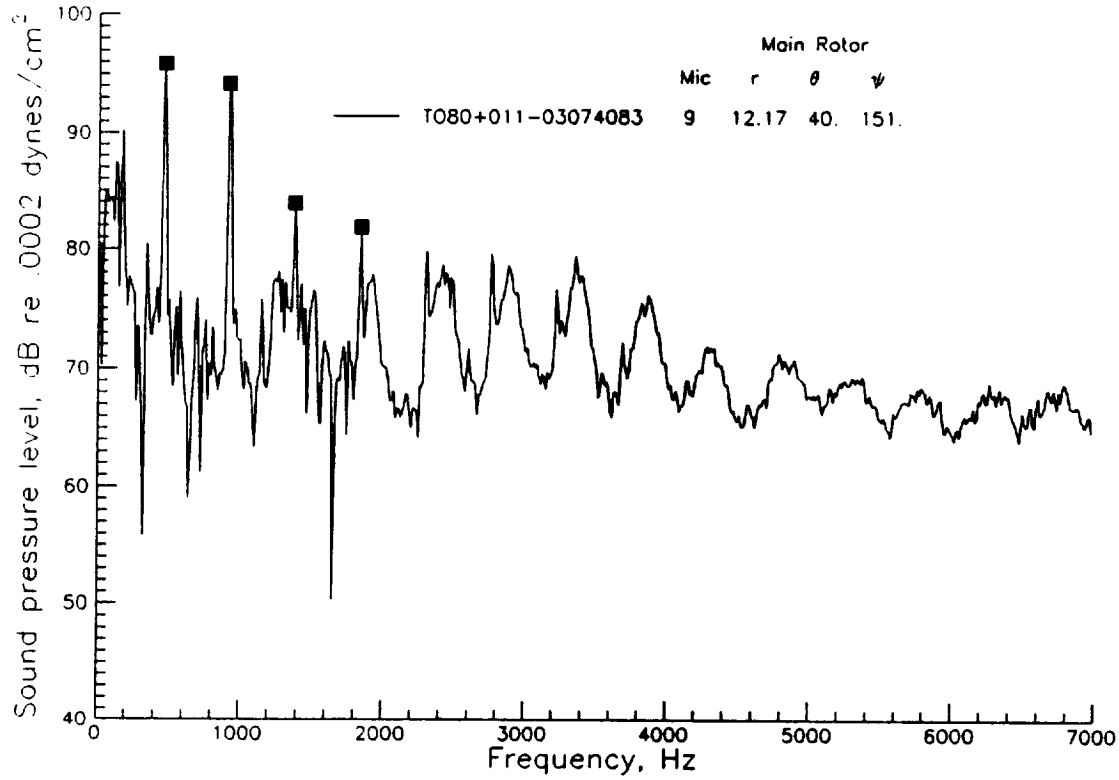

(a) isolated tail rotor

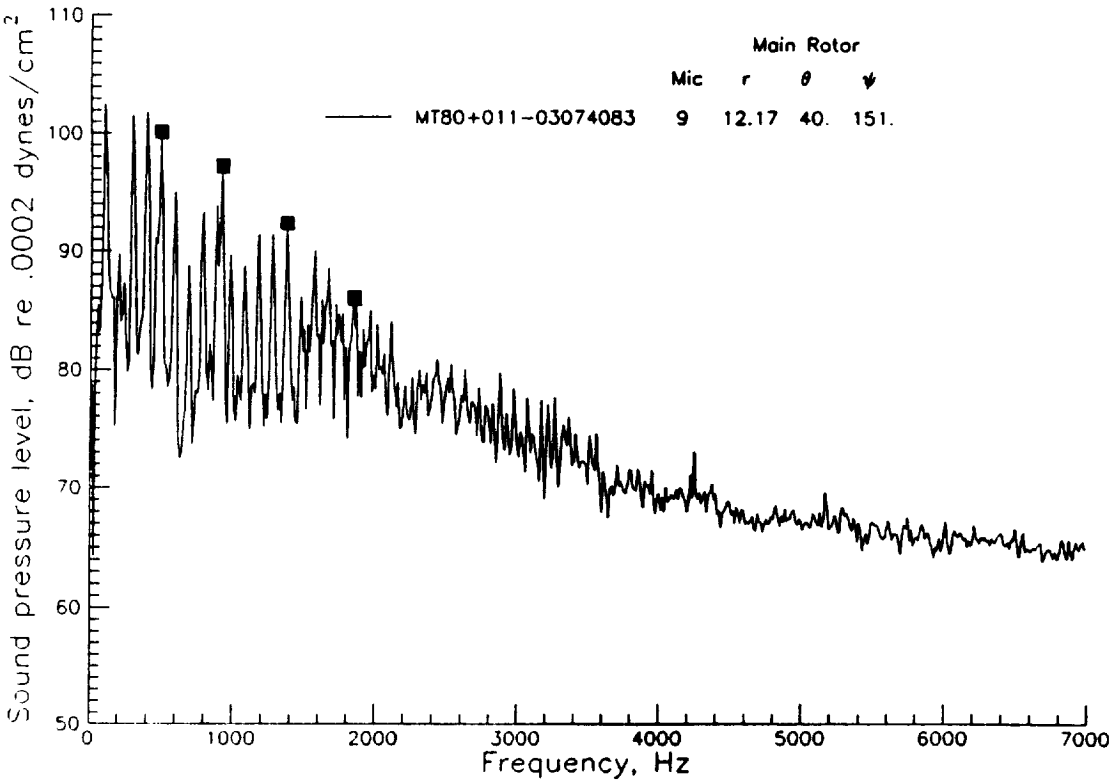

(b) main rotor and tail rotor (symbols mark tail rotor harmonics)

Figure 23. Comparison of isolated tail rotor with combined rotor configuration data at microphone 9 (V=80 kts, α_S=1°, α_{TPP}=-3°, $C_{T\text{-}M}$=.0074, tail rotor thrust 21 lb.).

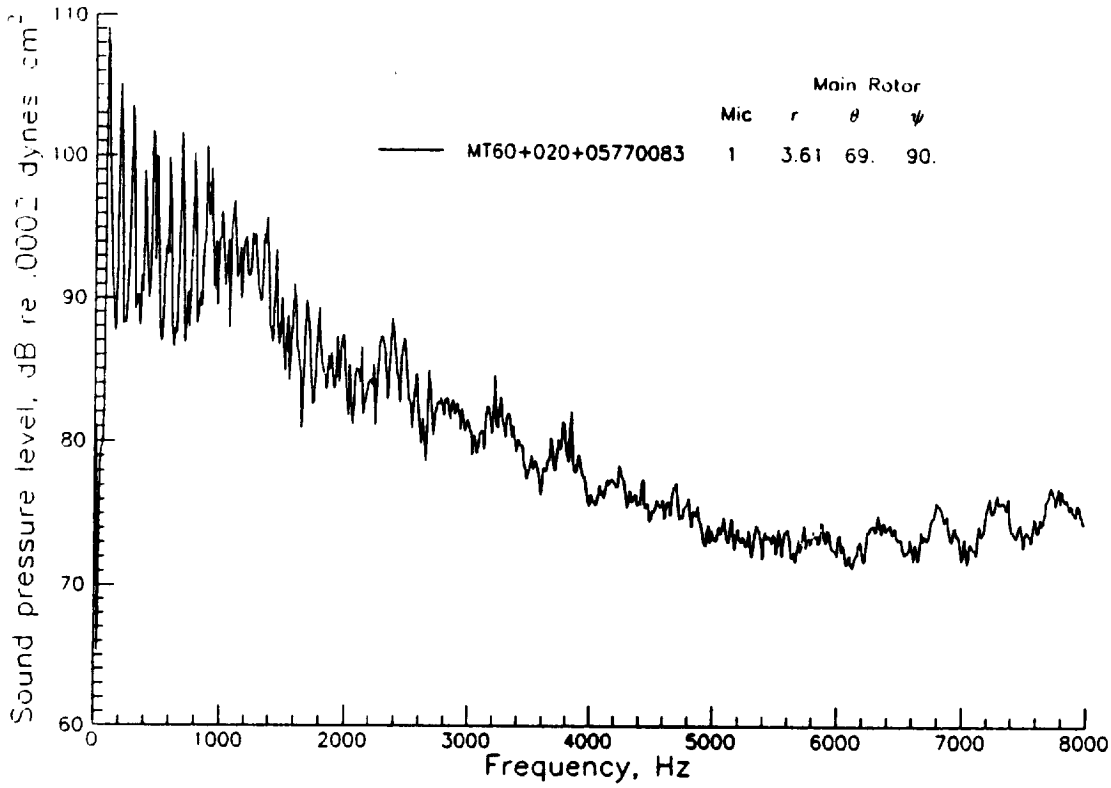

(a) descent, low tail rotor position (V=60 kts, α_{TPP}=5.7°, α_S=2°, $C_{T\text{-}M}$=.007, tail rotor thrust 16 lb)

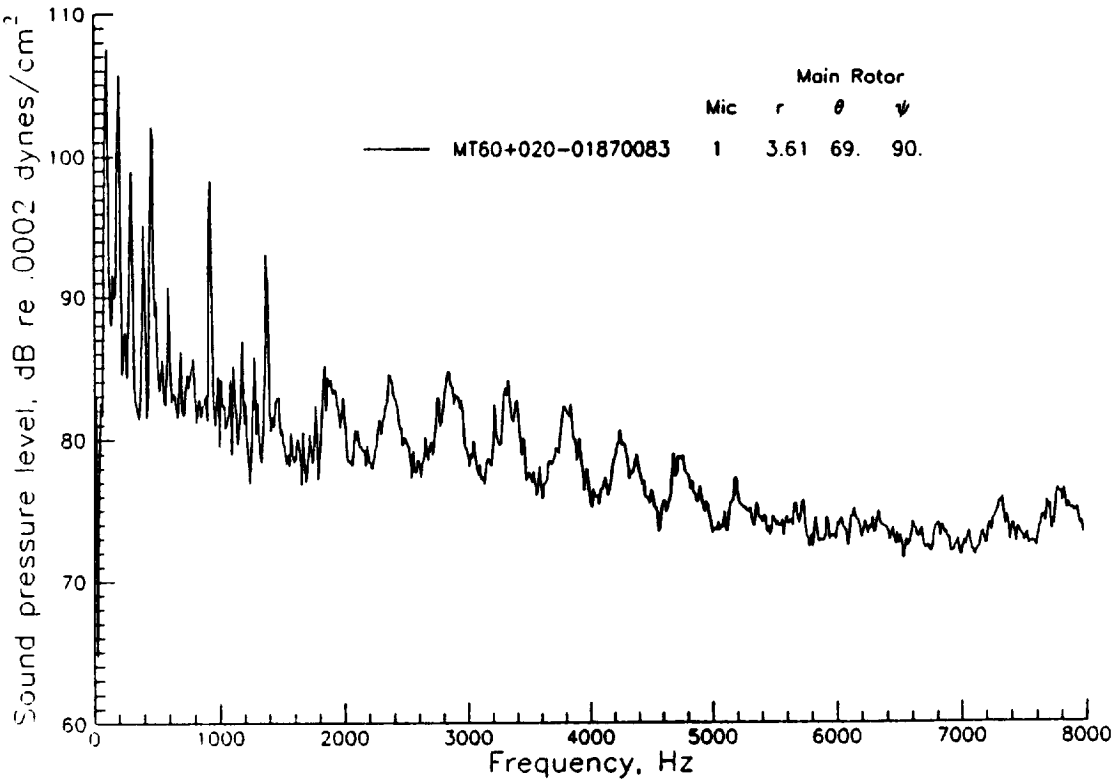

(b) ascent, high tail rotor position (V=60 kts, α_{TPP}=-1.8°, α_S=2°, C_T=.007, tail rotor thrust 9 lb).

Figure 24. Combined rotor configuration data at microphone 1.

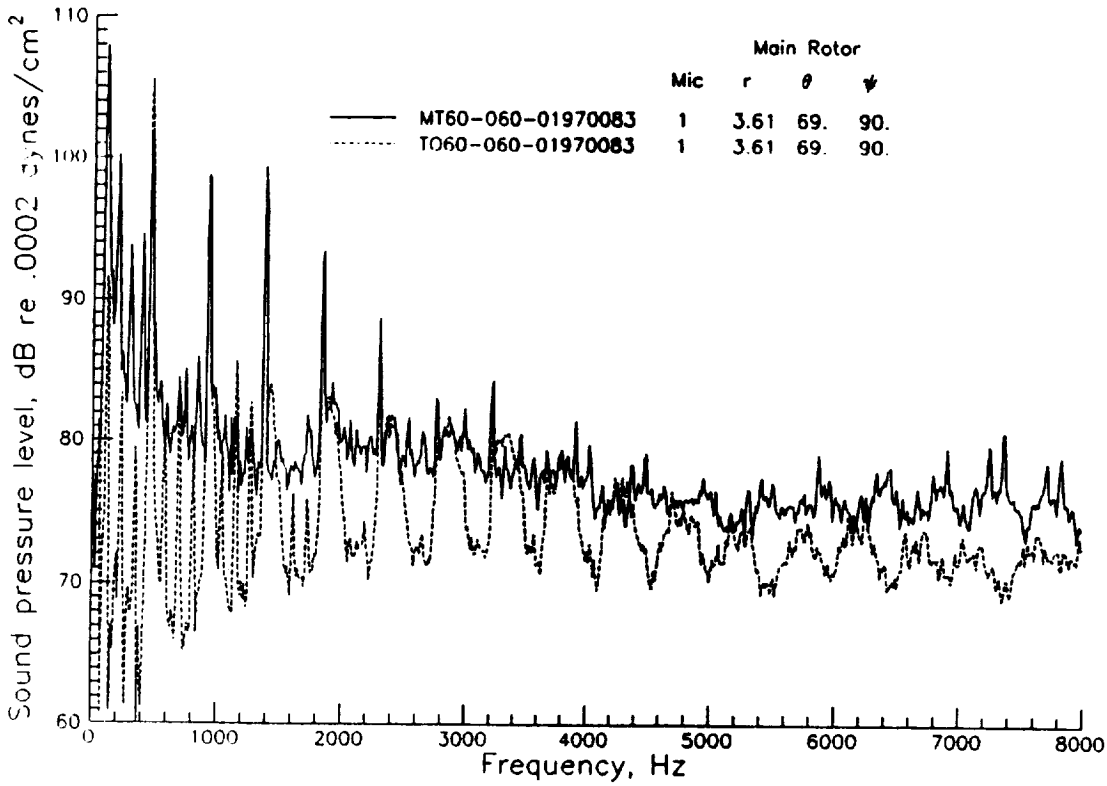

Figure 25. Comparison of combined rotors with isolated tail rotor data at microphone 1, high tail position (V=60 kts, α_{TPP}=-1.9°, α_S=-6.0°, C_{T-M}=.007, tail rotor thrust ~ 17 lb).

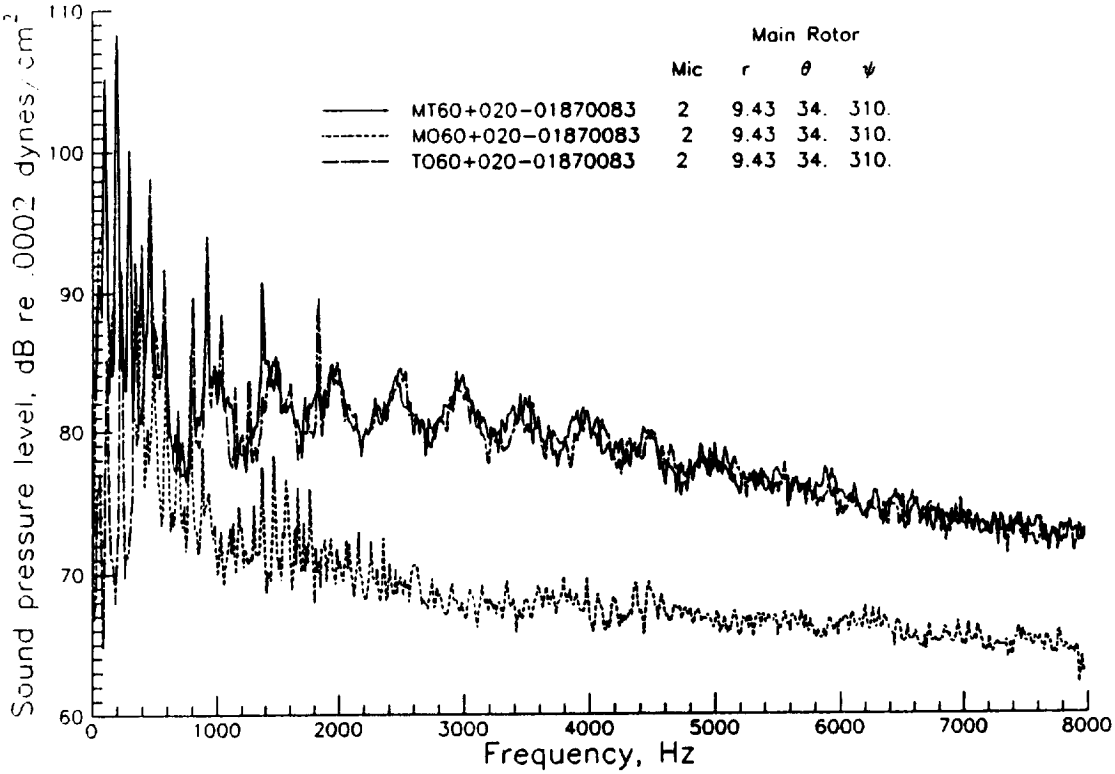

Figure 26. Spectra from the combined rotors, isolated main rotor and isolated tail rotor at microphone 2 for a low main rotor BVI condition (V=60 kts, α_{TPP}=-1.8°, α_S=2.0°, C_{T-M}=.007, tail rotor thrust ~ 17 lb).

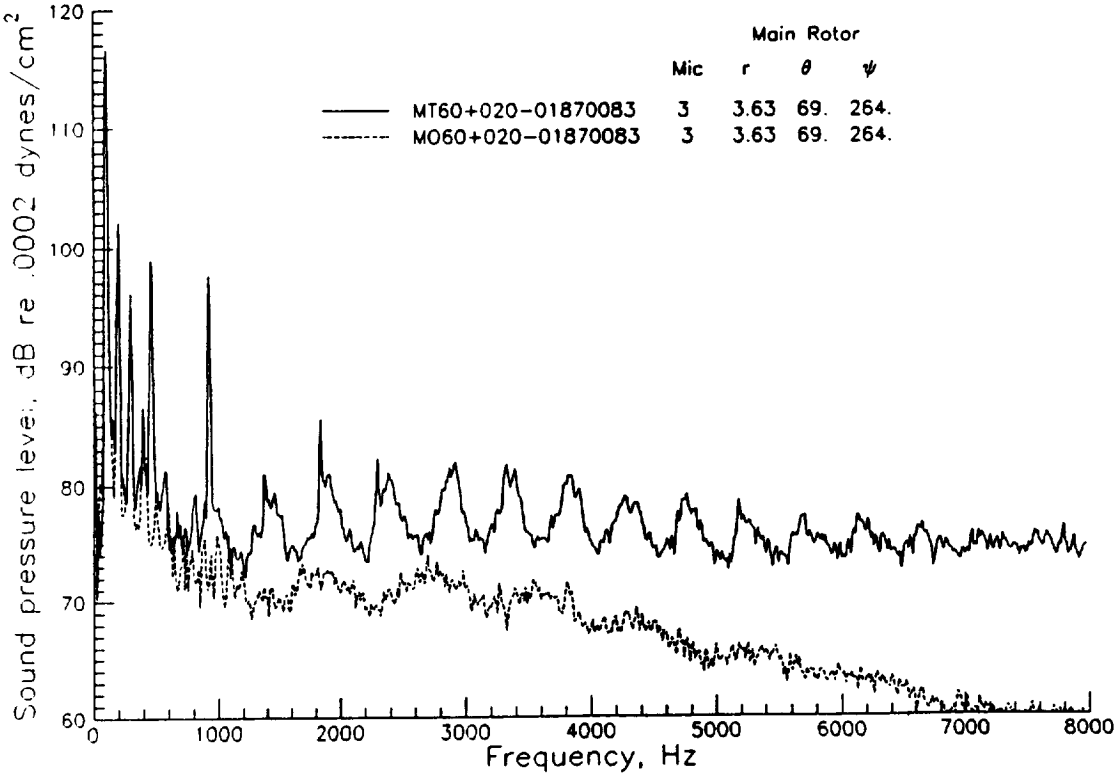

Figure 27. Spectra from the combined rotors and isolated main rotor for microphone 3 (V=60 kts, α_{TPP}=-1.8°, α_S=2.0°, C_{T-M}=.007, tail rotor thrust ~ 17 lb).

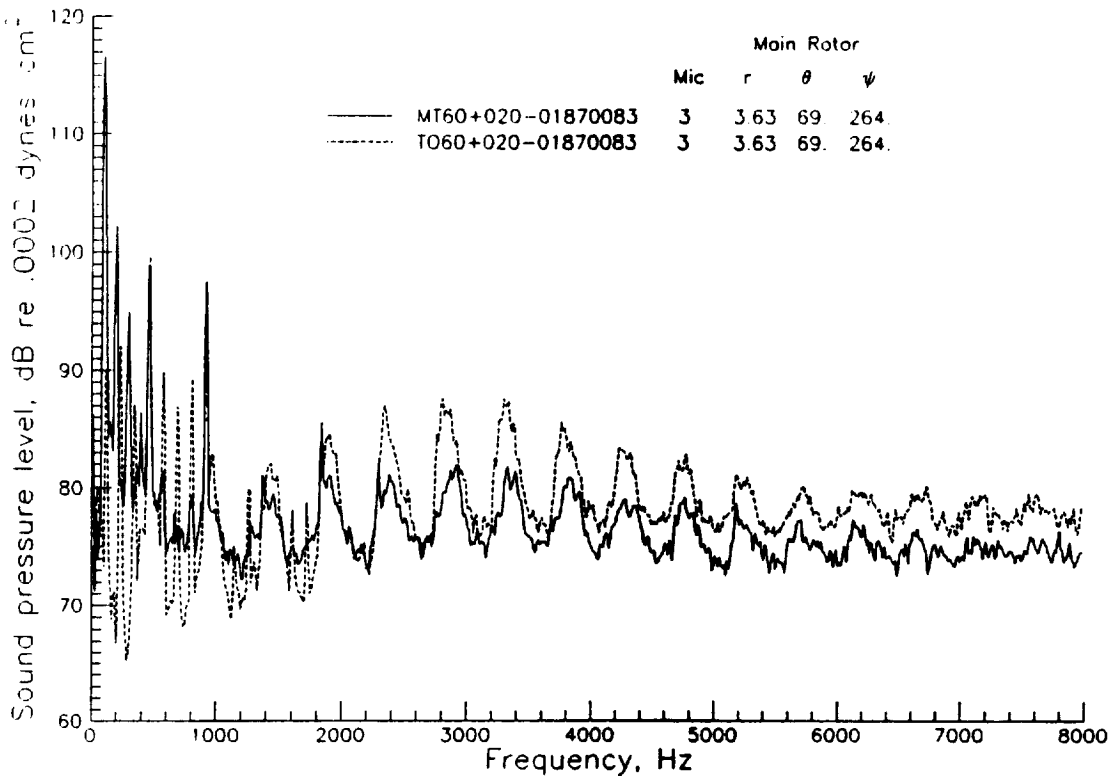

(a) low tail position (V=60 kts, α_{TPP}=-1.8°, α_S=2.0°, $C_{T\text{-}M}$=.007, tail rotor thrust ~ 17 lb).

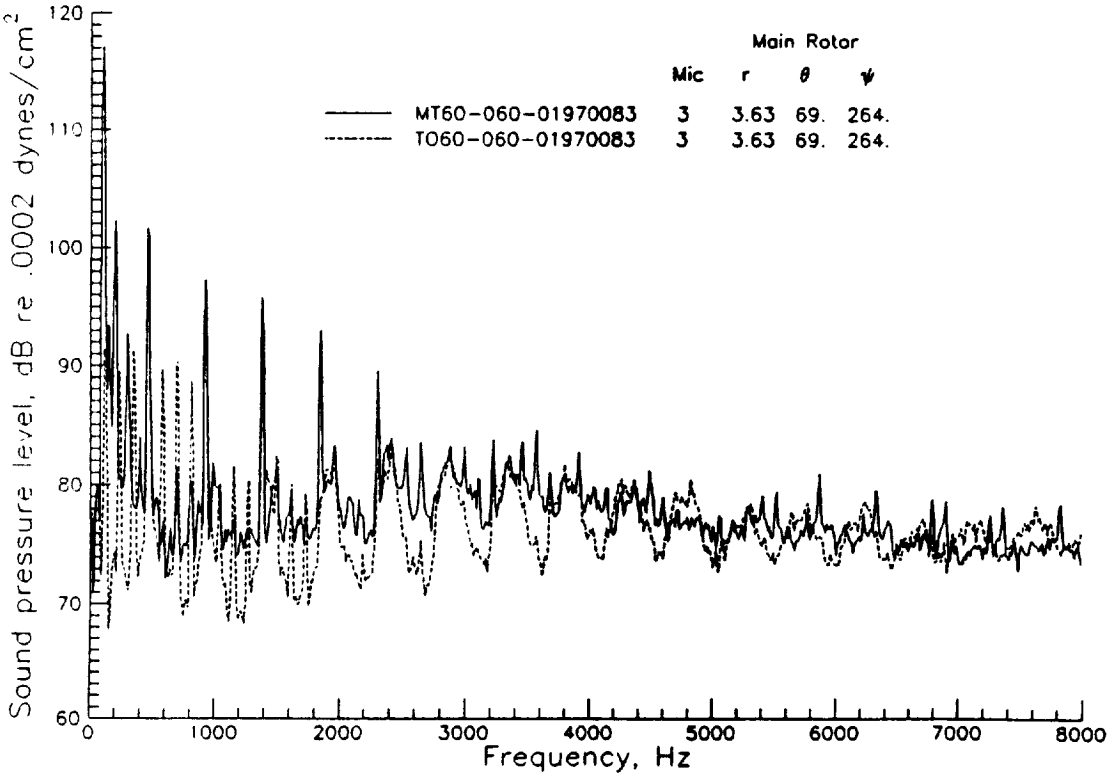

(b) high tail position (V=60 kts, α_{TPP}=-1.9°, α_S=-6.0°, $C_{T\text{-}M}$=.007, tail rotor thrust ~ 17 lb).

Figure 28. Spectra from the combined rotor configuration and isolated tail rotor for microphone 3.

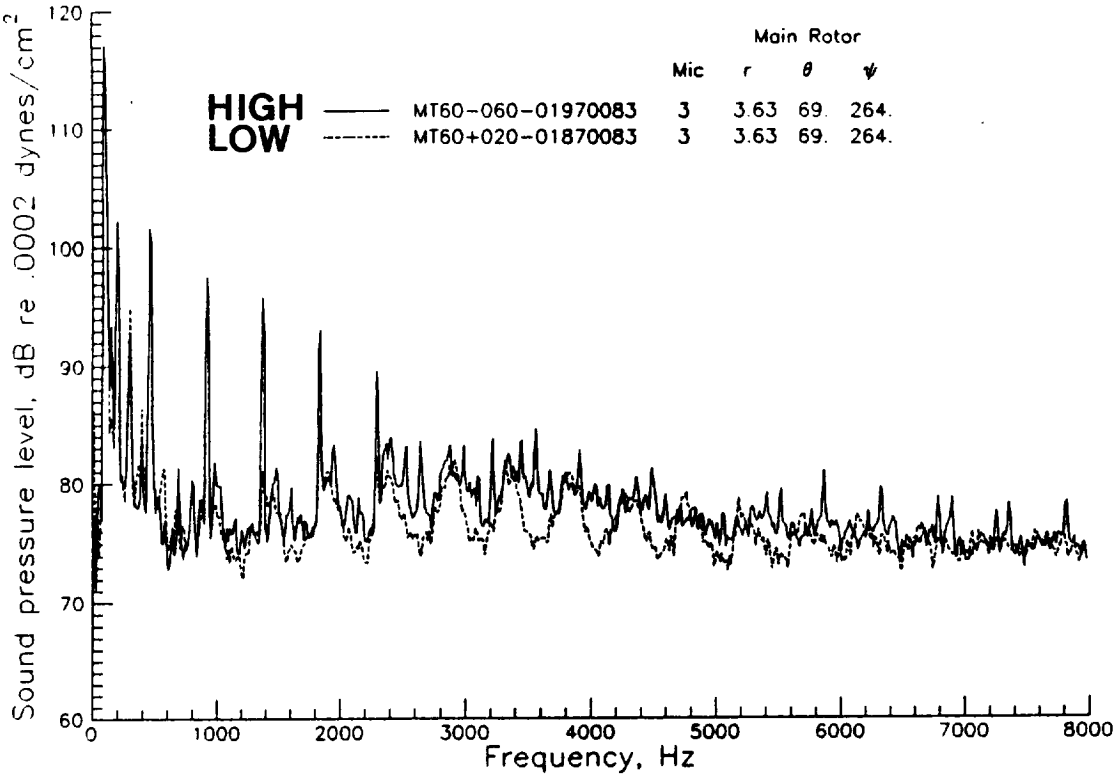

(a) V=60 kts

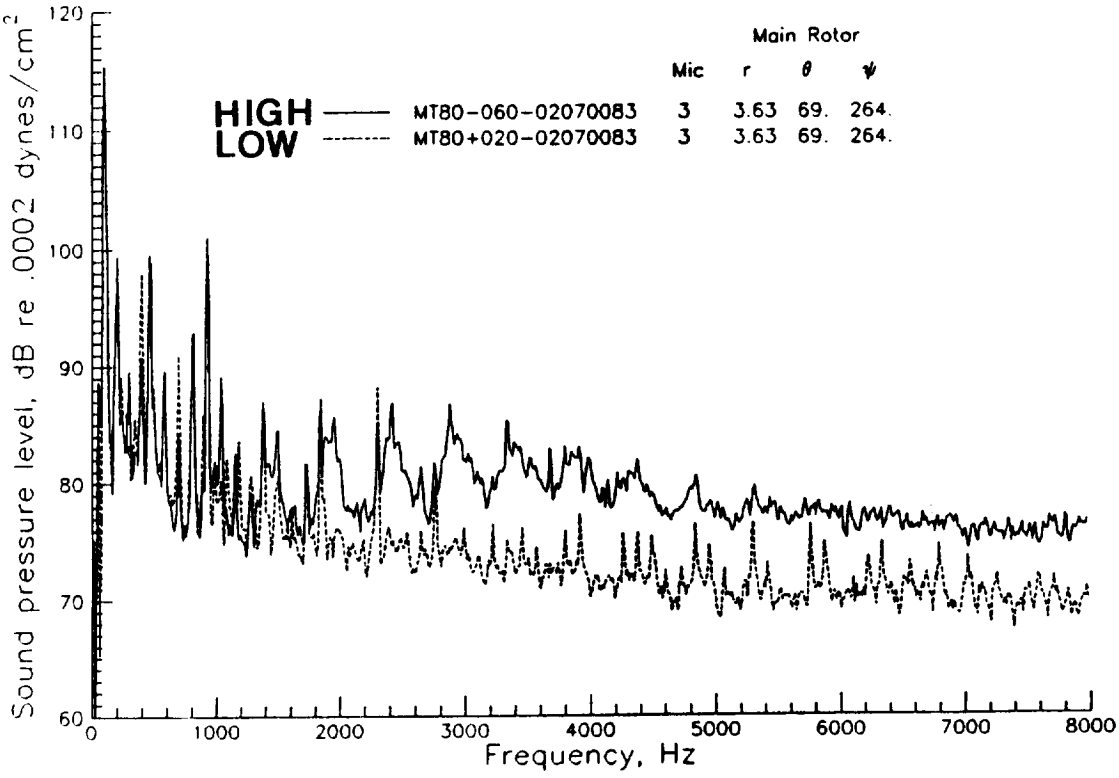

(b) V=80 kts

Figure 29. Comparison of spectra from the combined rotor configuration for microphone 3 at low and high tail rotor positions (α_{TPP}=-2.0°, $C_{T\text{-}M}$=.007).

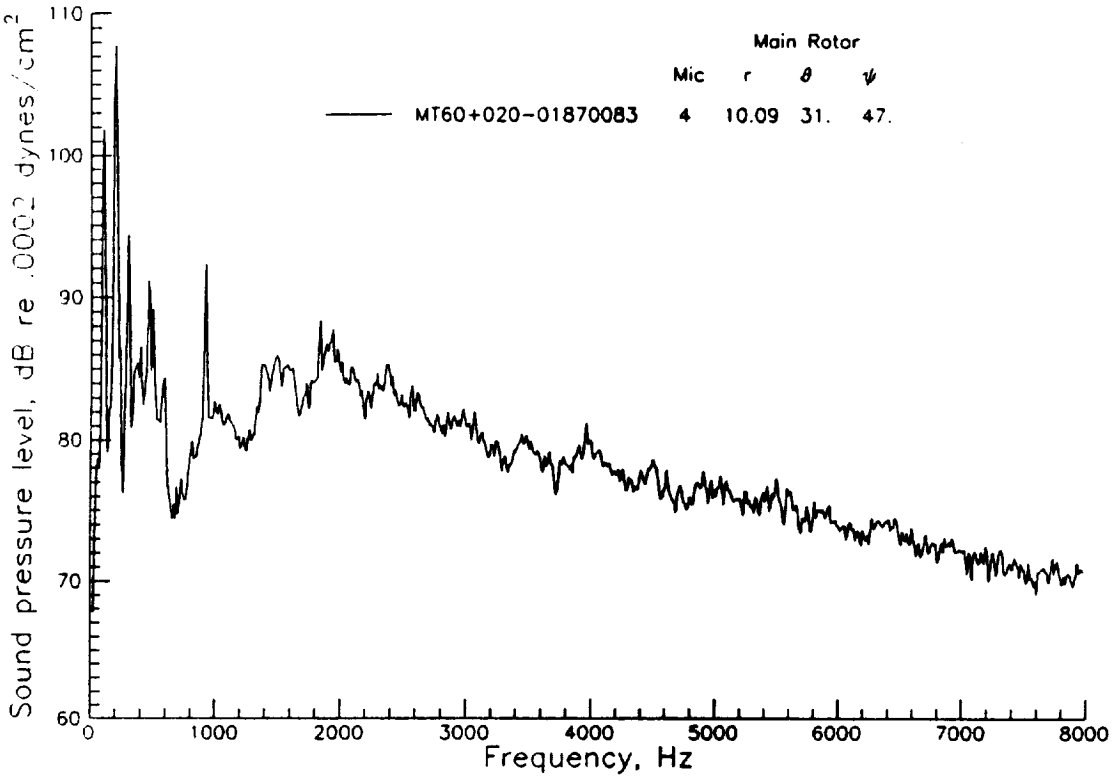

Figure 30. Spectrum from combined rotor configuration for microphone 4 (V=60 kts, α_{TPP}=-1.8°, α_S=2.0°, C_{T-M}=.007, tail rotor thrust 16 lb.).

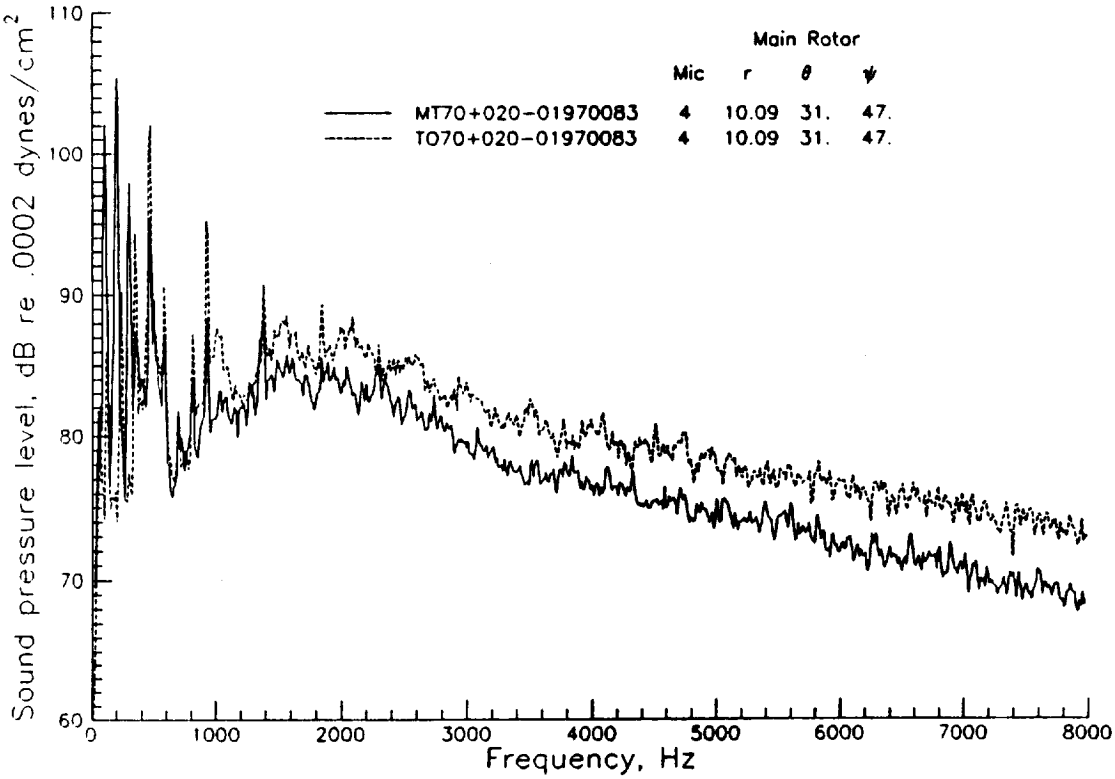

Figure 31. Spectra from the combined rotor configuration and isolated tail rotor for microphone 4 (V=70 kts, α_{TPP}=-1.9°, α_S=2.0°, C_{T-M}=.007, tail rotor thrust ~18 lb).

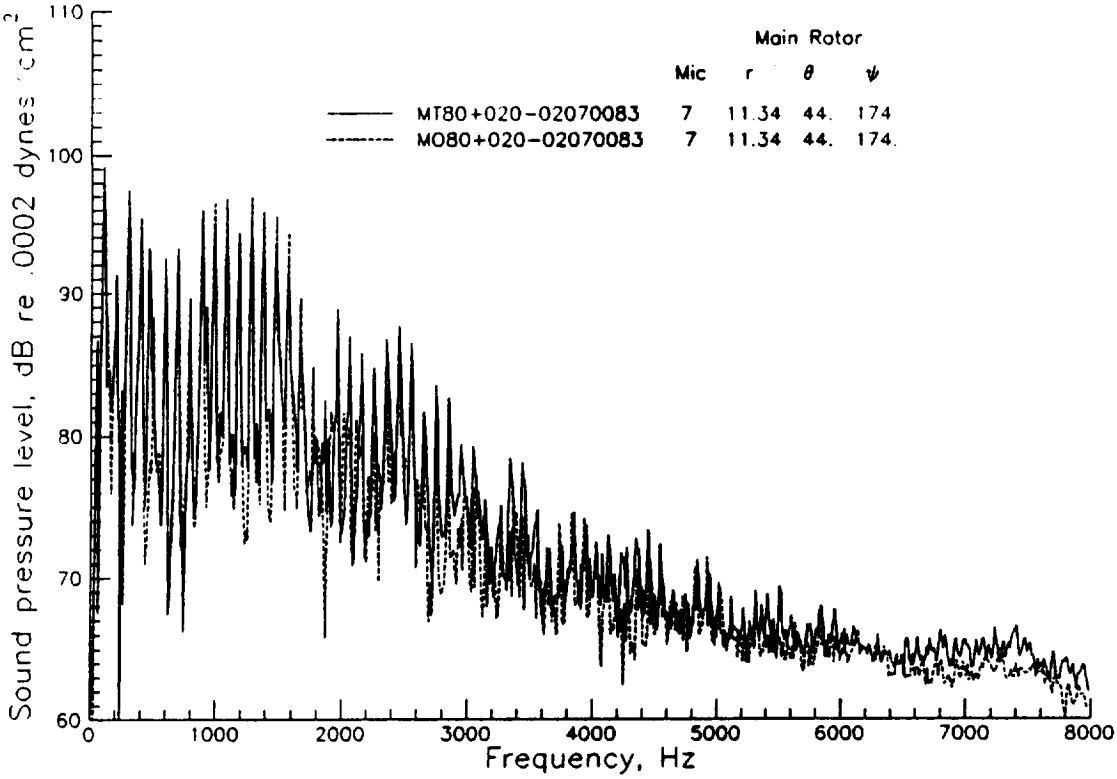

(a) spectra from the combined rotors and isolated main rotor

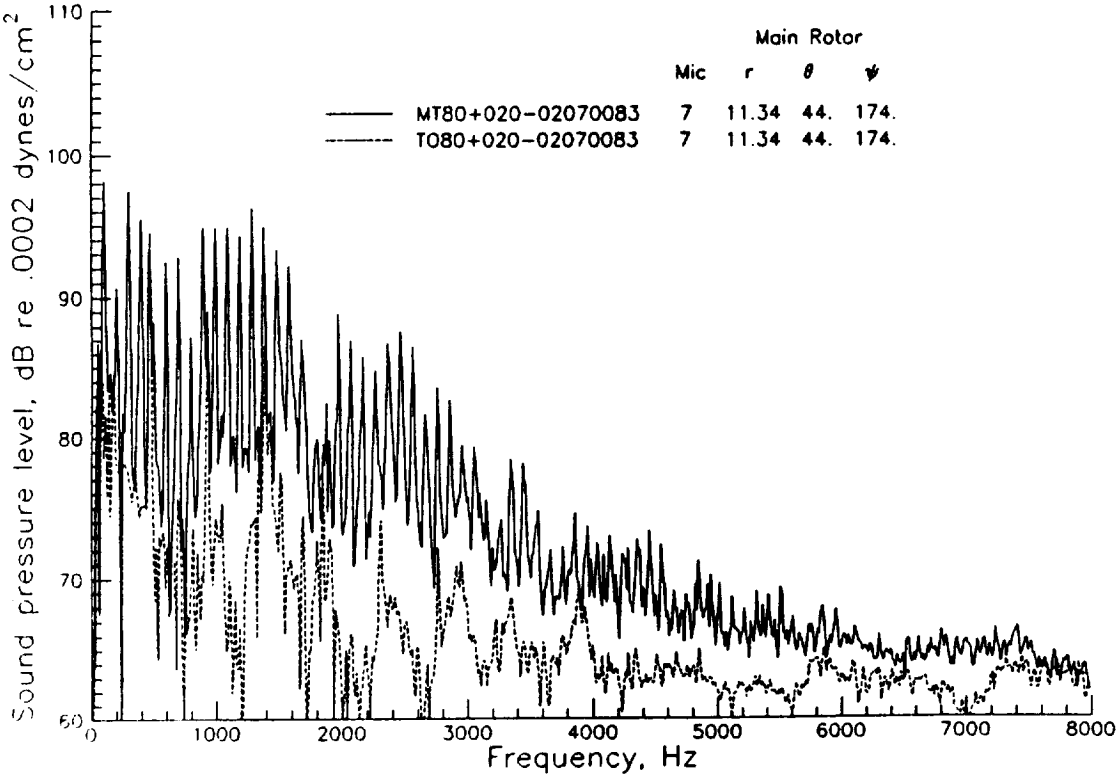

(b) spectra from the combined rotor and isolated tail rotor

Figure 32. Spectra for a low main rotor BVI condition from microphone 7 (V=80 kts, α_{TPP}=-2.0°, α_S=2.0°, $C_{T\text{-}M}$=.007, tail rotor thrust ~ 15 lb)

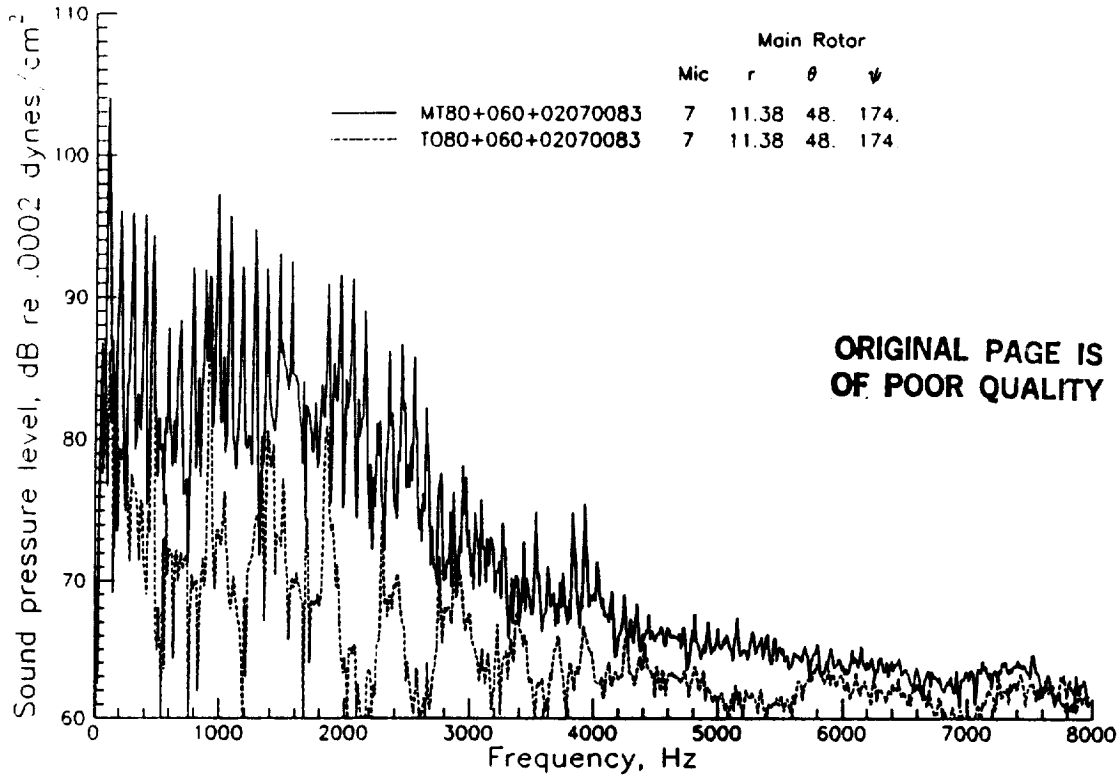

Figure 33. Spectra from the combined rotor and isolated tail rotor configurations for microphone 7 at a high main rotor BVI condition (V=80 kts, α_{TPP}=2°, α_S=6°, $C_{T\text{-}M}$=.007, tail rotor thrust 11 lb).

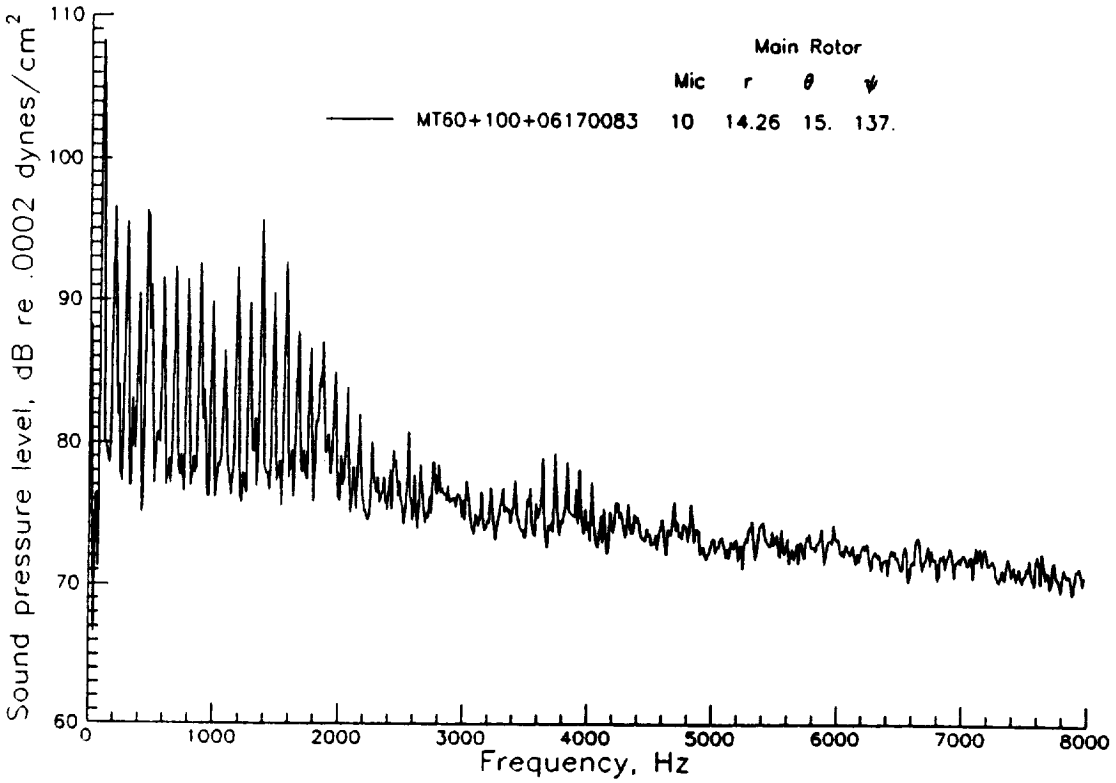

Figure 34. Spectrum from the combined rotor configuration for microphone 10 at a low tail position, high main rotor BVI condition (V=60 kts, α_{TPP}=6.1°, α_S=10°, $C_{T\text{-}M}$=.007, tail rotor thrust 10 lb).

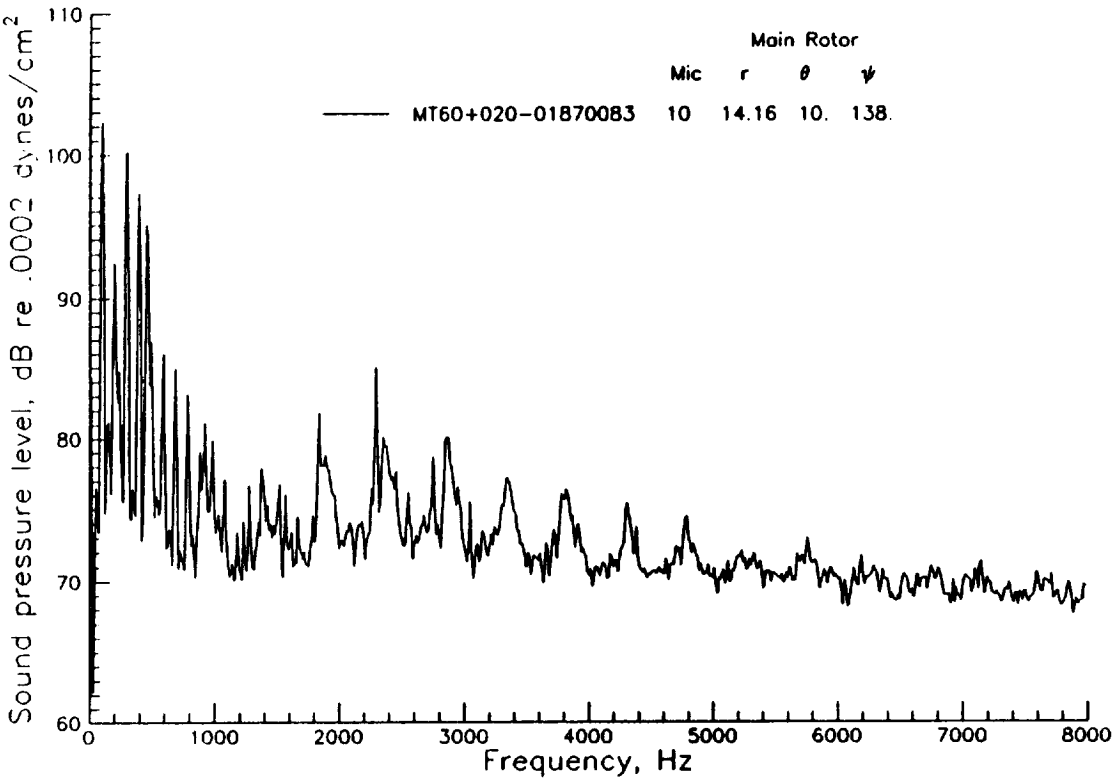

Figure 35. Spectrum from the combined rotor configuration for microphone 10 at a low tail rotor position, low main rotor BVI condition (V=60 kts, α_{TPP}=-1.8°, α_S=2°, $C_{T\text{-}M}$=.007, tail rotor thrust 16 lb).

Report Documentation Page

1. Report No.	2. Government Accession No.	3. Recipient's Catalog No.
NASA TM-101550		

4. Title and Subtitle
Acoustic Test of a Model Rotor and Tail Rotor: Results for the Isolated Rotors and Combined Configuration

5. Report Date
February 1989

6. Performing Organization Code

7. Author(s)
R. M. Martin
C. L. Burley
J. W. Elliott

8. Performing Organization Report No.

10. Work Unit No.
505-63-51

9. Performing Organization Name and Address
NASA Langley Research Center
Hampton, VA 23665-5225

11. Contract or Grant No.

13. Type of Report and Period Covered
Technical Memorandum

12. Sponsoring Agency Name and Address
National Aeronautics and Space Administration
Washington, DC 20546-0001

14. Sponsoring Agency Code

15. Supplementary Notes

16. Abstract

Acoustic data from a model scale main rotor and tail rotor experiment in the NASA Langley 14 by 22 Foot Subsonic Tunnel are presented for the main rotor and tail rotor in isolation and for the two rotors operating together. Results for the isolated main rotor show the importance of the rotor flapping conditions on mid-frequency noise content. High levels of main rotor retreating side blade-vortex interaction noise are shown to radiate downstream of the model. The isolated tail rotor noise results show the dominance of harmonic noise in the thrusting direction. The occurrence of tail rotor broadband noise is seen by the broadening of the tail rotor harmonics and is attributed to fuselage wake turbulence. The combined main and tail rotor data are presented to show the dominance of each rotor's different noise sources at different directivity locations.

17. Key Words (Suggested by Author(s))	18. Distribution Statement
helicopter noise, rotorcraft acoustics, main rotor/tail rotor interaction noise, tail rotor noise, broadband noise, blade-vortex interaction noise	Unclassified-Unlimited Subject Category 71

19. Security Classif. (of this report)	20. Security Classif. (of this page)	21. No. of pages	22. Price
Unclassified	Unclassified	72	A04